CUTOFF FREQUENCIES FOR ALFVÉN WAVES IN THE SOLAR ATMOSPHERE

by

B L HARSHA KALPANIE PERERA

Presented to the Faculty of the Graduate School of
The University of Texas at Arlington in Partial Fulfillment
of the Requirements
for the Degree of

DOCTOR OF PHILOSOPHY

THE UNIVERSITY OF TEXAS AT ARLINGTON
December 2014

To my loving parents, my husband Janitha and my daughter Nethuni who are always by my side and the great teacher Dr. Zdzislaw Musielak.

ACKNOWLEDGEMENTS

First, I would like to thank my advising professor Dr. Zdzislaw Musielak for his valuable guidance through the course of my Ph.D. graduate studies. His constant support, advice and unflinching encouragement have guided me through the most difficult moments of my research.

I wish to thank Dr. Chris Jackson, Dr. Krzysztof Murawski, Dr. Manfred Cuntz, Dr. Qiming Zhang and Dr. Sangwook Park for their interest in my research and for taking time to serve on my committee. I am indebted to Dr. Murawski for all his help with the numerical analysis performed in my PhD research. Also I would like to remember late Dr. Nail Fazleev who served on my committee during my comprehensive exam and gave me valuable advises and comments towards improving my research.

I am grateful to all the teachers who taught me during all the years I spent in school as well as to all the teachers at the University of Texas at Arlington for their words of encouragement. Collective and individual acknowledgments are also owed to my graduate friends at UTA, whose presence is somehow perpetually refreshing, helpful and memorable.

I would like to express my deep gratitude to my parents and siblings for providing me an encouraging environment for my academic career. I would like to express my appreciation to my loving husband Janitha Hapuwitharana for his continuous support, care and inspiring encouragements and thanks to my precious daughter for being by my side and making my life complete.

Finally, my thanks go to all the people who have supported me to complete the research work directly or indirectly.

This work has been supported by NSF under the grant AGS 1246074.

November 19, 2014

ABSTRACT

CUTOFF FREQUENCIES FOR ALFVÉN WAVES IN THE SOLAR ATMOSPHERE

B L HARSHA KALPANIE PERERA, Ph.D.

The University of Texas at Arlington, 2014

Supervising Professor: Zdzislaw Musielak

Propagation of linear Alfvén waves in the isothermal and non-isothermal solar atmosphere is investigated numerically and analytically. It is shown that the two wave variables, the velocity and magnetic field perturbations, behave differently and that there is a range of wave frequencies for which the wave behavior changes from propagating to non-propagating. The so-called transition and turning points corresponding to this change are determined analytically, and their locations in the atmosphere are calculated and verified against the numerical results. The transition and turning points are then used to introduce cutoff frequencies, which are different for different wave variables. The main result is that there isn't a unique cutoff frequency for Alfvén waves. Instead, a number of cutoff frequencies can be introduced depending upon the method used to define them, as well as on the choice of the wave variable used to describe the waves. Relevance of the obtained results to recent observations of Alfvén waves in the solar atmosphere is also discussed.

A concept of global cutoff frequencies is also introduced by using Leighton's, Hille's and Kneser's oscillation theorems, as well as the Sturm comparison theorems.

The oscillation theorems have been applied to bounded and unbounded Alfvén wave equations for both the velocity and magnetic field wave variables. The obtained results demonstrated that the global cutoff frequency and the local cutoff frequency are two different physical concepts. Furthermore, the latter exists if and only if the wave frequency is greater than the former. These analytical results have been verified using numerical solutions of the linear Alfvén wave equations. The original ideal MHD equations were modified by taking into account the displacement current, and several oscillations theorems were applied to the resulting wave equations. As expected, only oscillatory solutions were found.

The results presented in this PhD dissertation give strong theoretical evidence for the existence of local and global cutoff frequencies for Alfvén waves propagating in both isothermal and in more realistic non-isothermal solar atmospheres. The existence of these cutoffs has profound implications on the energy and momentum transport in the solar atmosphere and the role of Alfvén waves in heating of the solar atmosphere, as well as in acceleration of the solar wind.

TABLE OF CONTENTS

LIST OF FIGURES

LIST OF TABLES

CHAPTER 1

INTRODUCTION

1.1 Solar Atmosphere : An overview

Traditionally the atmosphere of the Sun is divided into four layers as illustrated in the Fig. 1.1 a, starting with the photosphere at the bottom, moving up through the chromosphere and transition region to the corona. The photosphere is the layer in which the temperature drops outwards from around 5800 K at the solar surface to around 4000 K at the temperature minimum. Beyond that point it rises again, first relatively gently (forming the chromospheric plateau), but then very rapidly in the transition region. The temperature profile becomes flatter again in the corona. The boundary between the corona and the transition region is often drawn at approximately 10^6 K. This boundary, like that between the chromosphere and transition region, is not sharp or well defined. At still greater distances from the solar surface the temperature gradually decreases again, achieving values of approximately 10^5 K at 1 AU (whereby electrons and ions need not have the same temperature in the heliosphere) as shown in the Fig. 1.1 b.

The solar photosphere is the layer that emits most of the solar radiative energy flux, with the emitted spectrum having its peak in the visible region. As such, the photosphere is the atmospheric layer most easily observed from the ground. The chromosphere is the second of the four layers in the Sun's atmosphere and is roughly 2000 km deep. It is located between the photosphere and the solar transition region. The transition region between the chromosphere and corona is one of the most fascinating parts of the solar atmosphere. It separates two vastly different temperature regimes,

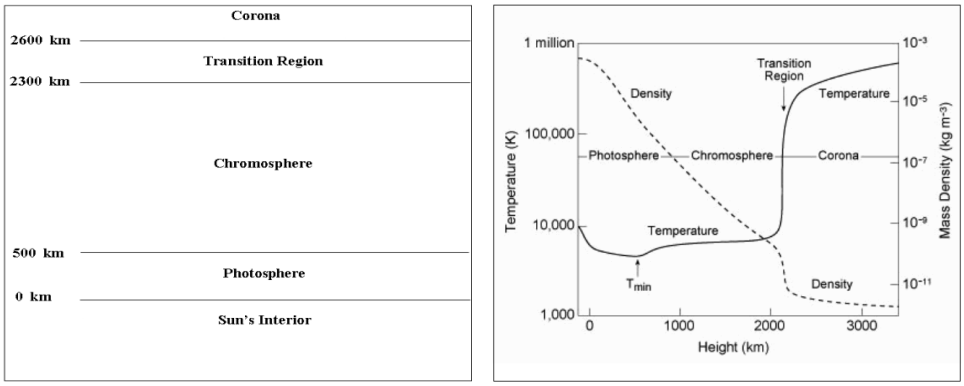

Figure 1.1: Schematic illustration (left) and temperature and density profiles (right) of the solar atmosphere

in which the energy balance between heating and cooling processes operates in different ways. The corona is the outermost layer of the solar atmosphere. It extends from the top of the chromosphere out to a distance of several million kilometres, where it becomes the solar wind. The corona is not as bright as the photosphere, hence it can only be seen when the photosphere is blocked out in some way; e.g., during a total solar eclipse or by using a coronagraph.

Solar observations from both ground-based and space borne facilities show that a wide range of magnetohydrodynamic (MHD) waves propagate throughout the solar atmosphere, however, the energy carried by some of those waves may not be sufficient to heat the solar atmosphere (e.g., (Fujimura & Tsuneta 2009), and references therein). There is strong observational evidence for the existence of Alfvén waves on the Sun (e.g., De Pontieu et al. (2007); Cirtain et al. (2007); Jess et al. (2009); McIntosh et al. (2011)). These waves can penetrate through the stratified solar atmosphere and could be the most promising wave mechanism to explain the heating of the Sun's outer atmosphere (e.g., Parker (1979); Priest (1982); Hollweg (1990); Roberts & Ulmschneider (1997); Ulmschneider & Musielak (2003)).

In 1942 Hannes Alfvén proposed that purely incompressible MHD waves can propagate through magnetized plasma under and carry energy approximately along the magnetic field lines. After over six decades of this Nobel prize wining discovery, solar physicists are still trying to figure out whether these waves are capable of heating the solar corona and accelerating the solar wind or not. The existence of Alfvén waves requires magnetic fields whose tension is the restoring force for the waves. Observations demonstrated that the solar atmosphere is highly inhomogeneous and that the solar magnetic field plays dominate role in forming these inhomogeneities. The most prominent magnetic structures in the solar photosphere are sunspots and magnetic flux tubes (e.g., Parker (1979); Priest (1982); Solanki (1993); (Saar 1996, 1998); Stix (2004); Cameron & Galloway (2005)); these structures are often called active regions. In addition, there are also regions of weak (or no) magnetic fields and they are called quiet regions (e.g., Foukal (2004)). According to traditional view, the most prominent source of non-radiative energy needed to heat the solar atmosphere is the solar convection zone, where different waves, including Alfvén waves, are generated. These waves carry their energy through the photosphere and dissipate in the overlying atmosphere (e.g., Foukal (2004); Stix (2004)). In magnetic-free regions, acoustic waves are likely to be responsible for the heating, however, in magnetic regions, where magnetic flux tubes dominate, longitudinal, transverse and torsional Alfvén tube waves may significantly contribute to the heating.

To account for the observed emissions, a significant amount of non-radiative energy is needed to heat different regions of the solar atmosphere. A heat input of the order 2×10^7 ergs / cm^2 s and 1×10^6 ergs / cm^2 s is required for the solar chromosphere and transition region, respectively (e.g., Schrijver & Title (2003); Linsky (1991); Anderson & Athay (1989)). The solar data also shows that the observed emission from magnetically active regions can be 10 (or more) times higher than that observed

in quiet (weak magnetic field) regions (e.g., Linsky (1991); (Priest et al. 2002, 2003); Foukal (2004); Stix (2004)).

In order to address the heating problem of the solar atmosphere, one must establish conditions for the propagation of Alfvén waves in the solar atmosphere, and this is one of the main goals of this dissertation.

1.2 Cutoff frequencies of Alfvén waves in the solar atmosphere

Linear Alfvén waves propagating in a uniform background medium with homogeneous magnetic fields are purely transverse waves and they can decouple from magnetohydrodynamics (MHD) waves. Alfvén waves also exist in the solar atmosphere, which is highly inhomogeneous with gradients in all its physical parameters, as it has been recently demonstrated by the solar observations performed by the Hinode satellite, the Solar Dynamic Observatory (SDO), the Swedish Solar Telescope (SST), and by the STEREO. Specific recent observational results include the outwardly-propagating Alfvén waves with amplitudes of the order of 20 km s^{-1} and periods within 100-500 s in the quiescent solar atmosphere as reported by McIntosh et al. (2011), and the propagating Alfvén waves with amplitudes of the order of 7.4 km s^{-1} and periods of the order of 45 s in solar spicules as reported by Okamoto & De Pontieu (2011). Earlier observational evidence for the existence of torsional Alfvén waves in the solar atmosphere was given by Jess et al. (2009), who found the waves with periods ranging from 2 min to 12 min, with the maximum power near 6-7 min. Interpretations and discussions of the observational results can be found in Erdélyi & Fedun (2007), De Pontieu et al. (2007), Dwivedi & Srivastava (2010), (Cargill & de Moortel 2011; Cargill 2013), and others.

Numerous papers were already published on different aspects of the Alfvén wave propagation in the solar atmosphere (e.g., Ferraro & Plumpton (1958); Hollweg (1978,

1981); Hollweg (1985); (Zhugzhda & Locans 1982); (Hollweg 1981); Thomas (1983); An et al. (1989); Hollweg (1990, 1992); Musielak et al. (1992); Velli (1993); Musielak & Moore (1995); Kudoh & Shibata (1999); Ofman (2002); Cally (2003); Suzuki & Inutsuka (2005); Hollweg & Isenberg (2007); Verdini & Velli (2007); Verdini et al. (2009); Matsumoto & Shibata (2010); Murawski & Musielak (2010); McKenzie & Hu (2010); Cally (2012); Webb et al. (2012); Chmielewski et al. (2013);Murawski et al. (2014); Perera et al. (2014); Perera et al. (2014), and many others). The topics covered in these papers range from the Alfvén wave propagation in isothermal and non-isothermal atmospheres to reflection, dissipation and momentum deposition by the waves. The presented results were used to explain the observed chromospheric and coronal heating, the solar wind acceleration, and the spectral line broadening in the solar atmosphere.

First indications that the propagation of Alfvén waves along a uniform magnetic field embedded in an isothermal solar atmosphere is affected by the density gradient were given by Ferraro & Plumpton (1958), who found analytical solutions to the problem (see also Thomas (1983)). The obtained solutions show that Alfvén waves form standing waves, which are caused by constructive interference between the propagating and reflected Alfvén waves. The formation of the standing wave patterns in the isothermal atmosphere was investigated numerically by An et al. (1989), who were able to reproduce full analytical solutions by their numerical simulations and identify a height in their atmospheric model at which Alfvén wave reflection is dominant. Their main result is that wave reflection occurs continuously and that the atmospheric height at which it reaches maximum is related to a characteristic frequency defined as the ratio of Alfvén velocity to two pressure (or density) scale heights. Recently, Cally (2012) argued that the boundary conditions used by the

above authors were equivalent to imposing a perfectly reflecting boundary in their models and, as a result, their solutions must naturally describe standing Alfvén waves.

The origin and physical meaning of the characteristic frequency identified by An et al. (1989) was further explored by Musielak et al. (1992) and Musielak & Moore (1995). In their approach, Alfvén wave equations were transformed into the corresponding Klein-Gordon equations, which explicitly displayed the so-called critical frequencies. Full analytical solutions as well as an oscillation theorem based on Euler's equation were used to establish criteria for the Alfvén wave propagation and reflection. The criteria were established for an isothermal atmosphere and only recently extended to a non-isothermal atmosphere by Murawski & Musielak (2010), who considered a model with realistic temperature distribution characteristic for the solar chromosphere, transition region and corona, and derived a local cutoff frequency.

Typically, this cutoff frequency separates wave frequencies into those that correspond to propagating and non-propagating waves (e.g., Lamb (1932); Rae & Roberts (1982); Roberts (1983, 2000); Musielak et al. (2000); Musielak et al. (2002); Musielak et al. (2006)), and its existence is caused by gradients of physical parameters (their characteristic scales) in the considered atmospheric model. Petukhov & Petukhov (2002) argued that uniform magnetic fields do not introduce any space or time characteristic scales and, as a result, the cutoff frequency should not be present for the Alfvén wave propagation. Similar conclusions were reached by Lopin & Nagorny (2013) for transverse (kink) tube waves, and by Musielak et al. (2007) for torsional tube waves; in both cases the waves are Alfvén-like and their propagation is confined to thin and isothermal magnetic flux tubes embedded in the solar atmosphere. However, cutoff frequencies may appear when temperature gradients are taken into account as shown by Routh et al. (2007, 2010); Routh et al. (2013) and Hammer et al. (2010). Moreover, Murawski & Musielak (2010) pointed out that in their analytical

and numerical studies the local cutoff frequency obtained for Alfvén waves is relevant for reflection of these waves, a point of view that seems to be consistent with earlier numerical studies performed by An et al. (1989).

According to the above results, the problem of existence or non-existence of cutoff frequencies for Alfveń waves still remains unsolved. Therefore, the main goal of this dissertation is to solve this problem by performing numerical simulations of linear Alfvén waves propagating in an isothermal and non-isothermal solar atmosphere models. Let us also point out that the purpose of our numerical simulations is different than those performed by An et al. (1989), who recovered the Ferraro & Plumpton (1958) solutions by running their code for a long period of time, and by Murawski & Musielak (2010), who studied the propagation of impulsively generated Alfvén waves of Fourier frequency spectrum in the solar atmosphere described by the VAL C model (Vernazza et al. (1981)). Instead, in this dissertation we solve the initial value problem for the propagation of Alfvén waves of different frequencies and identify heights in the atmosphere at which the wave behavior changes from propagating to non-propagating. We identify the locations of these heights with the so-called transition and turning points, and use them to introduce cutoff frequencies for Alfvén waves. We show that there is no one unique cutoff frequency for Alfvén waves but instead cutoff frequencies depend on the method used to define it as well as on the choice of the wave variable used to describe the waves. Our results present strong theoretical evidence for the existence of cutoff frequencies for the Alfvén wave propagation in the isothermal and non-isothermal solar atmospheres. We also briefly discuss the relevance of our findings to the current observational results.

We consider isothermal and non-isothermal models, however, we assume that the background magnetic field is uniform in our approach presented in this dissertation. A class of models in which the displacement currents (DC) are included in

the description of the Alfvén wave propagation (e.g., Leroy (1983)) will also be considered. In our studies, we shall use both analytical and numerical methods, with the former including integral transforms, methods to determine cutoff frequencies as well as some powerful oscillation theorems (e.g., Swanson (1968); Teschl (2011) and references therein).

Another goal is also to address properly boundary conditions in the considered atmospheric models. The fact that these conditions may profoundly affect even the well-known close form solutions was recently discussed by Cally (2012), who argued the boundary conditions used by several authors were equivalent to imposing a perfectly reflecting boundary in their models. A much broader range of boundary conditions will be considered in this dissertation and implications of these conditions on the Alfvén wave propagation in the solar atmosphere will be discussed.

CHAPTER 2

SOLAR MAGNETOHYDRODYNAMICS

2.1 Background

Plasma is an ionized gas that supports many plasma wave modes. Restoring forces include kinetic and magnetic pressure, and electric and magnetic forces. Wave phenomena are important for heating plasmas, instabilities and diagnostics of its physical properties. In order to describe the behavior of the plasma in the solar atmosphere various physical phenomena have to be taken into account. There are several theoretical models describing plasma:

- Single Particle Description
- Kinetic Model
- Magnetohydrodynamics
- Hybrid Model
- Gyro-kinetic Description

Henceforth, we will limit our discussion to one-fluid Magnetohydrodynamics. It is the most commonly used theoretical model as it provides the simplest description of plasma and can be applied to a wide variety of astrophysical contexts. It is also a preferred model when it comes to numerical simulations as it requires the least computational resources. The approach assumes that the plasma is able to maintain a local equilibrium and that studies of low-frequency wave phenomena in highly conducting gases or fluids immersed in magnetic fields can be performed.

2.2 Hydrodynamics

The behavior of non-viscous gases or fluids with zero heat conductivity is described by Euler equations. The first one is the equation of mass continuity (Milne-Thomson & Rott (1968))

$$\frac{\partial \rho}{\partial t} + \nabla \cdot (\rho \mathbf{V}) = 0, \tag{2.1}$$

where ρ is mass density and $\mathbf{V}$ is flow velocity. Then, there is the equation of motion as given in Milne-Thomson & Rott (1968) :

$$\rho \frac{\partial \mathbf{V}}{\partial t} + (\rho \mathbf{V} \cdot \nabla)\mathbf{V} + \nabla p = \mathbf{F}, \tag{2.2}$$

where p is gas pressure and $\mathbf{F}$ denotes external forces, such as gravity or Lorentz force. Finally, there is the energy equation, which for the case of $\mathbf{F} = 0$ has the following form (Priest (1982))

$$\frac{\partial E}{\partial t} + \nabla \cdot [\mathbf{V}(E + p)] = 0. \tag{2.3}$$

Here

$$E = \frac{\rho V^2}{2} + \frac{p}{\gamma - 1}, \tag{2.4}$$

is the total energy density, $\rho V^2/2$ stands for kinetic energy density, $p/(\gamma - 1)$ is the internal energy density and γ denotes adiabatic index. Equation 2.3 with the use of Eq. 2.1 can be written in the following form:

$$\frac{\partial p}{\partial t} + \mathbf{V} \cdot \nabla p = -\gamma p \nabla \cdot \mathbf{V}. \tag{2.5}$$

2.3 Maxwell equations

Maxwell's equations describe evolution of electric field $\mathbf{E}(\mathbf{r},\mathbf{t})$ and magnetic field $\mathbf{B}(\mathbf{r},\mathbf{t})$ in response to current density $\mathbf{j}(\mathbf{r},\mathbf{t})$ and space charge density $q(\mathbf{r},\mathbf{t})$:

Faraday's law of induction:

$$\nabla \times \mathbf{E} = -\frac{\partial \mathbf{B}}{\partial t}, \tag{2.6}$$

Ampere's law:

$$\nabla \times \mathbf{B} = \mu_0 \mathbf{j} + \frac{1}{c^2}\frac{\partial \mathbf{E}}{\partial t}, \tag{2.7}$$

where μ_0 is permeability of free space and c is the speed of light in a vacuum.

Gauss' law:

$$\nabla \cdot \mathbf{E} = \frac{q}{\epsilon_0}, \tag{2.8}$$

where ϵ_0 is permittivity of free space.

Solenoidal constraint:

$$\nabla \cdot \mathbf{B} = 0, \tag{2.9}$$

which together with Ohm's law:

$$\mathbf{j} = \sigma(\mathbf{E} + \mathbf{V} \times \mathbf{B}), \tag{2.10}$$

where σ denotes electrical conductivity.

2.4 MHD equations

Magnetohydrodynamics (MHD) describes a slow evolution (typical velocities are small when compared to the speed of light) of an electrically conducting fluid - most often a plasma consisting of electrons and protons. It is the study of highly conducting fluids in the presence of magnetic fields. It has broad applications in laboratory

plasmas, magnetospheric physics, space physics and astrophysics. MHD equations are coupled, non linear, partial differential equations, which are complicated to solve either analytically or numerically. The basic set of MHD equations is derived from conservation laws (i.e., conservation of mass, momentum and energy) in conjunction with Maxwell's equations.

2.4.1 MHD Approximations

A fluid embedded in the magnetic field is described by both Navier-Stokes equations of hydrodynamics and Maxwell's equations of electromagnetism. However, the most basic formulation of MHD equations, namely the ideal MHD, incorporates several simplifications to the model.

- First of all, in the limit of ideal MHD, viscosity and heat conductivity is set to zero, transforming the Navier-Stokes equations into Euler equations 2.1, 2.2 and 2.5 (Priest (1982)). This assumption results in an infinite Reynolds number:

$$R = \frac{\mathbf{V}\Lambda}{\nu}, \tag{2.11}$$

  where Λ stands for the length scale and ν is the kinematic viscosity. A large value of Reynolds number allows turbulent flow (Rahimi Tabar & Rouhani (1996)). The lack of heat conductivity excludes a number of physical phenomena connected with heat transfer from the consideration, including conduction, convection, thermal radiation or thermal diffusion. To simulate these processes other theoretical model has to be considered.
- In the next step the resistivity of the fluid is ignored, making the plasma a perfect conductor (Goedbloed & Poedts (2004)). This implies that magnetic advection surpasses magnetic diffusion, what makes magnetic Reynolds number

infinite. In this regime, the magnetic field is 'frozen' into the medium and travels with the plasma flow as in Davidson (2001). This assumption is valid for systems, in which, for the given length scale, the time of magnetic diffusion is longer than the considered time (Priest (1982)).

- The so-called MHD Approximation limits the considered velocities to non-relativistic: $V << c$ (Priest (1982)). Thus, the displacement current term in Ampre's law: $\frac{1}{c^2}\frac{\partial \mathbf{E}}{\partial t}$ can be ignored, transforming Eq. 2.7 into:

$$\nabla \times \mathbf{B} = \mu_0 \mathbf{j}. \tag{2.12}$$

  This assumption excludes from consideration electromagnetic waves, since changes of the electric field in time are neglected.

- Ideal MHD equations are applicable if characteristic time scales in the system are much longer than (Priest (1982))
  - the time lag between collisions of particles, what implies that the medium is strongly collisional and results in nearly Maxwellian distribution of particle speeds;
  - the ion gyration time.
- Characteristic lengths of the system pose another limitation of applicability of ideal MHD equations. The length scales should be much larger than (Priest (1982)):
  - the Debye length;
  - the Larmor gyration radius.

2.4.2 Ideal MHD equations

Due to the slow evolution, it is possible to consider the combined electrons and ions as a single fluid. The instantaneous state of this fluid is characterized by the following fields:

- $\rho(\mathbf{r}, t)$: Mass density. On the above mentioned time scales the plasma is charged neutral - the number densities of protons and electrons will therefore balance $n_p = n_e = n$. The protons are the most of the mass, so $\rho = nm_p$.
- $V(\mathbf{r}, t)$: Flow velocity. $\mathbf{V}$ is the center of mass velocity of all particles within a small neighborhood of the point $\mathbf{r}$.
- $p(\mathbf{r}, t)$: Pressure. This is the sum of electron pressure and proton pressure.
- $B(\mathbf{r}, t)$: Magnetic field. This is the fundamental field in MHD.

The assumptions described in sec. 2.4.1 lead to the following perfect fluid, ideal MHD equations (Parker (1979), Priest (1982)):

Mass continuity equation :

$$\frac{\partial \rho}{\partial t} + \nabla \cdot (\rho \mathbf{V}) = 0, \tag{2.13}$$

Momentum equation :

$$\rho \left(\frac{\partial \mathbf{V}}{\partial t} + (\mathbf{V} \cdot \nabla)\mathbf{V} \right) + \nabla p - \rho \mathbf{g} - \frac{1}{\mu_0} (\nabla \times \mathbf{B}) \times \mathbf{B} = 0, \tag{2.14}$$

Induction equation :

$$\frac{\partial \mathbf{B}}{\partial t} - \nabla \times (\mathbf{V} \times \mathbf{B}) = 0, \tag{2.15}$$

Energy equation :

$$\frac{\partial p}{\partial t} + \mathbf{V} \cdot \nabla p + \gamma p \nabla \cdot \mathbf{V} = 0. \tag{2.16}$$

These equations, together with the Ideal Gas law:

$$p = \frac{\rho}{m} k_B T, \tag{2.17}$$

provide a full description of a fluid embedded in the magnetic field in the limit of ideal magnetohydrodynamics. Here $\mathbf{g}$ is gravitational acceleration, T is temperature, m denotes mean particle mass and k_B is Boltzmann's constant. It is noteworthy that Eq. 2.14 was obtained from Eq. 2.2 by introducing gravity and Lorentz force in the following manner: $F = \rho\mathbf{g} + \frac{1}{\mu_0}(\nabla \times \mathbf{B}) \times \mathbf{B}$.

2.4.3 Linear MHD equations

We will investigate the MHD equations for small amplitude, plane wave solutions. Into the MHD equations 2.13 - 2.17 we substitute:

$$\mathbf{B} = \mathbf{B}_e(\mathbf{r}) + \mathbf{B}_1(\mathbf{r}, t) \ , \tag{2.18}$$

$$\mathbf{V} = \mathbf{V}_1(\mathbf{r}, t) \ , \tag{2.19}$$

$$\rho = \rho_e(\mathbf{r}) + \rho_1(\mathbf{r}, t) \ , \tag{2.20}$$

$$p = p_e(\mathbf{r}) + p_1(\mathbf{r}, t) \ , \tag{2.21}$$

where quantities with subscript $'1'$ represent small, linear perturbations from the values of the background quantities. Higher order perturbations are ignored and the equilibrium is assumed to be uniform, with $\mathbf{B}_e$ and acceleration of gravity, $\mathbf{g}$ being

constants. Then we substitute the above equations into the MHD equations, linearize them, and obtain (Ferraro & Plumpton (1958))

$$\frac{\partial \rho_1}{\partial t} + \nabla \cdot (\rho_e \mathbf{V}_1) = 0, \tag{2.22}$$

$$\rho_e \frac{\partial \mathbf{V}_1}{\partial t} = -\nabla p_1 + \frac{1}{\mu_0}(\nabla \times \mathbf{B}_1) \times \mathbf{B}_e + \rho_1 \mathbf{g}, \tag{2.23}$$

$$\frac{\partial \mathbf{B}_1}{\partial t} = \nabla \times (\mathbf{V}_1 \times \mathbf{B}_e). \tag{2.24}$$

2.4.4 MHD Equilibrium

Magneto-hydrodynamic equations are often solved by specifying an equilibrium state (denoted by subscript 'e') and then perturbing it by small disturbances. Let us consider stationary equilibrium state: $V_e = 0$ with a force-free magnetic field, i.e.

$$\frac{1}{\mu_0}(\nabla \times \mathbf{B}_e) \times \mathbf{B}_e = 0 \ . \tag{2.25}$$

In particular, straight magnetic field satisfies Eq. (2.25) with $\mathbf{B}_e = B_e \hat{\mathbf{y}}$, and it will be considered throughout this dissertation. As a result, in our state of equilibrium gravity force, acting along y-direction ($\mathbf{g} = [0, -g, 0]$), is balanced by a pressure gradient:

$$\rho_e g = \nabla p_e \ . \tag{2.26}$$

From this point forward, we assume that the plasma evolution occurs only along y-direction. It is clear that in such a system, all equilibrium quantities vary only with regard to altitude y, corresponding to one-dimensional equilibrium. Using the ideal gas law (Eq. (2.17)) and the y - component of the hydrostatic pressure balance given in Eq. (2.26), we express the following :

Pressure scale-height Λ_p :

$$\Lambda_p(y) = \frac{k_B T_e(y)}{mg} \ , \tag{2.27}$$

Equation (2.26) together with Eq. (2.17) implies that pressure profile has the following form:

$$p_e(y) = p_0 \exp\left(-\int_{y_0}^{y} \frac{d\xi}{\Lambda(\xi)}\right) \ , \tag{2.28}$$

where p_0 is gas pressure at a reference level $y = y_0$. Mass density is described by a relation:

$$\rho_e(y) = \frac{p_e(y)}{g\Lambda(y)} \ , \tag{2.29}$$

and the speed of sound

$$c_s(y) = \sqrt{\frac{\gamma p_e(y)}{\rho_e(y)}} \ . \tag{2.30}$$

2.5 MHD wave modes

Disturbances in fluids and plasmas propagate as waves which transport the energy of perturbations from one region to another. A wave is characterized by its amplitude and phase (frequency and wave number). If the amplitude of the disturbances is small, linear waves can be represented as a superposition of plane waves using Fourier analysis. In a dispersive medium such as a plasma, wave propagation follows a dispersion relation between wave frequency and wave number. The velocity of wave phase propagation is called phase velocity.

Within the linear limit of infinitesimally small wave amplitudes in uniform and magnetized plasma, there are three distinct types of MHD waves that can be mathematically described as: slow and fast magneto-acoustic waves, and Alfvén waves. The first two types of wave have an acoustic character modified by the magnetic

field, whereas the Alfvén waves exist purely because of the presence of a magnetic field. The three physically distinct MHD wave modes exist due to the following reasons. The MHD description of a magnetized plasma is using macroscopic quantities, lets say density (ρ), velocity (V), magnetic field (B) and a thermodynamics variable, say pressure (p). In ideal MHD (i.e. no dissipation or non-adiabatic processes) these quantities are coupled through a set of eight non-linear partial differential equations (PDEs) governing mass conservation, momentum conservation, governing magnetic flux and the energy conservation. If this is a closed system in a stationary state, one may expect eight eigenvalues corresponding to eight different physical wave modes.

However, there is the solenoidal condition, that will reduce the number of independent PDEs to seven, resulting in seven eigenvalues. One eigenvalue, $\omega = 0$, turns out to be describing the entropy wave that does not carry information, and may be disregarded, leaving six possible independent eigenvalues corresponding to six further independent modes. An interesting intrinsic feature of the remaining eigenvalues is that they appear squared, i.e. there is no distinction between forward and backward propagating MHD waves in a static (i.e. $V_e = 0$) magnetized plasma. Hence, there are three physically distinct MHD waves. These waves are a complete set and their appropriate linear superposition can be combined into any linear MHD wave perturbations. This also means that the individual eigen modes (slow, fast magneto-acoustic and Alfvén waves) are orthogonal to each other and there is no linear transformation that can transform one MHD eigen mode into the other. Henceforth, we will limit our discussion to Alfvén waves in the solar atmosphere.

CHAPTER 3

ALFV*É*N WAVES IN THE SOLAR ATMOSPHERE

3.1 Alfvén waves : An overview

One of the remarkable properties of magnetic fields in MHD is that they can transmit transverse waves, just like a plucked string. It relies on the fact that the **B**-field and fluid are virtually frozen together when the conductivity σ is high. To give an illustration, suppose that a portion of a field line is swept sideways by the lateral movement of the fluid (Fig. 3.1). The resulting curvature of the field line gives rise to a restoring force, $B^2/\mu R$, where R is the radius of the curvature of the field line. As the curvature increases, the restoring force rises and eventually the inertia of the fluid is overcome and the lateral movement is stopped. However, the Lorentz force is still present, and so the flow now reverses, carrying the field lines back with it. Eventually, the field lines return to their equilibrium position, only now the inertia of the fluid carries the field lines past the neutral point and the whole process starts in reverse. Oscillations then develop and this is called an Alfvén wave (Davidson

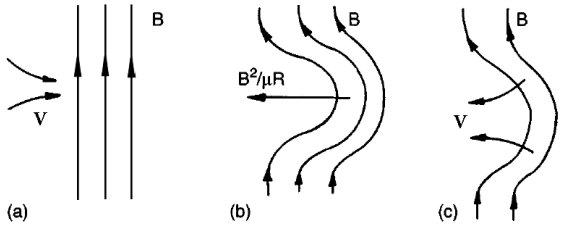

Figure 3.1: Formation of Alfvén waves

(2001)), which propagates with the Alfvén speed C_A along the magnetic field lines (Fig. 3.2) and is given by

$$C_A = \frac{B_e}{\sqrt{\mu_0 \rho_e}}, \tag{3.1}$$

where B_e and ρ_e are the background magnetic field and gas density, respectively.

Hannes Alfvén discovered the waves in 1942, and he explained them in his paper as follows (Alfvén (1942)):

"*If a conducting liquid is placed in a constant magnetic field, every motion of the liquid gives rise to an electromagnetic force, which produces electric currents. Owing to the magnetic field, these currents give mechanical forces which change the state of motion of the liquid. Thus a kind of combined electromagnetic-hydrodynamic wave is produced.*"
and since then these waves have been called Alfvén waves.

The propagation of transverse Alfvén waves has an interesting analogy with the propagation of waves on a vibrating string with beads, with the magnetic field providing the tension and the MHD fluid providing the mass per unit length that carries the charged particles in plasma along with it. This analogy also suggests that waves on different magnetic field lines propagate independently, as though they were on separate strings.

3.2 Alfvén wave equations in the solar atmosphere

Since the wave propagation is restricted to the y - direction, in order to describe the propagation of Alfvén waves in the solar atmosphere, we introduce the first order velocity perturbation $\mathbf{V}_1(y,t) = v_z(y,t)\hat{\mathbf{z}}$ and the magnetic field perturbation

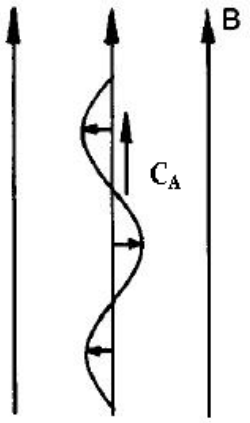

Figure 3.2: Alfvén waves

$\mathbf{B}_1(y,t) = b_z(y,t)\hat{\mathbf{z}}$. With these assumptions, the z - components of momentum (Eq. (2.23)) and induction (Eq. (2.24)) equations can be written as

$$\frac{\partial v_z}{\partial t} - \frac{B_e}{\mu\rho_e(y)}\frac{\partial b_z}{\partial y} = 0 \ , \tag{3.2}$$

and

$$\frac{\partial b_z}{\partial t} - B_e\frac{\partial v_z}{\partial y} = 0 \ . \tag{3.3}$$

We then eliminate one wave variable in terms of the other by combining these two equations, and obtain two wave equations for Alfvén waves propagating in the solar atmosphere. The wave equations are

$$\frac{\partial^2 v_z}{\partial t^2} - C_A^2(y)\frac{\partial^2 v_z}{\partial y^2} = 0 \ , \tag{3.4}$$

and

$$\frac{\partial^2 b_z}{\partial t^2} - C_A^2(y)\frac{\partial^2 b_z}{\partial y^2} - 2C_A(y)C_A'(y)\frac{\partial b_z}{\partial y} = 0 \tag{3.5}$$

where $C'_A(y)$ is the derivative of Alfvén velocity with respect to y. These two equations will be extensively used in this dissertation.

3.3 Role of Alfvén waves in the solar atmosphere

Alfvén waves are of considerable importance in astrophysical MHD, where they provide an effective mechanism for transferring the energy and momentum to different parts of the solar atmosphere. Since Alfvén waves transfer energy primarily along the magnetic field lines, the waves may be used to explain the observed association between the enhanced local heating of the solar atmosphere and the enhanced magnetic field strength. Extensive discussions of the role played by these MHD waves in the solar atmosphere can be found in early papers written by Kulsrud (1955), Osterbrock (1961), Parker (1979), Priest (1982), Hollweg (1985, 1990, 1992), Roberts & Ulmschneider (1997), and Ulmschneider & Musielak (2003).

Waves transport energy and momentum in the solar atmosphere, thus contributing to its heating and dynamics. Of particular interest are Alfvén waves propagating in the solar atmosphere with uniform magnetic fields, and waves in thin magnetic flux tubes, which support three basic types of waves: longitudinal, transverse, and torsional waves (e.g., Roberts (2000)). Longitudinal tube waves are acoustic waves confined to the tubes, however, both transverse and torsional tube waves are Alfvén-type waves. The interest in Alfvén waves and in torsional and transverse tube waves has significantly increased recently after they were reported to be observed in the solar atmosphere (see sec. 1.1).

CHAPTER 4

CUTOFF FREQUENCIES FOR ALFVÉN WAVES IN ISOTHERMAL SOLAR ATMOSPHERE

4.1 Governing equations and their numerical solutions

We consider an atmosphere with $\vec{g} = -g\hat{y}$, where $g = 274$ m s^{-2} for the solar atmosphere and $\hat{y}$ is a unit vector along the vertical direction. We assume that the atmosphere is isothermal with $T_0 = 6000$ K and permeated with an uniform magnetic field $\vec{B}_e = B_e\hat{y}$, with $B_e = 0.04$ T.

We solve numerically Eqs (3.2) and (3.3) by using CLAWPACK, a computer code designed to find numerical solutions to hyperbolic partial differential equations (Leveque (2002)). The computational domain for our numerical simulations is 0.0 $Mm < y < 2.5$ Mm, and it is covered by a uniform grid of approximately 10^4 numerical cells. We set open (with zero gradient) boundary conditions at the bottom and top of the simulation region. Alfvén waves are generated by imposing sinusoidal perturbations at the lower ($y = 0$) boundary: $v_z(y = 0, t) = v_0 sin(\omega_A t)$, $b_z(y = 0, t) = 0$, where $v_0 = 1.0 \times 10^{-4}$ Mm s^{-1} and ω_A is the frequency of the excited Alfvén waves. We also assume that $v_z(y, t = 0) = 0$ and $b_z(y, t = 0) = 0$. Using the above conditions, we numerically solve the initial value problem for the propagation of Alfvén wave of a given frequency, and determine the wave behavior within the computational domain. We now present the results of our numerical simulations.

4.2 Numerical results

The results of our numerical simulations are presented in Figs 4.1 and 4.2. We show plots of the velocity and magnetic field perturbations with respect to y in Figs 4.1 and 4.2, respectively. In all our results, the wave propagation time is approximately 114 s, which is a required time for Alfvén waves to propagate from $y = 0$, where they are generated, to the upper boundary of our computational domain located at $y = 2.5$ Mm. As shown in the panels of Figs 4.1 and 4.2, the period $P_A = 2\pi/\omega_A$ of Alfvén waves ranges from 10 s to 300 s, and it is clearly seen that within this range the behavior of the velocity and magnetic field perturbations changes from oscillatory to non-oscillatory. We identify the oscillatory behavior with propagating waves and the non-oscillatory behavior with non-propagating waves. Moreover, we determine heights in the solar atmosphere at which the wave behavior changes from oscillatory (propagating) to non-oscillatory (non-propagating). In the first-order approximation, these heights can be identified with the last zeros of $v_z(y,t)$ and $b_z(y,t)$, which are denoted respectively as y_{0v} and y_{0b} in the plots shown in Figs 4.1 and 4.2; our results clearly demonstrate that the location of such zeros is a sensitive function of the wave period.

Now, comparison between Figs 4.1 and 4.2 shows that the behavior of the velocity perturbations is different than that of the magnetic field perturbations, which means that both wave variables behave differently. Therefore, we must discuss them separately. Let us begin with the velocity perturbations presented in Fig. 4.1, which shows that Alfvén waves with $P_A = 10$ s are propagating through approximately half of the computational domain and that they are non-propagating in the other half. The region of propagation gets shorter with the increasing (decreasing) wave period (wave frequency) and for $P_A = 300$ s the wave becomes non-propagating in the entire computational domain. To approximately separate the propagating and non-

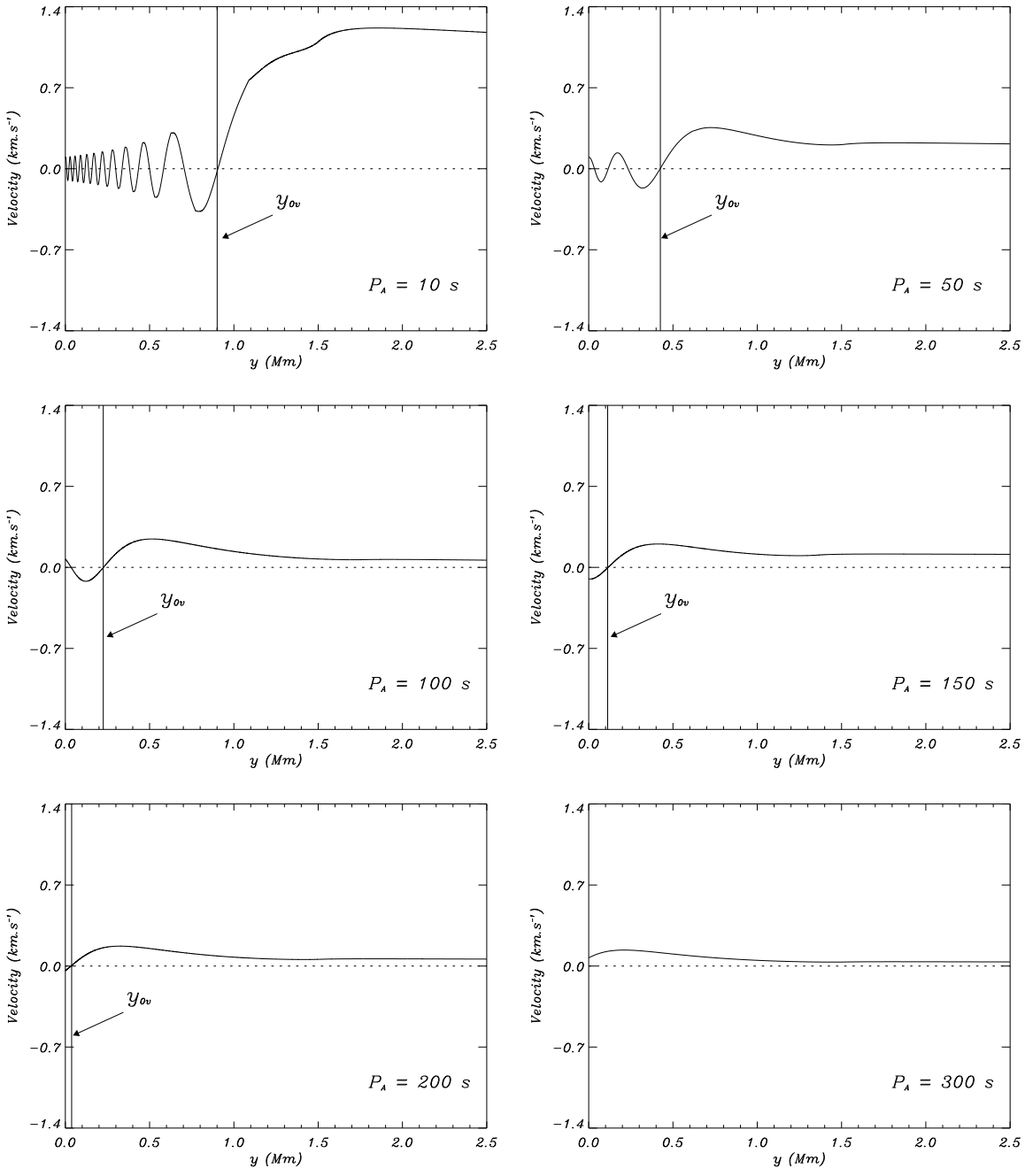

Figure 4.1: Plots of the velocity perturbation versus the atmospheric height with the locations of the last zeros y_{0v} depicted by vertical solid lines.

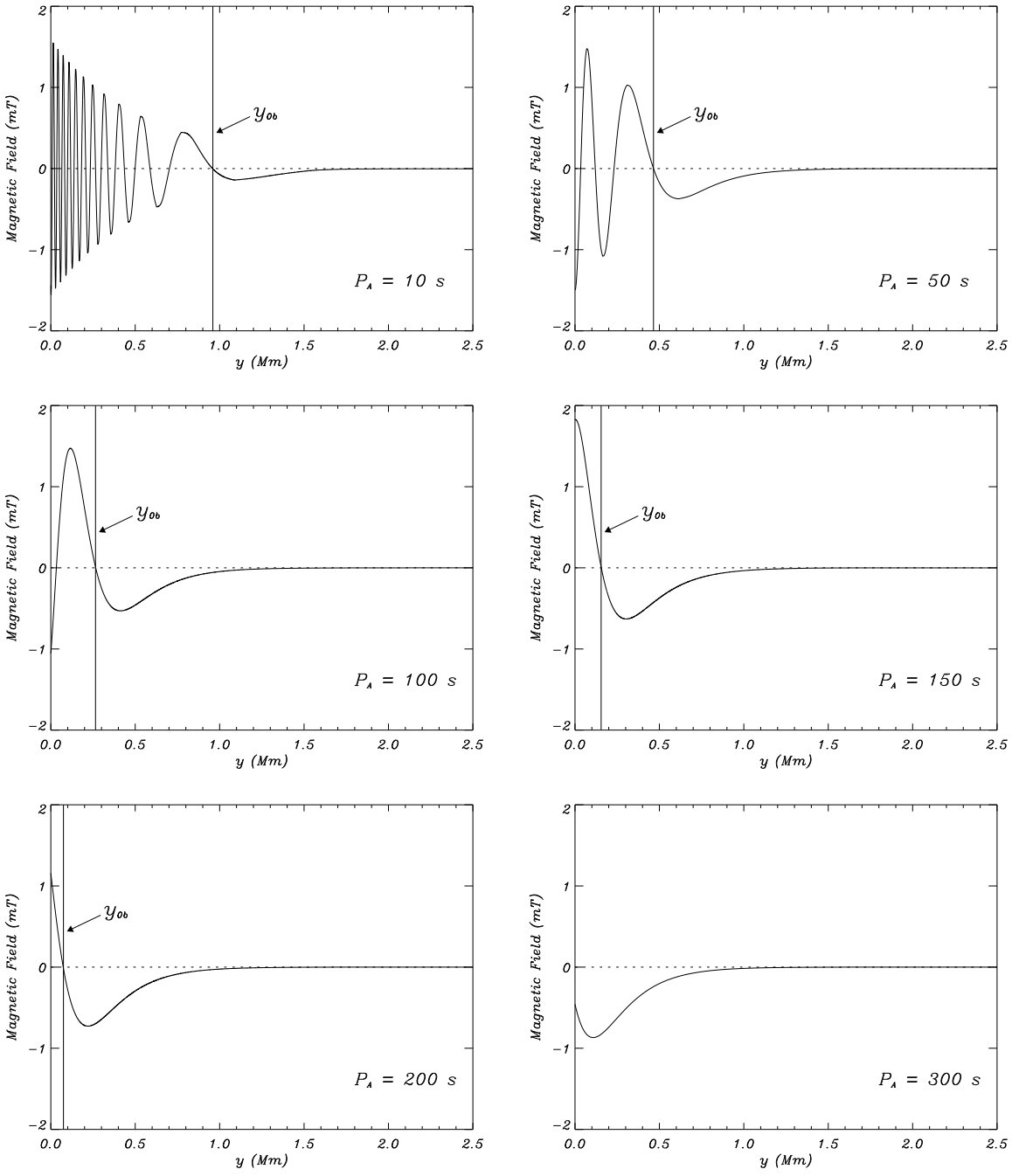

Figure 4.2: Plots of the magnetic field perturbation versus the atmospheric height with the locations of the last zeros y_{0b} depicted by the vertical solid lines...

propagating regions, we included solid lines in all panels of Fig. 4.1 at the heights corresponding to the last zeros in the plots; note that there is no such line in the last panel on the right because there is no other zero except at $y = 0$. We refer to the specific heights corresponding to those lines as transition and turning points, and define them more precisely in sec. 4.4.

In Fig. 4.2, we show plots of the magnetic field perturbations versus y. It is seen that the region of propagating waves decreases with the wave period. However, its size is bigger than that found for the velocity perturbations (see Fig. 4.1). Specifically, there is a narrow region of propagating waves even for Alfvén waves with $P_A = 300$ s. The differences between the behavior of the velocity and magnetic field perturbations are clearly seen by comparing the locations of the last zeros in Fig. 4.1 and 4.2. The fact that these locations are different has important physical consequences, namely, the behavior of Alfvén waves in the solar atmosphere depends on the wave variable chosen to describe it. In other words, one picture of wave behavior emerges by looking at the velocity perturbations, and a different picture is seen when one looks at the magnetic field perturbations. We discuss this phenomenon later in the chapter after the transition and turning points are defined in sec. 4.4 and computed in sec. 4.5 and 4.6.

4.3 Alfvén wave equations

We now demonstrate that the numerically established differences in the behavior of the wave variables has its origin in different forms of the wave equations describing the propagation of Alfvén waves. Let us eliminate one wave variable in terms of the other by combining Eqs (3.2) and (3.3), and obtain two wave equations

for Alfvén waves propagating in our isothermal model of the solar atmosphere. The wave equations are

$$\frac{\partial^2 v_z}{\partial t^2} - C_A^2(y)\frac{\partial^2 v_z}{\partial y^2} = 0 \ , \tag{4.1}$$

and

$$\frac{\partial^2 b_z}{\partial t^2} - C_A^2(y)\frac{\partial^2 b_z}{\partial y^2} - 2C_A(y)C_A'(y)\frac{\partial b_z}{\partial y} = 0 \ , \tag{4.2}$$

where $C_A(y) = B_e/\sqrt{\mu\rho_e(y)}$ is the Alfvén velocity and $C_A'(y)$ is the derivative with respect to y. It is seen that the derived Alfvén wave equations have different forms, which means that the wave variables behave differently. To write Eq. (4.2) in its standard form, we use the transformation $b_z(t,y) = b_{1z}(t,y)e^{-y/2\Lambda_p}$, where Λ_p is the pressure or density scale height given in Eq. (2.27), which is a constant for isothermal model we consider in this chapter and obtain

$$\frac{\partial^2 b_{1z}}{\partial t^2} - C_A^2(y)\frac{\partial^2 b_{1z}}{\partial y^2} + \Omega_{cr,b}^2(y)b_{1z} = 0 \ , \tag{4.3}$$

with

$$\Omega_{cr,b}^2(y) = \frac{C_A^2(y)}{4\Lambda_p^2} \ . \tag{4.4}$$

Since in our model the driver excites Alfvén waves with one given frequency ω_A, we make Fourier transforms in time by using $v_z(t,y) = e^{-i\omega_A t}\tilde{v}_z(y)$ and $b_{1z}(t,y) = e^{-i\omega_A t}\tilde{b}_{1z}(y)$. The resulting wave equations can be written as

$$\frac{d^2\tilde{v}_z}{dy^2} + \frac{\omega_A^2}{C_A^2(y)}\tilde{v}_z = 0 \ , \tag{4.5}$$

and

$$\frac{d^2\tilde{b}_{1z}}{dy^2} + \frac{\omega_A^2 - \Omega_{cr,b}^2(y)}{C_A^2(y)}\tilde{b}_{1z} = 0 \ . \tag{4.6}$$

The Fourier transformed Alfvén wave equations will now be used to introduce the concepts of transition and turning points.

4.4 Transition and turning points

The concept of transition and turning points are known in mathematics but their specific definitions vary from one author to another (e.g., Wasow 2002). For example, in calculus a turning point is a point at which the derivative of a function changes sign or where the function has either a relative minimum or maximum. Moreover, the transition and turning points are defined for second order linear differential equations and often used to find asymptotic solutions of these equations (e.g., Langer 1949; Anyanwu 1988; Wasow 2002) or to establish a uniform asymptotic turning point theory for these equations (e.g., Zauderer 1972).

One of the main goals of this study is to define the transition and turning points for the Alfvén wave equations (see Eqs (7.27) and (7.28)), and determine the locations of these points in the solar atmosphere. Since the locations of the transition and turning points are established analytically, we compare them to our numerical results presented in Figs 4.1 and 4.2. Using the comparison, we introduce the concept of cutoff frequency for Alfveń waves and give it a physical interpretation.

Let us begin with Eq. (7.28), which has one constant parameter ω_A^2 and the $y-$dependent parameter $\Omega_{cr,b}^2$. Since ω_A^2 is essentially a free parameter, we may set it to be larger than $\Omega_{cr,b}^2$ at $y = 0$. With ω_A^2 being constant and $\Omega_{cr,b}^2$ increasing in the solar atmosphere, there is a height y_{tr} at which

$$\omega_A^2 = \Omega_{cr,b}^2(y_{tr}) \ . \tag{4.7}$$

We use this condition as our definition of the *transition point* whose location in the solar atmosphere is given by the height y_{tr}.

To introduce a *turning point*, we must first find a second order ordinary differential equation in which such point is clearly defined. To the best of our knowledge, the Euler equation has the well-defined turning point (e.g., Murphy 2011). We write the Euler equation as $u'' + (C_E/4x^2)u = 0$, where C_E is the so-called Euler constant. The solutions to this equation are: oscillatory, when $C_E > 1$, and non-oscillatory, when $C_E < 1$, and they are separated by the turning point that corresponds to $C_E = 1$. To define the turning points for our Fourier transformed Alfvén wave equations (see Eqs ((7.27) and (7.28)), we cast these equations in their Euler's forms by taking

$$\frac{\omega_A^2}{C_A^2(y_{tv})} = \frac{1}{4y_{tv}^2} \ , \tag{4.8}$$

and

$$\frac{\omega_A^2 - \Omega_{cr,b}^2(y_{tb})}{C_A^2(y_{tb})} = \frac{1}{4y_{tb}^2} \ , \tag{4.9}$$

and use these conditions to determine the locations y_{tv} and y_{tb} of the turning points for the velocity and magnetic field perturbations in the solar atmosphere, respectively.

4.5 Approximate travel time for Alfvén waves

We define the approximate wave travel time, t_{ap}, as

$$t_{ap}(y) = \frac{y}{C_A(y)} \ , \tag{4.10}$$

and the scale height time, t_H, as

$$t_H(y) = \frac{\Lambda_p}{C_A(y)} \ . \tag{4.11}$$

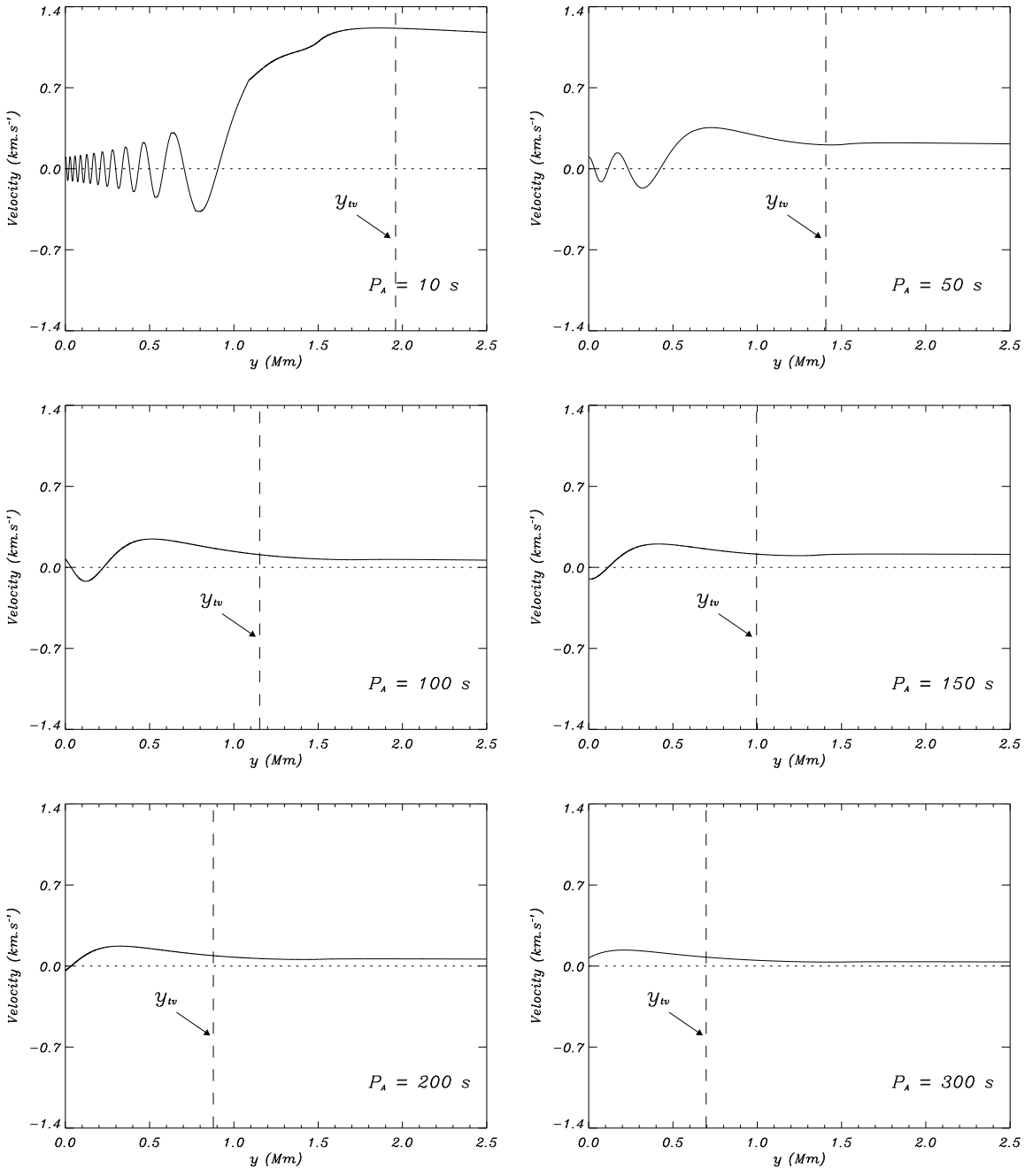

Figure 4.3: Plots of the velocity perturbation versus the atmospheric height with the locations of the turning points y_{tv} depicted by the vertical dashed lines.

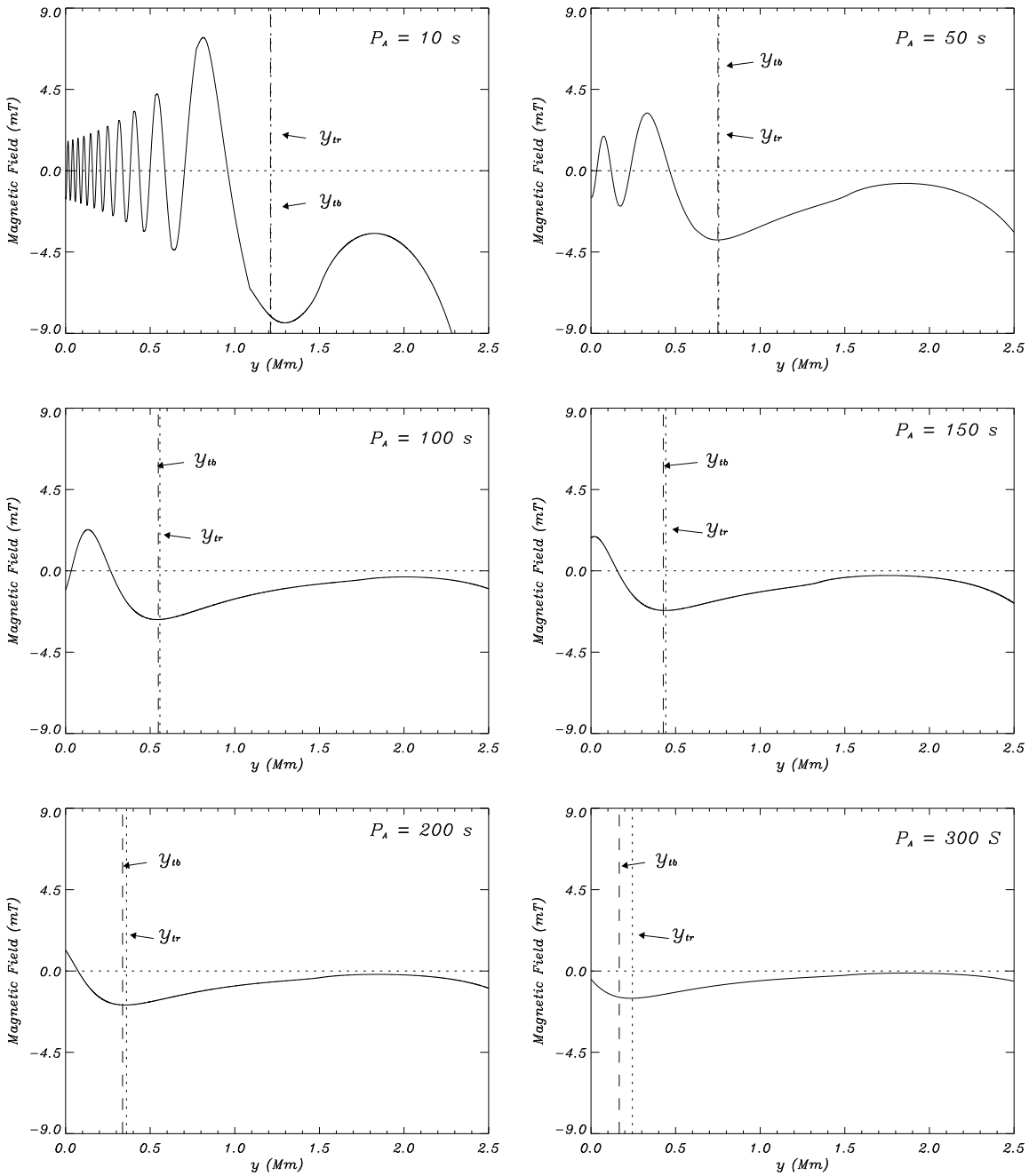

Figure 4.4: Plots of the transformed magnetic field perturbation: $[b_{1z}(t, y) = b_z(t, y)e^{y/2\Lambda_p}]$ versus the atmospheric height with the location of the turning, y_{tb}, and transition, y_{tr}, points depicted by the vertical dashed and dotted lines, respectively.

Using our definition of the transition point given by Eq. (4.7), we write the condition that determines the location y_{tr} of the transition point in the solar atmosphere for the magnetic field perturbations in the following form:

$$P_A = 4\pi t_H(y_{tr}) \ , \tag{4.12}$$

where P_A is period of Alfvén waves.

Now, our definitions of the turning points for the velocity and magnetic field perturbations are given by Eqs (4.8) and (4.9), respectively. We use these definitions to determine the locations y_{tv} and y_{tb} of the turning points in the solar atmosphere, and obtain

$$P_A = 4\pi t_{ap}(y_{tv}) \ , \tag{4.13}$$

and

$$P_A = 4\pi \frac{t_{ap}(y_{tb}) t_H(y_{tb})}{\sqrt{t_{ap}^2(y_{tb}) + t_H^2(y_{tb})}} \ . \tag{4.14}$$

Note that in the limit $t_H >> t_{ap}$, $P_A \approx 4\pi t_{ap}(y_{tb})$ and $y_{tb} \approx y_{tv}$, however, in the limit $t_H << t_{ap}$, $P_A \approx 4\pi t_H(y_{tb})$.

The values of y_{tr}, y_{tv} and y_{tb} obtained from Eqs (4.12), (4.13) and (4.14), respectively, are shown in Figs 4.3 and 4.4. The velocity perturbations presented in Fig. 4.3 are the same as those depicted in Fig. 4.1, however, the magnetic field perturbations plotted in Fig. 4.4 are different than those given in Fig. 4.2; to be specific, we plot b_{1z} in Fig. 4.4 instead of b_z, which is shown in Fig. 4.2 (see sec. ref4.4 for the relationship between the two variables). Our results demonstrate that there are well-defined turning points for both the velocity and magnetic field perturbations, and that there is also the well-defined transition point for the latter. It is interesting that the locations of the turning and transition points for the magnetic

field perturbations are very similar except for the wave period $P_A = 300$ s (see Fig. 4.4). However, as long as the locations of the turning points for the velocity and magnetic field perturbations are concerned, they are not similar but larger for the former. We further discuss these results in sec. 4.7 devoted to our definition of cutoff frequencies.

4.6 Actual travel time for Alfvén waves

After introducing the approximate wave travel time t_{ap} in the previous section and using it to determine the locations of the transition and turning points in the solar atmosphere, we now define the actual wave travel time t_{ac}. Let us begin with the following transformation

$$d\tau = \frac{dy}{C_A(y)} \ , \tag{4.15}$$

which gives

$$t_{ac}(y) \equiv \tau(y) = \int_0^y \frac{d\tilde{y}}{C_A(\tilde{y})} \ , \tag{4.16}$$

with $t_{ac}(y)$ and $\tau(y)$ representing the actual time that is required by Alfvén waves to propagate from $y = 0$ to any given atmospheric height y.

Since in the isothermal solar atmosphere, $C_A(y) = C_{A0} \exp(y/2\Lambda_p)$, where $C_{A0} = C_A(y = 0)$, we may explicitly calculate τ and obtain

$$\tau(y) = \frac{2\Lambda_p}{C_{A0}} \left(1 - \exp\left(-y/2\Lambda_p\right)\right) \ , \tag{4.17}$$

which can also be written as

$$y = -2\Lambda_p \ln\left(1 - \frac{C_{A0}}{2\Lambda_p}\tau\right) \ . \tag{4.18}$$

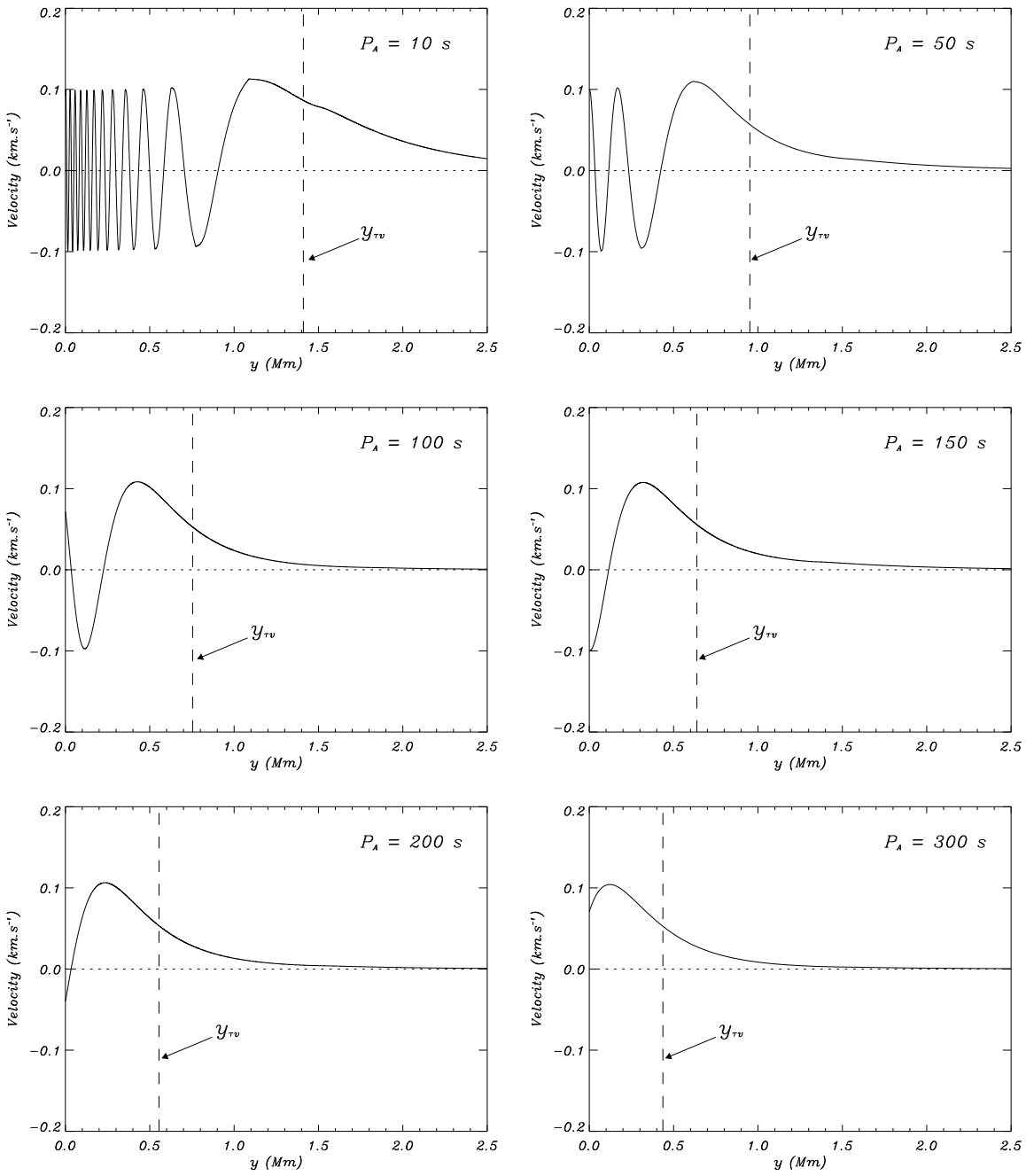

Figure 4.5: Plots of the transformed velocity perturbation: $[v(t, \tau(y)) = v_z(t, y)e^{-y/4\Lambda_p}]$ versus the atmospheric height with the locations of the turning points $y_{\tau v}$ depicted by the vertical dashed lines.

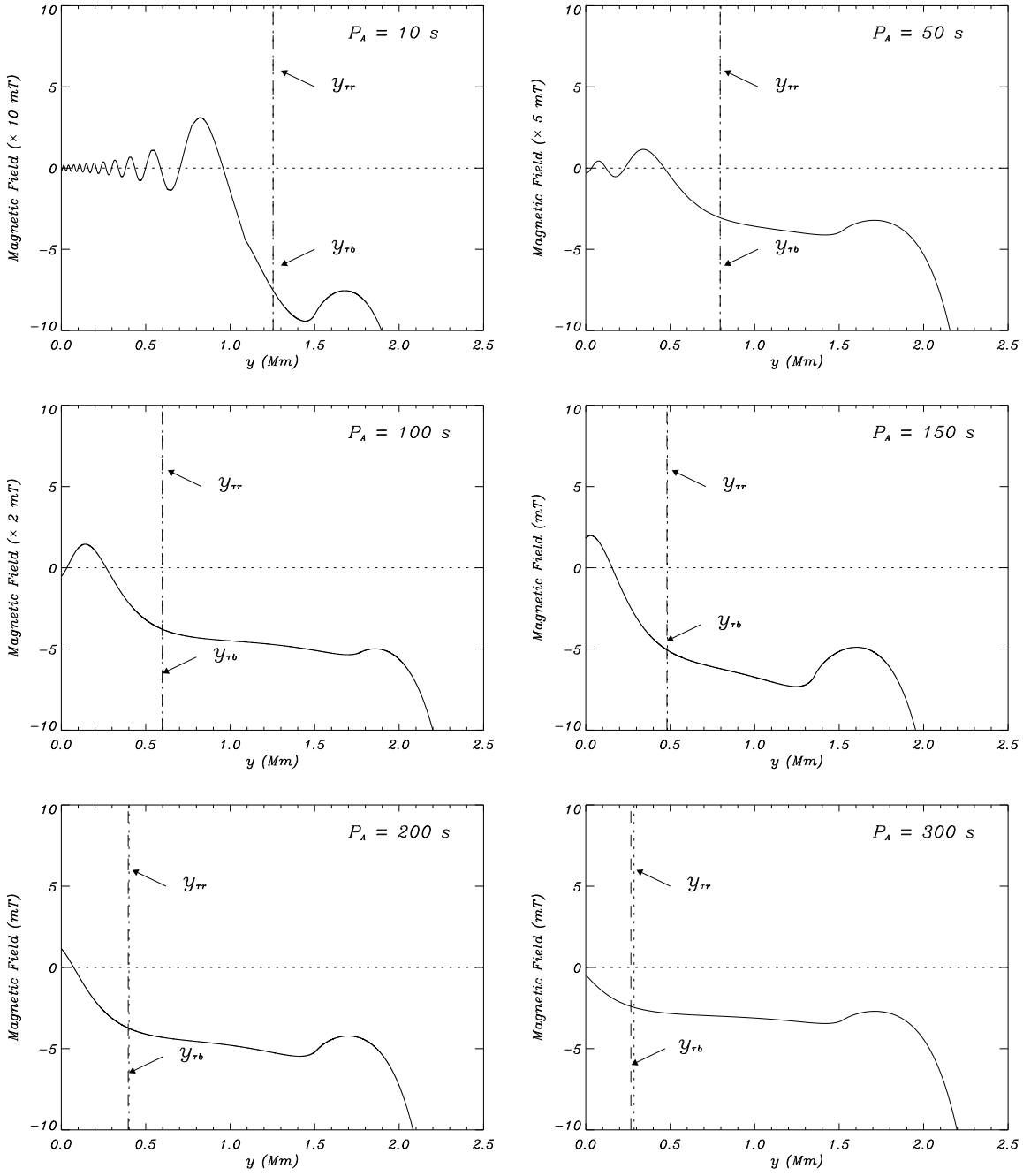

Figure 4.6: Plots of the transformed magnetic field $[b(t, \tau(y)) = b_z(t, y)e^{3y/4\Lambda_p}]$ versus the atmospheric height with the locations of the turning, $y_{\tau b}$, and transition, $y_{\tau r}$, points depicted by the vertical dashed and dotted lines, respectively.

Using Eq. (4.15), we write the Alfvén wave equations given by Eqs (4.1) and (4.3) in the following forms

$$\frac{\partial^2 v_z}{\partial t^2} - \frac{\partial^2 v_z}{\partial \tau^2} + \frac{C_A'(\tau)}{C_A(\tau)} \frac{\partial v_z}{d\tau} = 0 \ , \tag{4.19}$$

and

$$\frac{\partial^2 b_{1z}}{\partial t^2} - \frac{\partial^2 b_{1z}}{\partial \tau^2} - \frac{C_A'(\tau)}{C_A(\tau)} \frac{\partial b_{1z}}{d\tau} = 0 \ , \tag{4.20}$$

where $C_A' = dC_A/d\tau$.

With the transformations

$$v_z(t,\tau) = v(t,\tau) \exp\left[\frac{1}{2}\int^{\tau} \frac{C_A'(\tilde{\tau})}{C_A(\tilde{\tau})} d\tilde{\tau}\right] \ , \tag{4.21}$$

and

$$b_{1z}(t,\tau) = b(t,\tau) \exp\left[-\frac{1}{2}\int^{\tau} \frac{C_A'(\tilde{\tau})}{C_A(\tilde{\tau})} d\tilde{\tau}\right] \ , \tag{4.22}$$

we obtain

$$\frac{\partial^2 v}{\partial t^2} - \frac{\partial^2 v}{\partial \tau^2} + \Omega_{cr,v}^2(\tau) v = 0 \ , \tag{4.23}$$

and

$$\frac{\partial^2 b}{\partial t^2} - \frac{\partial^2 b}{\partial \tau^2} + \Omega_{cr,b}^2(\tau) b = 0 \ , \tag{4.24}$$

where

$$\Omega_{cr,v}^2(\tau) = -\frac{\Omega_0^2}{4(1-\Omega_0\tau)^2} \ , \tag{4.25}$$

and

$$\Omega_{cr,b}^2(\tau) = \frac{3\Omega_0^2}{4(1-\Omega_0\tau)^2} \ , \tag{4.26}$$

with $\Omega_0 = C_{A0}/2\Lambda_p$.

Let us now make Fourier transforms in time $v(t,\tau) = e^{-i\omega_A t}\tilde{v}(\tau)$ and $b(t,\tau) = e^{-i\omega_A t}\tilde{b}(\tau)$, and write Eqs (4.23) and (4.24) as

$$\frac{d^2\tilde{v}}{d\tau^2} + \left[\omega_A^2 - \Omega_{cr,v}^2(\tau)\right]\tilde{v} = 0 \ , \tag{4.27}$$

and

$$\frac{d^2\tilde{b}}{d\tau^2} + \left[\omega_A^2 - \Omega_{cr,b}^2(\tau)\right]\tilde{b} = 0 \ . \tag{4.28}$$

Using our definition of the transition point (see Eq. (4.7)), we find that Eq. (4.27) does not have any transition point and that the location τ_r of the transition point of Eq. (4.28) is given by

$$\tau_r = \frac{1}{\Omega_0} - \frac{\sqrt{3}}{4\pi}P_A \ , \tag{4.29}$$

which can be used to determine

$$y_{\tau r} = -2\Lambda_p \ln\left(1 - \Omega_0\tau_r\right) \ . \tag{4.30}$$

To determine the locations τ_v and τ_b of the turning points of Eqs (4.27) and (4.28), we use our definition of the turning point given by Eq. (4.9) and obtain

$$P_A = \pm 4\pi\tau_v \frac{1 - \Omega_0\tau_v}{\sqrt{1 - 2\Omega_0\tau_v}} \ , \tag{4.31}$$

and

$$P_A = \pm 4\pi\tau_b \frac{1 - \Omega_0\tau_b}{\sqrt{1 - 2\Omega_0\tau_b + 4\Omega_0^2\tau_b^2}} \ . \tag{4.32}$$

Once τ_v and τ_b are determined, we use Eq. (4.18) to calculate the corresponding values of $y_{\tau v}$ and $y_{\tau b}$.

Table 4.1. Roots of Eq. (33) for the velocity perturbations

P_A	τ_{v1}	τ_{v2}	$\tau_{v3,4}$	$y_{\tau,v3}$
10	0.7957546	-0.7957552	112.8222106 $\pm$ 0.7958083 i	1.4102849
50	3.9762177	-3.9765668	112.8223849 $\pm$ 3.9814098 i	0.9519656
100	7.9349416	-7.9405254	112.8250022 $\pm$ 7.9774549 i	0.7541281
150	11.8540670	-11.8823091	112.8363314 $\pm$ 12.0018977 i	0.6378578
200	15.7059772	-15.7950201	112.8667318 $\pm$ 16.0666406 i	0.5548257
300	23.0709956	-23.5154435	113.0444343 $\pm$ 24.3482266 i	0.4364756

Table 4.2. Roots of Eq. (34) for the magnetic field perturbations

P_A	τ_{b1}	τ_{b2}	τ_{b3}	τ_{b4}	$y_{\tau,b2}$
10	0.7958350	111.4438292	114.2005899	-0.7958333	1.2542929
50	3.9868748	105.9256129	119.7177501	-3.9858171	0.7956479
100	8.0274865	98.9939989	126.6329672	-8.0100319	0.5975738
150	12.1968522	91.9706542	133.5804449	-12.1035307	0.4806442
200	16.6120048	84.7560226	140.5675453	-16.2911520	0.3960534
300	27.2701476	68.7258856	154.6741054	-25.0257178	0.2674319

All roots of Eqs (4.31) and (4.32) are shown in Tables 4.1 and 4.2, respectively. Among the four roots given in Table 4.1, the positive real root gives $y_{\tau v}$ well below the location of the last zero (see Fig. 4.1) and it is therefore neglected. The negative real root leads to negative values of $y_{\tau v}$, which are not included in our numerical domain. Both complex roots give the same value of $y_{\tau v}$, which is calculated from Eq. (4.18) by taking the principal value of the logarithm of the complex root. The value of $y_{\tau v}$ for this root is located above the location of the last zero and it is shown in both Table 4.3 and Fig. 4.5.

Now, among the four roots given in Table 4.2, the smallest positive root is neglected because it leads to the values of $y_{\tau b}$ located well below the last zero (see Fig. 4.2). The negative root is also not considered because it leads to the values of $y_{\tau b}$ being outside of our computational domain. The positive real root τ_{b3} is also excluded because it gives negative arguments of the logarithmic function in Eq. (4.18). Finally,

Table 4.3. Locations of the turning and transition points in the isothermal solar atmosphere

P_A	y_{tv}	y_{tb}	y_{tr}	$y_{\tau v}$	$y_{\tau b}$	$y_{\tau r}$
10	1.9594513	1.2110348	1.2129875	1.4102951	1.2539260	1.2539340
50	1.4070229	0.7497981	0.7548368	0.9519751	0.7955822	0.7957833
100	1.1530383	0.5482381	0.5575221	0.7541376	0.5975458	0.5984686
150	0.9959149	0.4271117	0.4421003	0.6378673	0.4806288	0.4830469
200	0.8782216	0.3368218	0.3602073	0.5548352	0.3960444	0.4011538
300	0.6970168	0.1672348	0.2447856	0.4364853	0.2674301	0.2857321

the positive real root τ_{b2} is the only root that gives $y_{\tau b}$ within the computational domain and above the last zero, and only the location of the turning point described by this root is presented in Table 4.3 and depicted in Fig. 4.6.

Figures 5 and 6 present our numerical solutions for the velocity and magnetic field perturbations, respectively, and we marked the locations $y_{\tau v}$ and $y_{\tau b}$ of the turning points inside our computational domain. The velocity and magnetic field perturbations plotted in Fig. 4.5 and 4.6 are different than those given in Fig 4.3 and 4.4, as we transformed the wave variables $v_z(t, y)$ and $b_{1z}(t, y)$ into $v(t, y)$ and $b(t, y)$ by using Eqs (4.21) and (4.22), respectively. Since the magnetic field perturbation has also the transition point, we marked its locations in all the panels of Fig. 4.6. An interesting result is that the locations of the turning and transition points coincide so well for all studied wave periods except $P_A = 300$ s, for which a small discrepancy is seen.

4.7 Cutoff frequencies

Our numerical results clearly indicate that linear Alfveń waves propagating in the isothermal solar atmosphere change their behavior from propagating to non-propagating for some range of wave frequencies. To identify the height in the atmo-

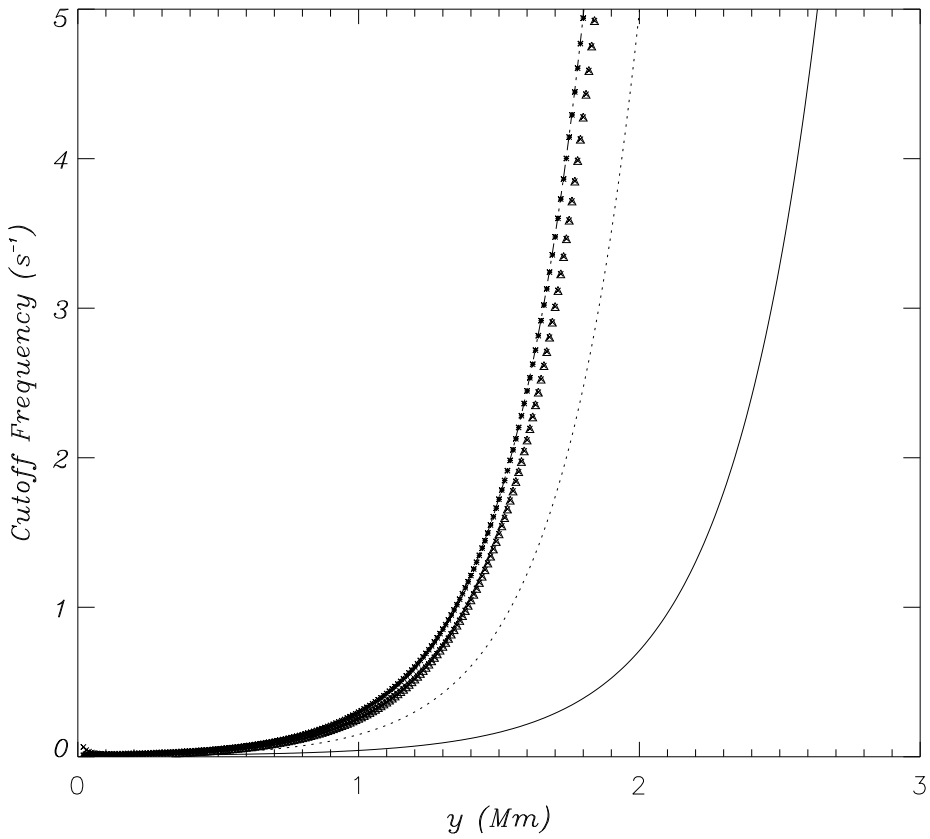

Figure 4.7: Plots of different cutoff frequencies versus the atmospheric height. The cutoff frequencies $\Omega_{cut,v}(y)$ and $\Omega_{cut,v}(\tau)$ are represented by solid and dotted lines, respectively. Moreover, the frequencies $\Omega_{cut,b}(y)$, $\Omega_{cut,tr}(y)$, $\Omega_{cut,b}(\tau)$ and $\Omega_{cut,tr}(\tau)$ are represented by star-symbols, solid-dotted, x-symbols and triangle-symbols, respectively.

sphere at which this change takes place, we determined the locations of the last zeros in the numerical solutions. Then, we defined the so-called transition and turning points, calculated their locations in the atmosphere, and compared these locations to the locations of the last zeros. Comparison of the results presented in Figs 4.1 and 4.3, and 2 and 4, shows that the turning points for the velocity perturbations, and the transition and turning points for the magnetic field perturbations are always located at larger atmospheric heights than the last zeros.

Our numerical results also demonstrate that the behavior of the velocity and magnetic field perturbations is different, namely, the former has only the turning point, and the latter has both the turning and transition points. The location of the turning point for the velocity perturbations is always above the location of the turning point for the magnetic field perturbations. On the other hand, the location of the transition point for the magnetic field perturbations is very close to the location of the turning point for all considered wave periods except $P_A = 300$ s. We used two different analytical methods to establish the locations of the transition and turning points. In the first method, we used the so-called approximate wave travel time, and the second method is based on the actual wave travel time. The methods lead to some small differences in the locations of the transition and turning points, and according to Table 4.3 the following inequalities are always satisfied: $y_{\tau r} > y_{tr}$, $y_{tv} > y_{\tau v}$ and $y_{\tau b} > y_{tb}$.

An important result of our numerical simulations is that only Alfvén waves of certain periods explicitly show the transition and turning points in our computational domain; for the atmosphere considered in this chapter, the wave periods range from 10 s to 300 s with the periods shorter than 10 s corresponding to the propagating waves in the entire computational domain. The latter demonstrates that the transition and turning points may not be explicitly seen for some other ranges of wave periods and for different sizes of computational domains. Nevertheless, in the atmospheric model considered here Alfvén velocity can become infinite and the waves can reach infinity. This means that Alfvén waves of all periods will show the transition and turning points once the full atmospheric model that extends from $y = 0$ to $y = \infty$ is taken into account.

The main result of this chapter is our strong theoretical evidence for the existence of the transition and turning points for Alfvén waves propagating in the isother-

mal solar atmosphere (Perera et al. (2014)); note that the result was obtained by using independently our numerical and analytical methods. In our approach, the turning points are obtained by comparing our wave equations to the Euler equation because the latter has a well-defined turning point that separates the oscillatory and non-oscillatory (exponential) solutions. Moreover, we introduced the transition points by using the standard mathematical definition in the theory of differential equations (e.g., Wasow 2002). Let us now relate this result to the concept of cutoff frequency, which separates propagating and non-propagating waves as already discussed in section 1.

The role played by turning points in the propagation of different waves was already recognized by Musielak et al. (2006), Routh et al. (2007, 2010) and Hammer et al. (2010), who used the turning points to define cutoff frequencies. Specific applications to the propagation of Alfvén waves in the solar atmosphere and definition of the cutoff frequency for these waves were done by Murawski & Musielak (2010). According to these authors, a cutoff frequency is identified with the largest turning point among all wave variables. However, in this dissertation we take a different approach, namely, we identify a cutoff frequency with every transition and turning point considered in here. This shows that there is no unique cutoff frequency for the propagation of Alfvén wave but instead different cutoff frequencies are associated with different transition and turning points (Perera et al. (2014)). Since these points are not the same for the velocity and magnetic field perturbations, different wave variables have different cutoff frequencies. Based on our results, we write down the explicit forms of cutoff frequencies obtained for the turning and transition points considered in this chapter.

We begin with the cutoffs expressed in terms of t_{ap} and obtained from the turning points for the velocity perturbation

$$\Omega_{cut,v}(y) = \frac{1}{2t_{ap}(y)} \ , \tag{4.33}$$

and for the magnetic field perturbation

$$\Omega_{cut,b}(y) = \frac{1}{2}\sqrt{\frac{1}{t_{ap}^2(y)} + \frac{1}{t_H^2(y)}} \ . \tag{4.34}$$

Now, we present the cutoffs expressed in terms of τ and obtained from the turning points for the velocity perturbation

$$\Omega_{cut,v}(\tau) = \frac{1}{2}\sqrt{\frac{1}{\tau^2} - \Omega_0^2(1-\Omega_0\tau)^{-2}} \ , \tag{4.35}$$

and for the magnetic field perturbation

$$\Omega_{cut,b}(\tau) = \frac{1}{2}\sqrt{\frac{1}{\tau^2} + 3\Omega_0^2(1-\Omega_0\tau)^{-2}} \ . \tag{4.36}$$

Finally, we write the cutoffs obtained from the transition points for the magnetic field perturbations; note that there are no transition points for the velocity perturbations. The cutoff expressed in terms of t_{ap} is given by

$$\Omega_{cut,tr}(y) = \frac{C_A(y)}{2\Lambda_p} \ , \tag{4.37}$$

and the cutoff expressed in terms of τ is

$$\Omega_{cut,tr}(\tau) = \frac{\sqrt{3}\Omega_0}{2(1-\Omega_0\tau)} \ . \tag{4.38}$$

All above cutoffs vary with the atmospheric height y (τ is also related to y), which means that they can be used to determine heights in the atmosphere at which the wave frequency ω becomes equal to one of these cutoffs. In general, the condition can be written as $\omega = \Omega_{cut}$, where the latter is any of the cutoffs. Moreover, we also have $\omega > \Omega_{cut}$ for propagating waves (or oscillatory solutions), and $\omega < \Omega_{cut}$ for non-propagating waves (or exponential solutions).

According to the above results, there are six cutoff frequencies introduced in this study. The velocity perturbation has two cutoffs obtained from the turning points, and the magnetic field perturbation has four cutoffs, two correspond to the turning points and the other two to the transition points. All cutoffs vary with the atmospheric height y (τ is also related to y) and they are plotted in Fig. 4.7, which shows that $\Omega_{cut,b}(y)$, and $\Omega_{cut,tr}(y)$ are practically the same, and $\Omega_{cut,b}(\tau)$ and $\Omega_{cut,tr}(\tau)$ are also similar. However, the cutoffs for the velocity perturbation $\Omega_{cut,v}(y)$ and $\Omega_{cut,v}(\tau)$ are different between themselves and also significantly different from the cutoffs for the magnetic field perturbation; note that there are no cutoffs corresponding to the transition points for the velocity perturbation.

Based on the above results, we conclude that there is no one unique cutoff frequency for Alfvén waves (Perera et al. (2014)) and that a number of cutoffs depends on the method used to define them as well as on the choice of the wave variable used to describe the waves. We also demonstrated that some of these cutoffs may have the same or similar values and that others may be significantly different. An important result is that our description of the propagation of Alfvén waves depends on whether we use the velocity or magnetic field perturbations, and that the main difference between these two descriptions is the location of the turning and transition points, and the values of the corresponding cutoff frequencies. It is likely that by using different ordinary differential equations with different turning points than the Euler

equation could give different locations of these points; and further exploration of this idea has been discussed in a later chapter.

Having defined the cutoff frequencies for the velocity and magnetic field perturbations of linear Alfvén waves, we may now compare our results to those previously discussed in sec. 1.1. The results that are the most relevant to ours were obtained by Petukhov & Petukhov (2002), who argued that uniform magnetic fields do not introduce any space or time characteristic scales and therefore no cutoff frequency should be present for the Alfvén wave propagation. Clearly, the conclusion reached by these authors is not consistent with our results presented in this study. The main reason for this difference is the fact that Petukhov and Petukhov studied the wave patterns formed after long wave travel times, which correspond to the formation of standing waves, instead of the finite time wave propagation investigated in this dissertation. We shall discuss the role of cutoff frequencies for Alfvén waves forming standing wave patterns (e.g., Ferraro & Plumpton (1958)) in another chapter.

4.8 Relevance to observations

Our results can be used to determine whether Alfvén waves with periods ranging from 100 s to 500 s observed by McIntosh et al. (2011) and Alfvén waves with period of 45 s observed by Okamoto & De Pontieu (2011) are propagating or evanescent. Comparison of our theoretically established cutoff frequencies to the observational data shows that Alfvén waves with periods ranging from 45 s to 200 s are partially propagating within our computational domain, whose physical parameters are described by the isothermal solar atmosphere, and partially evanescent in the upper part of the domain; as shown in Figs 4.1 through 4.7, the result is a sensitive function of wave period.

According to our results, Alfvén waves with periods higher than 200 s are evanescent in the entire computational domain. We want to point out that this range of wave periods corresponding to the propagating and non-propagating waves may actually change once a realistic temperature distribution in the solar atmosphere is included (see chapter 5).

4.9 Summary

We investigated numerically the propagation of linear Alfvén waves in the isothermal solar atmosphere. Our results showed that the two wave variables, the velocity and magnetic field perturbations, behave differently and that there is a range of wave frequencies for which our numerical solutions change from oscillatory, representing propagating waves, to non-oscillatory, representing non-propagating waves. To identify a height in the atmosphere at which this change occurs, we determined the locations of the last zeros in our numerical solutions, and then used analytical methods to establish the locations in the atmosphere the so-called transition and turning points. Comparison of the locations of the last zeros and the transition and turning points shows that the latter are located at atmospheric heights at which the change from propagating to non-propagating (exponential) wave solutions occurs. We used the obtained transition and turning points to define cutoff frequencies, and we showed that there were two different cutoffs for the velocity perturbations and four different cutoffs for the magnetic field perturbations.

Therefore, the main result of the study is that there is no one unique cutoff frequency for Alfvén waves but instead we have a number of cutoffs whose specific forms depend on the method used to define them as well as on the choice of the wave variable used to describe the waves. In other words, the description of Alfvén waves depends on which wave variable is used and the main difference between the

description using the velocity perturbations or the magnetic field perturbations is the location of the turning points the specific values of the cutoff frequencies related to these points. We used the cutoffs to establish a range of frequencies corresponding to the propagating Alfvén waves and compared it to some recent solar observations of these waves. Our results presented in this chapter give strong evidence for the existence of cutoff frequencies for Alfvén waves propagating in the isothermal solar atmosphere.

CHAPTER 5

CUTOFF FREQUENCIES IN NON-ISOTHERMAL ATMOSPHERIC MODELS

5.1 Background

So far in this dissertation we have focused only on isothermal solar atmosphere, which only roughly approximates the temperature plateau in the solar chromosphere. Henceforth, we extend our study to more realistic cases, namely, to two different non-isothermal models: (i) the power law temperature model, and (ii) the model used by Murawski & Musielak (2010), which will be called here the MM model. The first model is still not realistic as it only roughly approximates only the solar transition region, while the MM model accounts for the whole solar atmosphere, from the chromosphere to the corona, and hence it is close to the real solar atmosphere. In the following two sections, we will briefly explain the general concept of transition and turning points starting with the Alfvén wave equations in the non isothermal medium.

5.2 Governing equations

We introduce the small-amplitude velocity $\vec{v}(y,t) = v_z(y,t)\hat{z}$ and magnetic field $\vec{b}(y,t) = b_z(y,t)\hat{z}$ perturbations to describe propagation of Alfvén waves in the solar atmosphere, and we refer Eqs (3.2) and (3.3) for the velocity and magnetic field perturbations respectively:

$$\frac{\partial v_z}{\partial t} - \frac{B_e}{\mu\rho_e(y)}\frac{\partial b_z}{\partial y} = 0 \ , \tag{5.1}$$

and

$$\frac{\partial b_z}{\partial t} - B_e \frac{\partial v_z}{\partial y} = 0 \ . \tag{5.2}$$

The resulting wave equations for the velocity and magnetic field perturbations become (see Eqs (4.1) and (4.2))

$$\frac{\partial^2 v_{\rm z}}{\partial t^2} = C_{\rm A}^2(y) \frac{\partial^2 v_{\rm z}}{\partial y^2} \tag{5.3}$$

$$\frac{\partial^2 b_{\rm z}}{\partial t^2} = \frac{\partial}{\partial y} \left(C_{\rm A}^2(y) \frac{\partial b_{\rm z}}{\partial y} \right) \ . \tag{5.4}$$

where $C_{\rm A}$ is the Alfvén speed.

Now we follow sec. 4.3 and eliminate the first derivative from Eq. (5.4) and write it in its standard form by using the transformation $b_z(t,y) = (C_{\rm A0}/C_{\rm A}) b_{1z}(t,y)$, where $C_{\rm A0}$ is the Alfvén speed at $y = y_0$, and obtain

$$\frac{\partial^2 b_{1z}}{\partial t^2} - C_{\rm A}^2(y) \frac{\partial^2 b_{1z}}{\partial y^2} + \Omega_{\rm cr,b}^2(y) b_{1z} = 0 \ , \tag{5.5}$$

with

$$\Omega_{cr,b}^2(y) = C_{\rm A} \frac{d^2 C_{\rm A}}{dy^2} \ . \tag{5.6}$$

Since in our model the driver excites Alfvén waves with one given frequency ω_A, we make Fourier transforms in time by using $v_{\rm z}(t,y) = e^{-i\omega_A t} \tilde{v}_{\rm z}(y)$ and $b_{1z}(t,y) = e^{-i\omega_A t} \tilde{b}_{1z}(y)$. The resulting wave equations can be written as

$$\frac{d^2 \tilde{v}_z}{dy^2} + \frac{\omega_A^2}{C_A^2(y)} \tilde{v}_z = 0 \ , \tag{5.7}$$

and

$$\frac{d^2 \tilde{b}_{1z}}{dy^2} + \frac{\omega_A^2 - \Omega_{cr,b}^2(y)}{C_{\rm A}^2(y)} \tilde{b}_{1z} = 0 \ . \tag{5.8}$$

The Fourier transformed Alfvén wave equations will now be used to introduce the concepts of transition and turning points.

5.3 Transition and turning points

One of the main goals of this chapter is to define transition and turning points for the Alfvén wave equations (see Eqs (5.7) and (5.8)), and determine the locations of these points in the solar atmosphere. Since the concept is well established analytically (see sec. 4.4) we compare our numerical results to analytically obtained transition and turning points. Then we explain the physical significance of the cutoff frequency for Alfvén waves.

5.3.1 Transition and turning points in terms of approximate wave travel time

It is clearly seen that there is no critical frequency term in Eq. (5.3) and hence no transition point. Therefore only Eq. (5.5), which is the Alfvén wave equation for magnetic field perturbation will show a transition point. Since $\Omega_{\rm cr,b}$ is a function of y, and the wave frequency $\omega_{\rm A}$ is a free parameter, there is a height in the atmosphere, $y_{\rm tr}$, at which this critical frequency becomes equal to the wave frequency. So we find transition point using the following condition

$$\omega_{\rm A}^2 = \Omega_{\rm cr,b}^2(y_{\rm tr}). \tag{5.9}$$

Now we begin with a second order differential equation with well defined turning point, namely the Euler equation (e.g., Murphy 2011) which we can write as

$$u'' + \frac{C_{\rm E}}{4x^2}u = 0\ . \tag{5.10}$$

where $C_{\rm E}$ is the Euler constant.

The solutions of the above equation is said to be oscillatory (non-oscillatory) when $C_{\rm E} > 1$ ($C_{\rm E} < 1$) and the point at which it separates these two regions is called the turning point that corresponds to $C_{\rm E} = 1$. Now we compare our Fourier transformed Alfvén wave equations, Eqs (5.7) and (5.8) with the Euler equation and get the following set of equations

$$\omega_A^2 = \frac{C_{\rm A}^2(y_{\rm tv})}{4y_{\rm tv}^2} \ , \tag{5.11}$$

and

$$\omega_A^2 = \Omega_{cr,b}^2(y_{\rm tb}) + \frac{C_{\rm A}^2(y_{\rm tb})}{4y_{\rm tb}^2} \ . \tag{5.12}$$

Then we determine the locations $y_{\rm tv}$ and $y_{\rm tb}$ of the turning points for the velocity and magnetic field perturbations respectively, using the above conditions.

5.3.2 Transition and turning points in terms of actual wave travel time

In order to obtain transition and turning points in terms of actual wave travel time, $t_{\rm ac}$, we follow the method described in sec. 4.6 and start with the transformation

$$d\tau = \frac{dy}{C_{\rm A}(y)} \ , \tag{5.13}$$

and cast the Alfvén wave equations given by Eqs (5.3) and (5.4) for the velocity and magnetic field perturbations to the following form:

$$\frac{\partial^2 v_{\rm z}}{\partial t^2} - \frac{\partial^2 v_{\rm z}}{\partial \tau^2} + \omega_{\rm A}\frac{\partial v_{\rm z}}{\partial \tau} = 0 \ , \tag{5.14}$$

$$\frac{\partial^2 b_{\rm z}}{\partial t^2} - \frac{\partial^2 b_{\rm z}}{\partial \tau^2} - \omega_{\rm A}\frac{\partial b_{\rm z}}{\partial \tau} = 0 \ , \tag{5.15}$$

with

$$\omega_{\rm A}(\tau) = \frac{1}{C_{\rm A}} \frac{dC_{\rm A}}{d\tau} \ . \tag{5.16}$$

Now using the following transformations

$$v_{\rm z}(t,\tau) \ = \ v(t,\tau) \ \exp\left[\frac{1}{2}\int^{\tau} \omega_{\rm A}(\tilde{\tau}) d\tilde{\tau}\right] \ , \tag{5.17}$$

and

$$b_{\rm z}(t,\tau) \ = \ b(t,\tau) \ \exp\left[-\frac{1}{2}\int^{\tau} \omega_{\rm A}(\tilde{\tau}) d\tilde{\tau}\right] \ , \tag{5.18}$$

we eliminate the first derivative and write Eqs (5.14) and (5.15) in their standard forms:

$$\frac{\partial^2 v}{\partial t^2} - \frac{\partial^2 v}{\partial \tau^2} + \Omega^2_{\rm cr,v}(\tau) \ v \ = \ 0 \ , \tag{5.19}$$

and

$$\frac{\partial^2 b}{\partial t^2} - \frac{\partial^2 b}{\partial \tau^2} + \Omega^2_{\rm cr,b}(\tau) \ b \ = \ 0 \ , \tag{5.20}$$

where the critical frequencies are defined as

$$\Omega^2_{\rm cr,v}(\tau) \ = \ \frac{1}{2}\left[\frac{1}{2}\omega^2_{\rm A} - \frac{d\omega_{\rm A}}{d\tau}\right] \ , \tag{5.21}$$

and

$$\Omega^2_{\rm cr,b}(\tau) \ = \ \frac{1}{2}\left[\frac{1}{2}\omega^2_{\rm A} + \frac{d\omega_{\rm A}}{d\tau}\right] \ . \tag{5.22}$$

Then we make Fourier transforms in time $v(\tau,t) = \tilde{v}(\tau)e^{-i\omega t}$ and $b(\tau,t) = \tilde{b}(\tau)e^{-i\omega t}$ and obtain the second order ordinary differential equations as follows

$$\frac{d^2\tilde{v}}{d\tau^2} + [\omega^2 - \Omega^2_{\rm cr,v}(\tau)]\tilde{v} \ = \ 0 \ , \tag{5.23}$$

and

$$\frac{d^2\tilde{b}}{d\tau^2} + [\omega^2 - \Omega^2_{\rm cr,b}(\tau)]\tilde{b} \;=\; 0 \;. \tag{5.24}$$

Using these two equations we can define turning point frequencies in terms of τ, where τ being the actual wave travel time, $t_{\rm ac}$ and can be determined by

$$\tau(y) = \int^{y} \frac{d\tilde{y}}{C_{\rm A}(\tilde{y})} + \tau_{\rm c} = t_{\rm ac}(y) \;, \tag{5.25}$$

where τ_c is the integration constant and can be evaluated once the boundary conditions are introduced. Then we obtain turning point frequencies $\Omega_{\rm tp,v}$ and $\Omega_{\rm tp,b}$ for the velocity and magnetic field perturbations, respectively,

$$\Omega^2_{\rm tp,v}(\tau) \;=\; \Omega^2_{\rm cr,v}(\tau) + \frac{1}{4\tau^2} \;, \tag{5.26}$$

$$\Omega^2_{\rm tp,b}(\tau) \;=\; \Omega^2_{\rm cr,b}(\tau) + \frac{1}{4\tau^2} \;. \tag{5.27}$$

These turning point frequencies are now being expressed in terms of y, and we have

$$\Omega^2_{\rm tp,v}(y) \;=\; \Omega^2_{\rm cr,v}(y) + \frac{1}{4t^2_{\rm ac}(y)} \;, \tag{5.28}$$

and

$$\Omega^2_{\rm tp,b}(y) \;=\; \Omega^2_{\rm cr,b}(y) + \frac{1}{4t^2_{\rm ac}(y)} \;, \tag{5.29}$$

with the actual wave travel time $t_{\rm ac}$ defined by Eq. (5.25). In addition, the explicit forms of the critical frequencies are

$$\Omega^2_{\rm cr,v}(y) \;=\; \frac{1}{2}\left[\frac{1}{2}\left(\frac{dC_{\rm A}}{dy}\right)^2 - C_{\rm A}\left(\frac{d^2C_{\rm A}}{dy^2}\right)\right] \;, \tag{5.30}$$

$$\Omega^2_{\rm cr,b}(y) \;=\; \frac{1}{2}\left[\frac{1}{2}\left(\frac{dC_{\rm A}}{dy}\right)^2 + C_{\rm A}\left(\frac{d^2C_{\rm A}}{dy^2}\right)\right] \;. \tag{5.31}$$

Once the turning point frequencies are determined in terms of y, we find locations of the turning points in τ-space namely, $y_{\tau v}$ and $y_{\tau b}$ for the velocity and magnetic field perturbations, respectively, by equating turning point frequency to the wave frequency ($\omega_{\rm A}$). The results are:

$$\omega^2_{\rm A} \;=\; \Omega^2_{\rm cr,v}(y_{\tau \rm v}) + \frac{1}{4t^2_{\rm ac}(y_{\tau \rm v})} \;, \tag{5.32}$$

and

$$\omega^2_{\rm A} \;=\; \Omega^2_{\rm cr,b}(y_{\tau \rm b}) + \frac{1}{4t^2_{\rm ac}(y_{\tau \rm b})} \;, \tag{5.33}$$

Also note that in τ-space the critical frequency terms are present in both the velocity and magnetic field perturbations; however, only the magnetic field Fourier transformed wave equation has the critical frequency. Hence there are two transition points as well as two turning points given by

$$\omega_{\rm A} = \Omega_{\rm cr,v}(y_{\rm vr}) \;, \tag{5.34}$$

$$\omega_{\rm A} = \Omega^2_{\rm cr,b}(y_{\rm vb}) \;. \tag{5.35}$$

5.4 Application to the power law model

Let us consider the temperature distribution

$$T_{\rm e}(y) = T_0\left(\frac{y}{y_0}\right)^m \;, \tag{5.36}$$

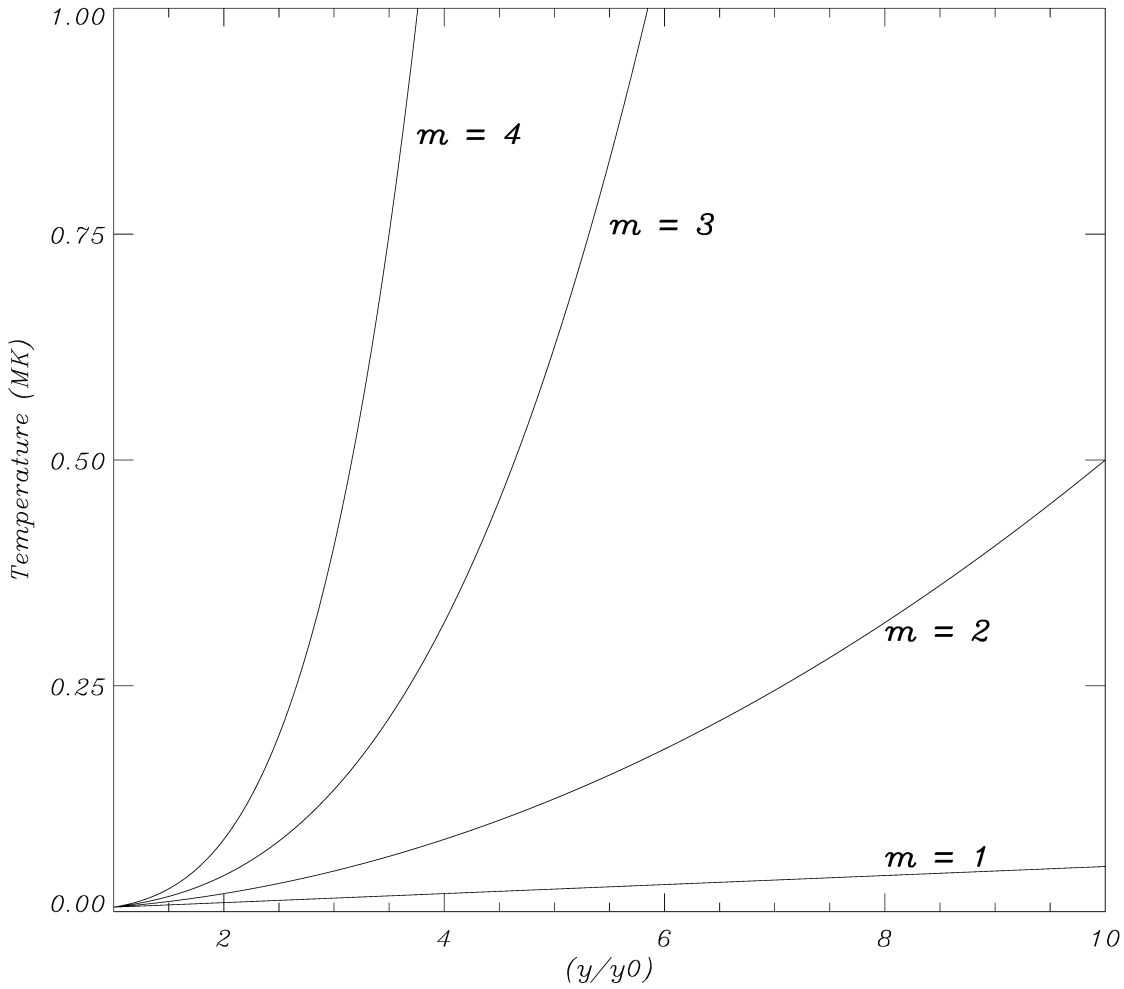

Figure 5.1: Temperature (MK) as a function of distance ratio for power law model.

where y_0 is a fixed height in the atmosphere, T_0 is the temperature at y_0 and m can be any real number. We use T_0 to be 6000 K and $y_0 = 1$ Mm. The resulting temperature profile is given in Fig. (5.1) In this section we consider one special case when $m = 1$ and one general case when $m > 1$. In order to obtain turning point frequencies for each wave variable, we first recall that the equations derived for the scale height, pressure and density in Chapter 2 are given by Eqs (2.27), (2.28) and (2.29), respectively.

5.4.1 Linear temperature model: m = 1 case

In this special case, we first obtain the pressure scale height using Eq. (2.27), which is given by

$$\Lambda_{\rm p}(y) = \Lambda_{\rm p0}\left(\frac{y}{y_0}\right) , \tag{5.37}$$

where $\Lambda_{\rm p0} = (k_B T_0)/(mg)$. Then, we obtain an expression for the gas pressure

$$p_e(y) = p_0\left(\frac{y_0}{y}\right)^{\frac{y_0}{\Lambda_{\rm p0}}} , \tag{5.38}$$

and the gas density

$$\rho_e(y) = \rho_{00}\left(\frac{y_0}{y}\right)^{\frac{y_0}{\Lambda_{\rm p0}}+1} , \tag{5.39}$$

with $\rho_{00} = p_0/g\Lambda_{p0}$.

Using all the above equations, we evaluate the Alfvén speed and obtain

$$C_A(y) = C_{A0}\left(\frac{y}{y_0}\right)^a , \tag{5.40}$$

where $2a = y_0/\Lambda_{p0}+1$ and C_{A0} is the Alfvén speed at y_0. For simplicity, we introduce $b = C_{A0}/y_0^a$ and obtain the Fourier transformed Alfvén wave equations for the velocity and magnetic field perturbations:

$$\frac{d^2\tilde{v}_z}{dy^2} + \frac{\omega_A^2}{b^2 y^{2a}}\tilde{v}_z = 0 , \tag{5.41}$$

and

$$\frac{d^2\tilde{b}_{1z}}{dy^2} + \frac{\omega_A^2 - \Omega_{cr,b}^2(y)}{b^2 y^{2a}}\tilde{b}_{1z} = 0 . \tag{5.42}$$

where $\Omega^2_{crit}(y) = a(a-1)b^2y^{2a-2}$. Hence we obtain the turning point frequencies

$$\Omega^2_{tp,v}(y) = \frac{b^2}{4}y^{2a-2} \ , \tag{5.43}$$

and

$$\Omega^2_{tp,b}(y) = \frac{b^2}{4}(2a-1)^2y^{2a-2} \ . \tag{5.44}$$

for the velocity and magnetic field perturbations, respectively.

Using Eqs (5.43) and (5.44), we calculate the turning points y_{tv} and y_{tb} and depict them by vertical lines in Figs 5.2 and 5.3. Also we find the transition point by using Eq. (5.9) and denote it by y_{tr}; note that it exists only for magnetic field. Figure 5.3 illustrates the magnetic field versus the atmospheric height and both the transition and turning points are explicitly shown.

5.4.2 Other temperature models: m > 1 cases

In these cases the general temperature profile is given by Eq. (5.36) and we use it to calculate the Alfvén speed

$$C_A(y) = C_{A0}\left(\frac{y}{y_0}\right)^{m/2}\exp\left(\frac{y_0}{2\Lambda_{p0}(m-1)}\left[1-\left(\frac{y_0}{y}\right)^{m-1}\right]\right), \tag{5.45}$$

and the turning point frequencies for the wave variables

$$\Omega^2_{tp,v}(y) = C^2_{A0}\left(\frac{y}{y_0}\right)^{m}\frac{1}{y^2}\exp\left(\frac{y_0}{\Lambda_{p0}(m-1)}\left[1-\left(\frac{y_0}{y}\right)^{m-1}\right]\right), \tag{5.46}$$

and

$$\Omega^2_{tp,b}(y) = C^2_A(y)\left\{\frac{1}{2\Lambda_{p0}}\frac{1}{y}\left(\frac{y_0}{y}\right)^{m}\left(\frac{2}{y}+\frac{1}{2\Lambda_{p0}}-m\right)+\frac{1}{4y^2}\right\} \ . \tag{5.47}$$

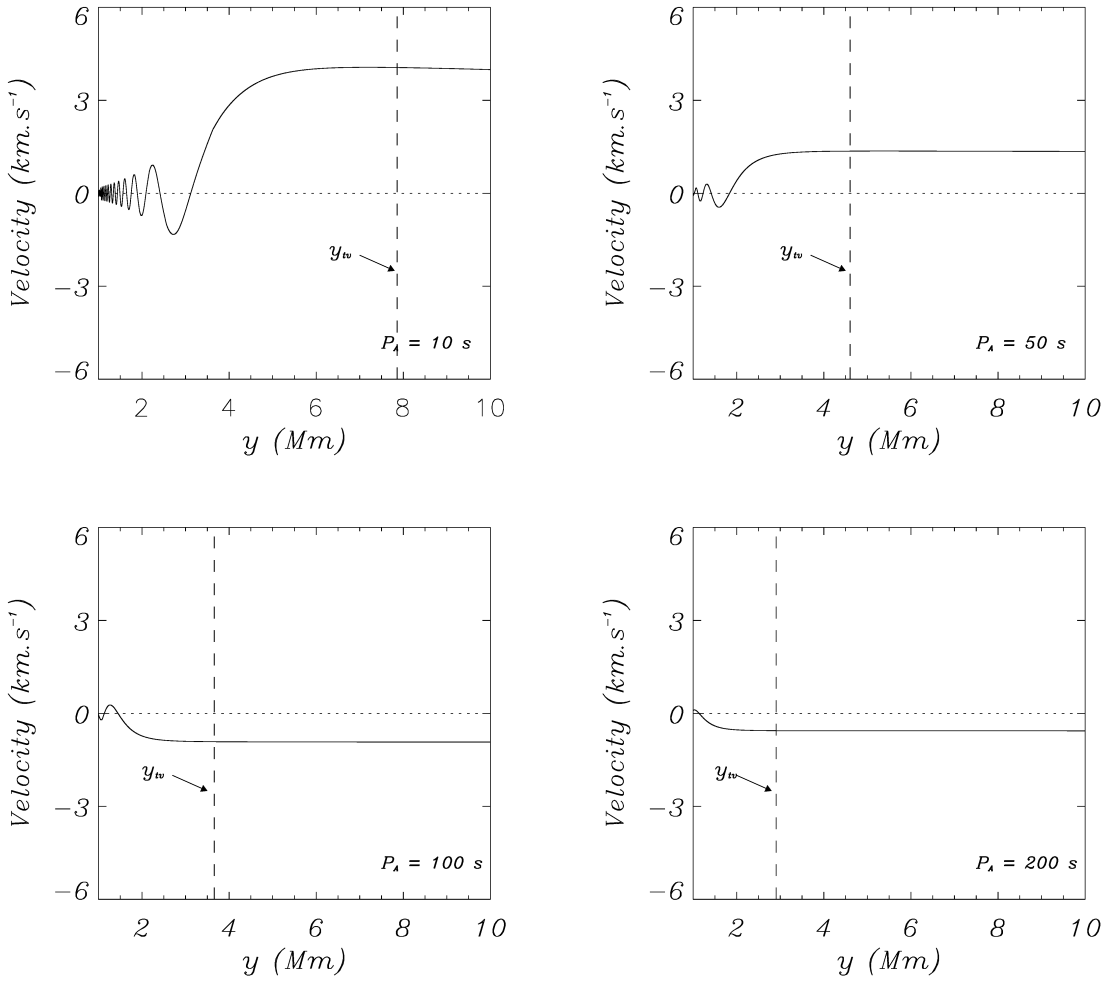

Figure 5.2: Velocity perturbation versus atmospheric height for $m = 1$ case

Let us represent these turning point frequencies graphically in Figs 5.4 and 5.5 for the velocity and magnetic field perturbations, respectively.

As shown in Figs. 5.4 and 5.5, all the turning point frequencies are higher for the steeper temperature gradients except for the m = 2 case. For the magnetic field, the turning point frequency for m = 2 becomes constant at least for the range shown in the figure. When the range is increased it goes down slightly. For all the other cases, the turning point frequency increases gradually by reducing the range of the

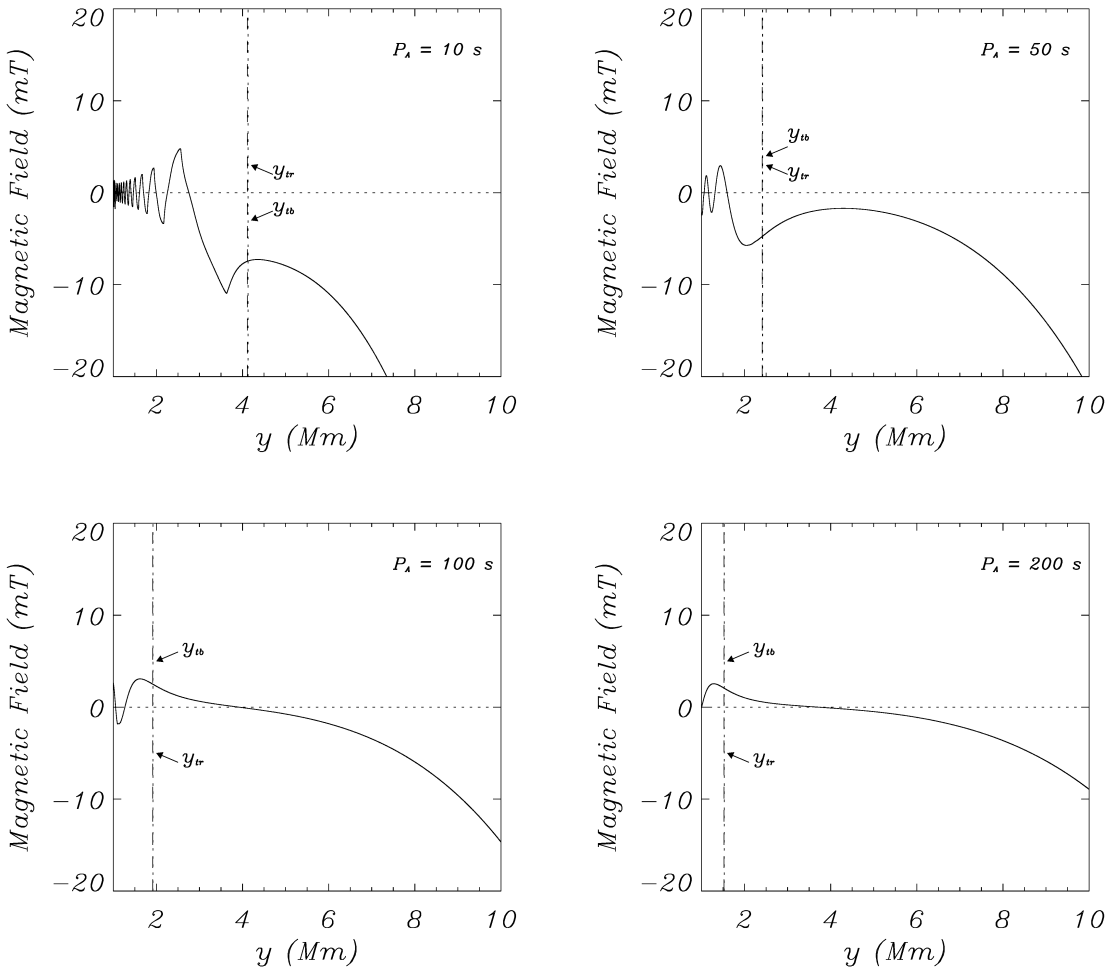

Figure 5.3: Magnetic field perturbation versus atmospheric height for $m = 1$ case

propagation of Alfvén waves in the solar atmosphere with the power law temperature distributions.

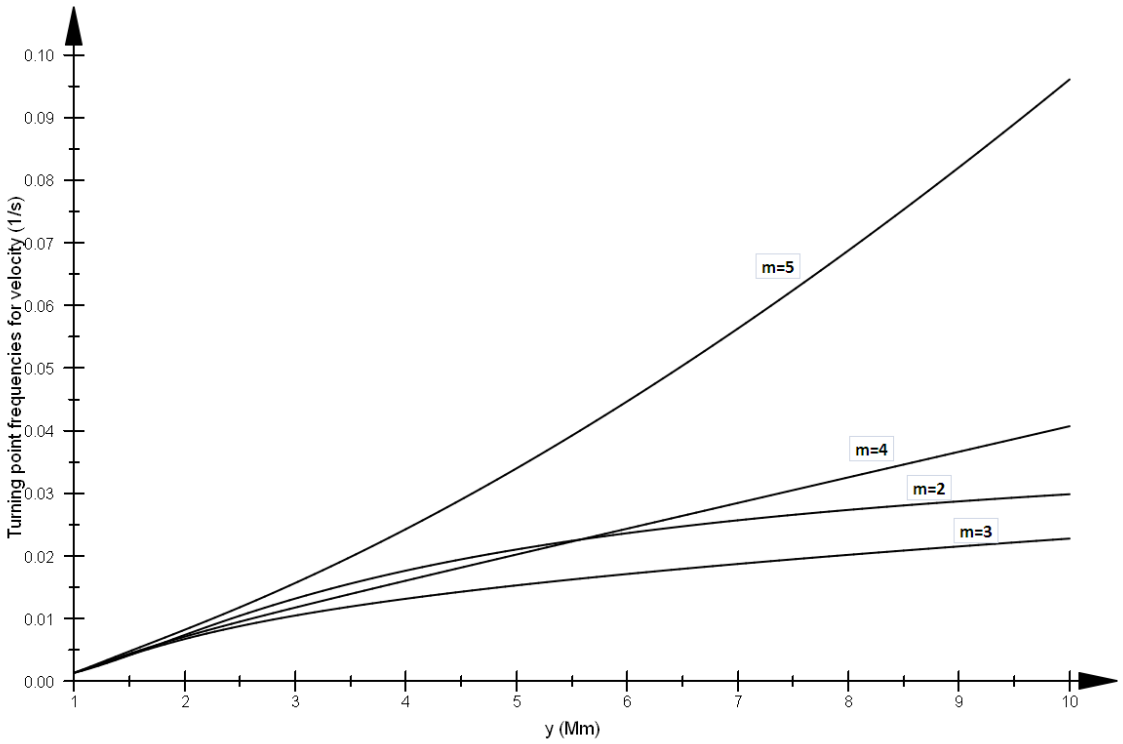

Figure 5.4: Turning point frequencies versus atmospheric height for velocity.

5.5 Application to the MM Model

We now consider the solar atmosphere with a smoothed step-function profile for the plasma temperature (see Murawski & Musielak (2010)) given by

$$T_{\rm e}(y) = \frac{1}{2} T_{\rm c} \left[1 + d_{\rm t} + (1 - d_{\rm t}) \tanh \left(\frac{y - y_{\rm t}}{y_{\rm w}} \right) \right] , \tag{5.48}$$

where $d_{\rm t} = T_{\rm ch}/T_{\rm c}$ and $T_{\rm ch}$ denotes the chromospheric temperature at its lower part. The symbol $T_{\rm c}$ corresponds to the temperature of the solar corona that is separated from the chromosphere by the transition region that is located at $y_{\rm t} = 2$ Mm. A width of the transition region is $y_{\rm w} = 200$ km. We set and hold fixed $T_{\rm c} = 200\, T_{\rm ch}$ with $T_{\rm ch} = 5000$ K. We assume that the atmosphere is permeated with an uniform magnetic field $\vec{B}_{\rm e} = B_{\rm e}\hat{y}$ with $B_{\rm e} = 1.5 \times 10^{-3}$ T and $\vec{g} = -g\hat{y}$ with $g = 274$ ms^{-2}

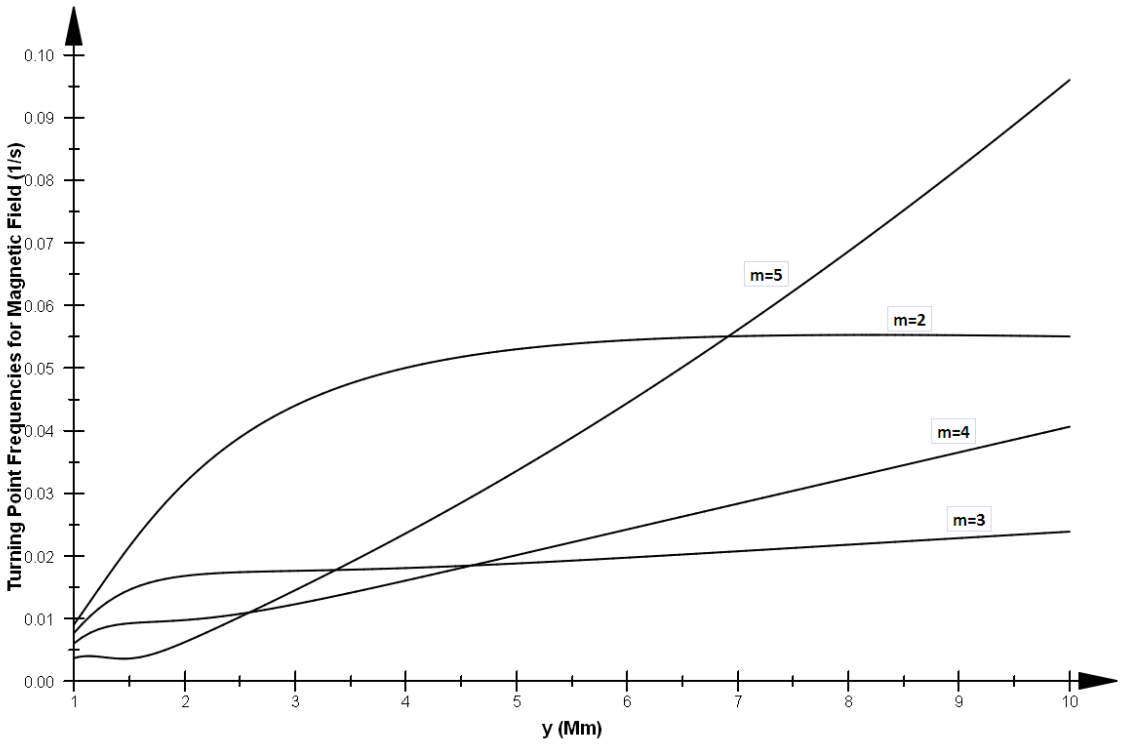

Figure 5.5: Turning point frequencies versus atmospheric height for magnetic field

and $\hat{y}$ is a unit vector along the vertical direction. In such atmosphere equilibrium mass density is given by (see Eq. (2.29))

$$\varrho_{\rm e}(y) = \frac{p_{\rm e}(y)}{g\Lambda_{\rm p}(y)} \tag{5.49}$$

and the pressure is

$$p_{\rm e}(y) = p_0 \, \exp\left\{-\alpha\left[2(\xi - \xi_{\rm r}) - b\ln\left(\frac{d_t + \exp(2\xi)}{d_t + \exp(2\xi_r)}\right)\right]\right\} \tag{5.50}$$

with the pressure scale height

$$\Lambda_{\rm p}(\xi(y)) = \frac{1}{2}\Lambda_{\rm pc}[a + b\,\tanh(\xi)]\ , \tag{5.51}$$

where $\xi(y) = (y - y_{\rm t})/y_{\rm w}$, $\xi_{\rm r}(y) = (y_{\rm r} - y_{\rm t})/y_{\rm w}$, $\alpha = y_{\rm w}/(2d_{\rm t}\Lambda_{\rm pc})$ with $\Lambda_{\rm pc} = k_{\rm B}T_{\rm c}/mg$, $a = 1 + d_{\rm t}$ and $b = 1 - d_{\rm t}$ and p_0 denotes the gas pressure at the reference level that is set and hold fixed at $y_{\rm r} = 10$ Mm with a value of 0.01 Pa.

5.5.1 Numerical results

Numerical solutions were obtained for Eqs (5.1) and (5.2) by using CLAWPACK, a computer code designed to find numerical solutions to hyperbolic partial differential equations (Leveque (2002)). The computational domain for our numerical simulations is 0.5 Mm $< y <$ 3.0 Mm and it is covered by a uniform grid of approximately 5×10^3 numerical cells. We set the open (zero gradient) boundary conditions at both boundaries of the simulation region. Alfvén waves are generated by imposing sinusoidal perturbation at the lower ($y = 0.5$) boundary; $v_{\rm z}(y = 0.5, t) = v_0 \sin(\omega_{\rm A} t)$, $b_{\rm z}(y = 0.5, t) = 0$ where $\omega_{\rm A}$ is the frequency of the excited wave. We set and hold fixed the amplitude of the imposed sinusoidal perturbation, $v_0 = 1 \times 10^{-4}$ Mm s^{-1}. Using these conditions, we numerically solve the initial value problem for the propagation of Alfvén waves of a given frequency and determine the wave behavior within the computational domain.

Numerical results for Eqs (5.1) and (5.2) were obtained for six different wave periods ranging from 50 s to 500 s. Figures 5.7 and 5.8 illustrate the velocity and magnetic field perturbations with respect to y, respectively. Waves were generated at the lower boundary, i.e. $y = 0.5$ and it requires approximately 224 s of propagating time for the waves to reach the upper boundary, which is located at $y = 3.0$ Mm.

There are a few different ways that the turning point, which separates oscillatory and non-oscillatory regions, can be defined. The concept is already explained in sec. 5.3. First we present the results with last zero and then we calculate the so-called turning and transition points using the method described in sec. 5.3.

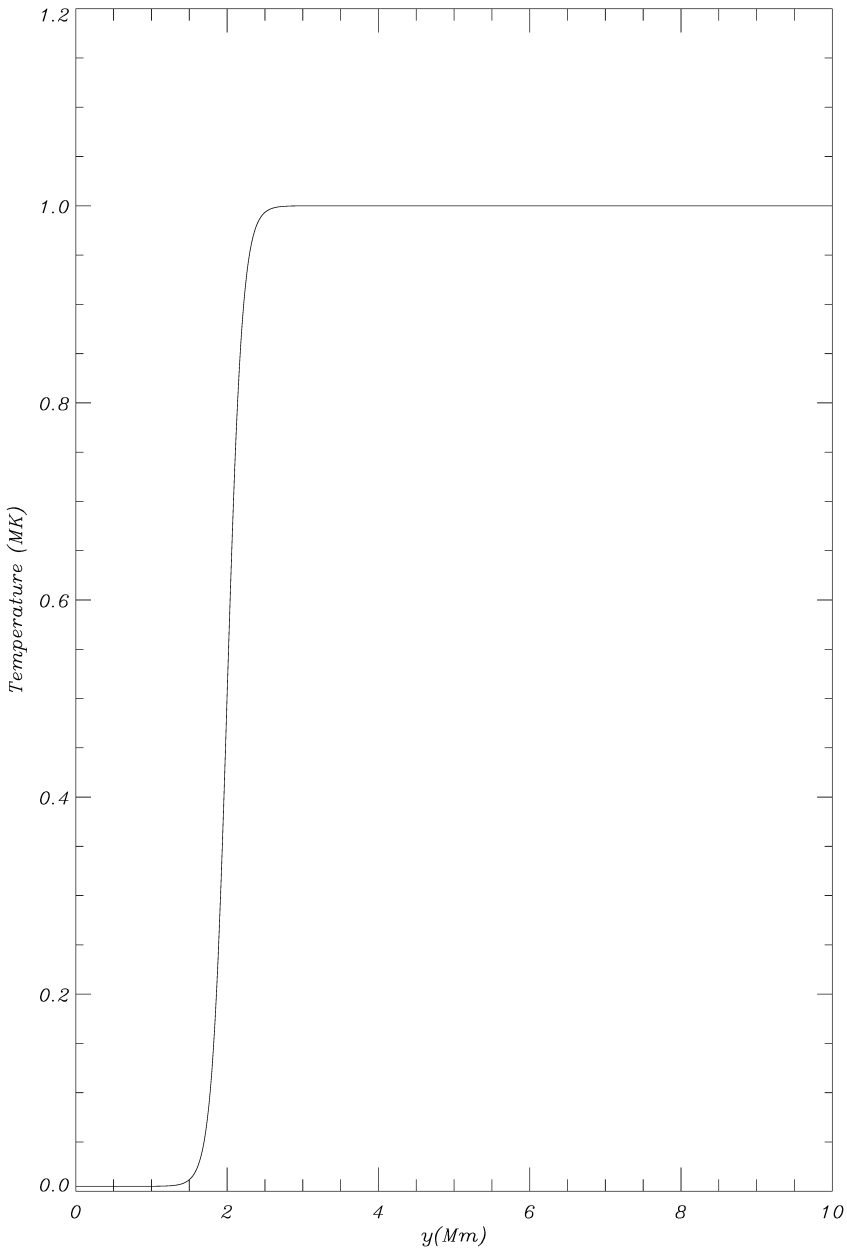

Figure 5.6: Temperature profile for MM model

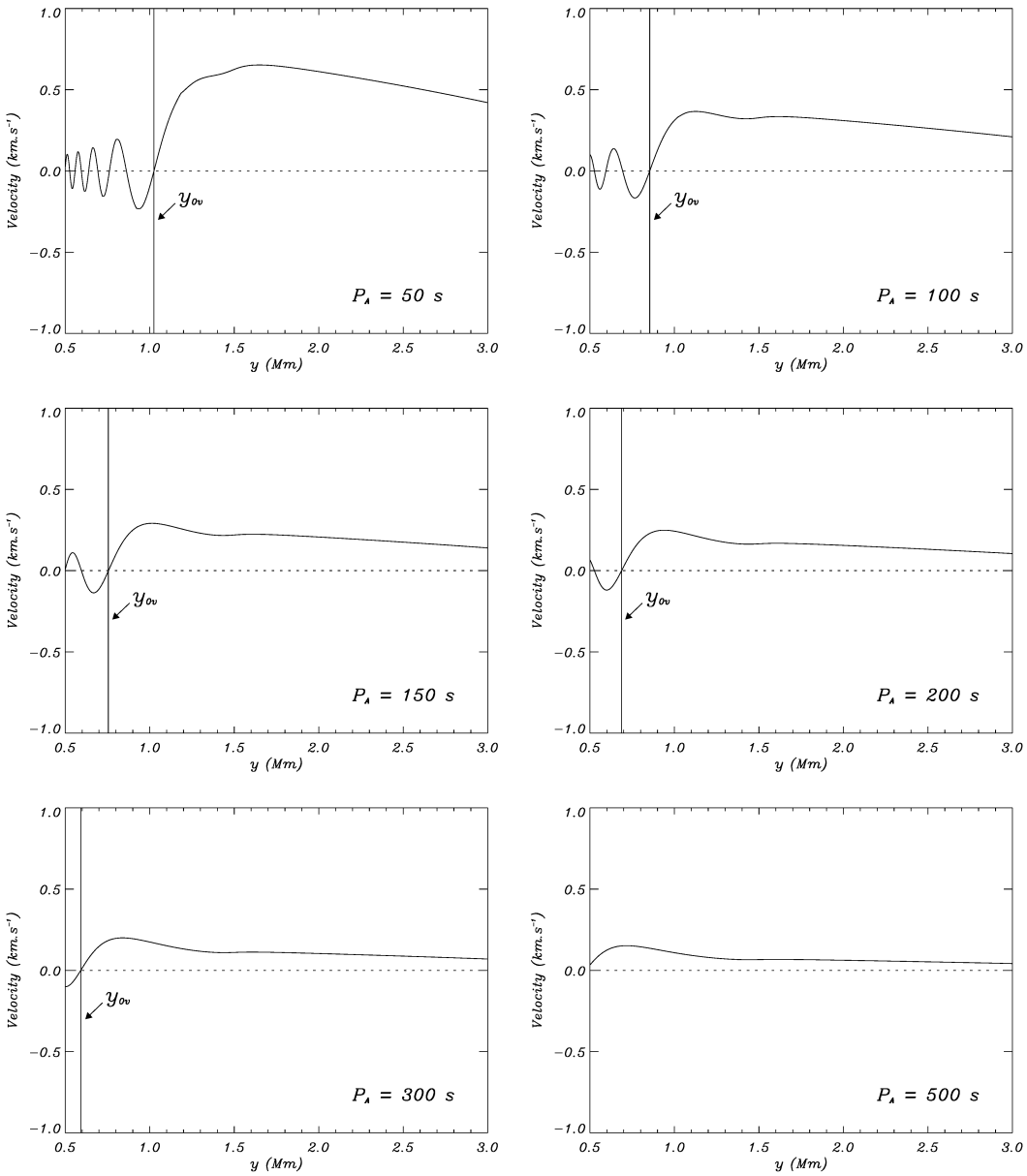

Figure 5.7: Plots of velocity perturbations versus atmospheric height with the location of the last zero, $y_{0\mathrm{v}}$ depicted by vertical solid line.

In Figs. 5.7 and 5.8, we present the numerical solutions for the velocity and magnetic field perturbations with the points at which the last zero locate and we call these points y_{ov} and y_{ob}, respectively. Since the results for both the velocity and magnetic field perturbations look different, we have to treat them separately. Let us begin with the velocity perturbations presented in Fig. 5.7 and it can be clearly seen that for lower periods the wave is propagating more in the atmosphere than in higher periods. Hence the solid line, which represents the last zero is moving toward the lower boundary, i.e. $y = 0.5$, by making the oscillatory region smaller when period (frequency) gets larger (smaller) and in the last panel there is no zero and as a result y_{ov} does not exist for period 500 s.

In Fig. 5.8, we show plots of the magnetic field versus y. Here also the position of last zero of each panel is getting closer to the lower boundary of the computational domain when the wave period gets higher. However, the corresponding location of the last zero for each wave period is different than in the velocity perturbations. Furthermore, in the last panel y_{ob} is present but very close to the lower boundary, whereas there is no such point in the velocity perturbation. It explains that these two wave variables behave differently and the results depend on which variable is chosen to describe the behavior of Alfvén waves in the solar atmosphere.

Figure 5.9 shows the numerical solutions of Eq. (5.1) along with turning points $y_{\rm tv}$ depicted by the vertical dashed lines. The plots given in Figs 5.7 and 5.9 are the same, except the latter shows turning points. The values of $y_{\rm tv}$ were calculated directly using Eq. (5.11) for given frequencies $\omega_{\rm A}$. However, the magnetic field perturbations given in Fig. 4 are different than those given in Fig. 5.8, as we plot $b_{1\rm z}$ instead of $b_{\rm z}$ and the relationship between $b_{\rm z}$ and $b_{1\rm z}$ is given in sec. 5.2. In order to show a consistency between analytically and numerically obtained results it is necessary to use the transformed wave variable $b_{1\rm z}$ instead of the original ($b_{\rm z}$). Also the values for

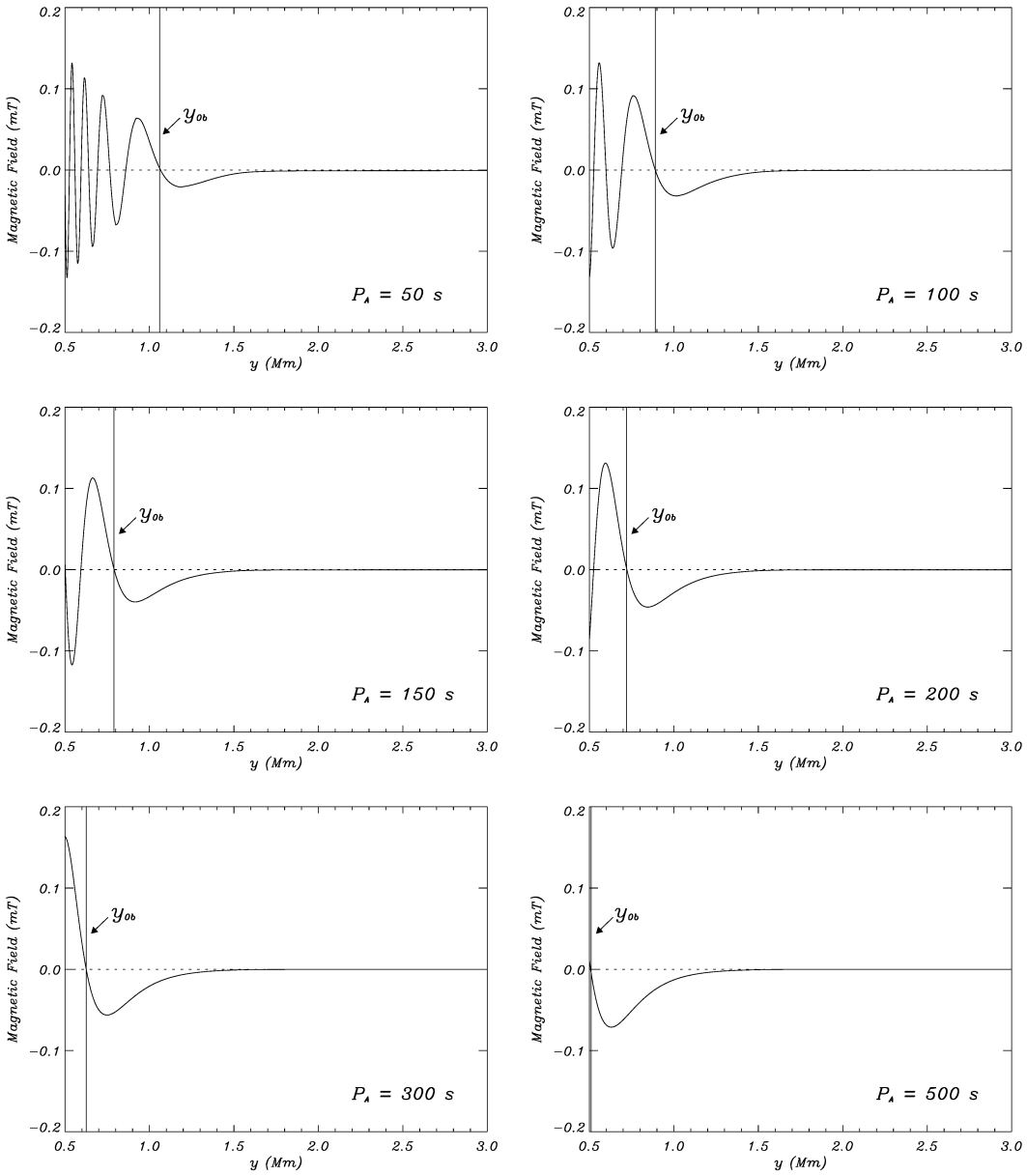

Figure 5.8: Plots of magnetic field perturbations versus atmospheric height with the location of the last zero, $y_{0\mathrm{b}}$ depicted by vertical solid line.

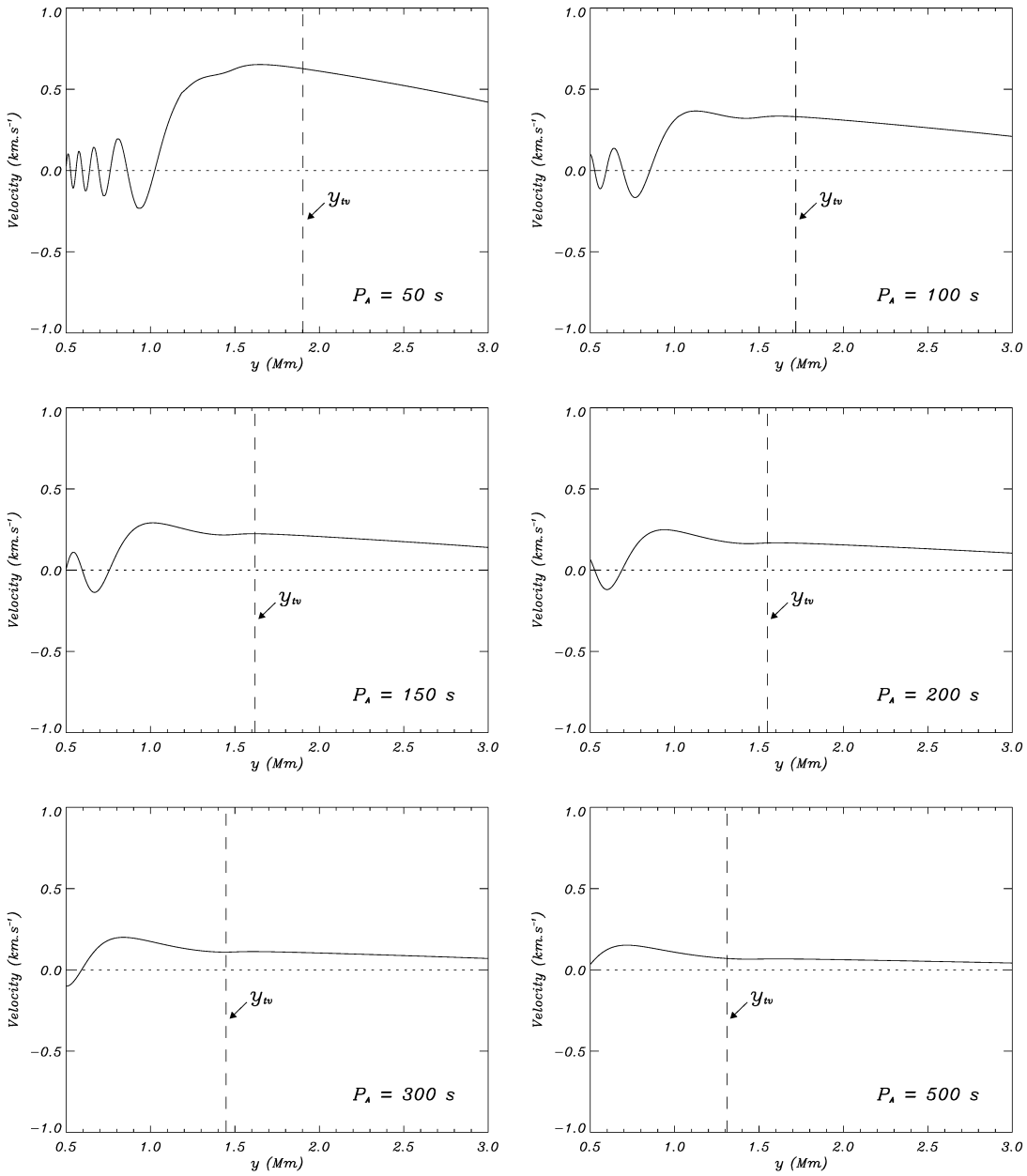

Figure 5.9: Plots of velocity perturbations versus atmospheric height with the location of the turning point, $y_{\rm tv}$ is depicted by vertical dashed line.

turning and transition points were calculated from Eqs (5.12) and (5.9), respectively, for given frequencies and they are shown in Fig. 5.10 as the vertical dotted lines. These results demonstrate that there are well-defined turning points for both velocity and magnetic field perturbations and also a well-defined transition point for the latter.

The location of the turning points for transformed magnetic field perturbation is always the first minimum after the last zero. Furthermore both the transition and turning points are very similar in all the panels (see Fig. 5.10) and different from the turning points for the velocity perturbations (see Fig. 5.9). The turning point frequencies for the velocity and magnetic filed perturbations are presented in Fig. 5.11. The two horizontal dashed-dotted lines represent the frequency range considered in this chapter. It is interesting to see that there are more than one turning point for each wave variable and that the wave frequency reaches a maximum in the transition region (see Fig. 5.11). However in this chapter we mainly focus only on the first turning point, which is located within our computational domain and it is clearly shown in Figs 5.9 and 5.10. Further discussion of these turning point frequencies is given below.

Now let us look at the turning points given in terms of the actual wave travel time. Figs 5.12 and 5.13 represent the locations of the transition and turning points for the transformed the velocity and magnetic field perturbations, respectively. We use Eqs (5.17) and (5.18) to transform the original velocity and magnetic field perturbations into wave variables in the τ - space. These figures present a new set of the turning and transition points which corresponds to each period, obtained from Eqs (5.32) through (5.35) as explained in the previous section. The transition points are shown as $y_{\rm vr}$ and $y_{\rm br}$ whereas the turning points are represented by $y_{\tau \rm v}$ and $y_{\tau \rm b}$ for the velocity and magnetic field perturbations, respectively. Since for this case, the turning point frequency cannot be found analytically, we computed $t_{\rm ac}$ numerically

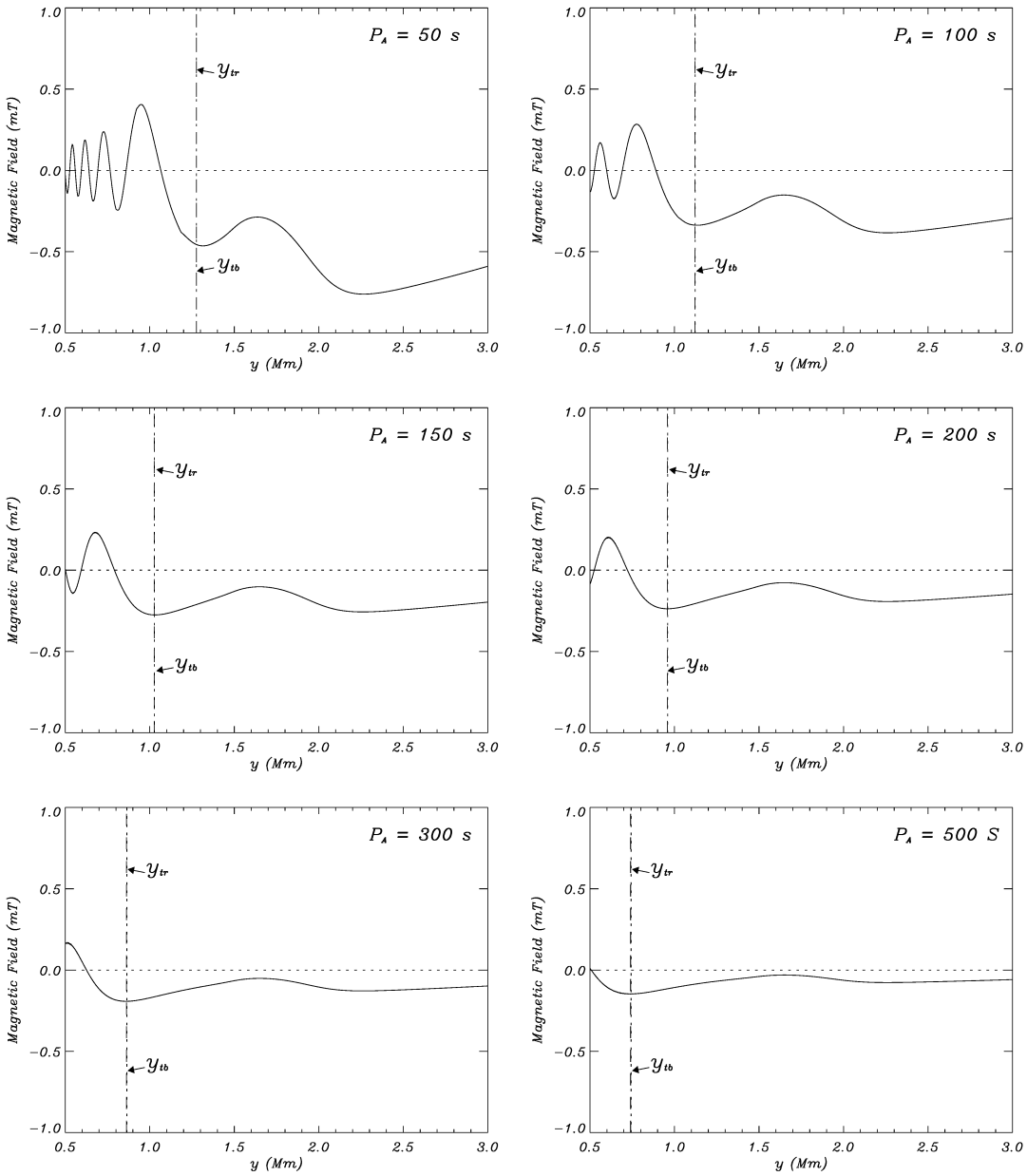

Figure 5.10: Plots of the transformed magnetic field perturbation: $[b_z(t,y) = (C_{\rm A0}/C_{\rm A})b_{1z}(t,y)]$ versus atmospheric height with the location of the transition, $y_{\rm tr}$ and turning points $y_{\rm tb}$ depicted by vertical dotted and dashed lines, respectively.

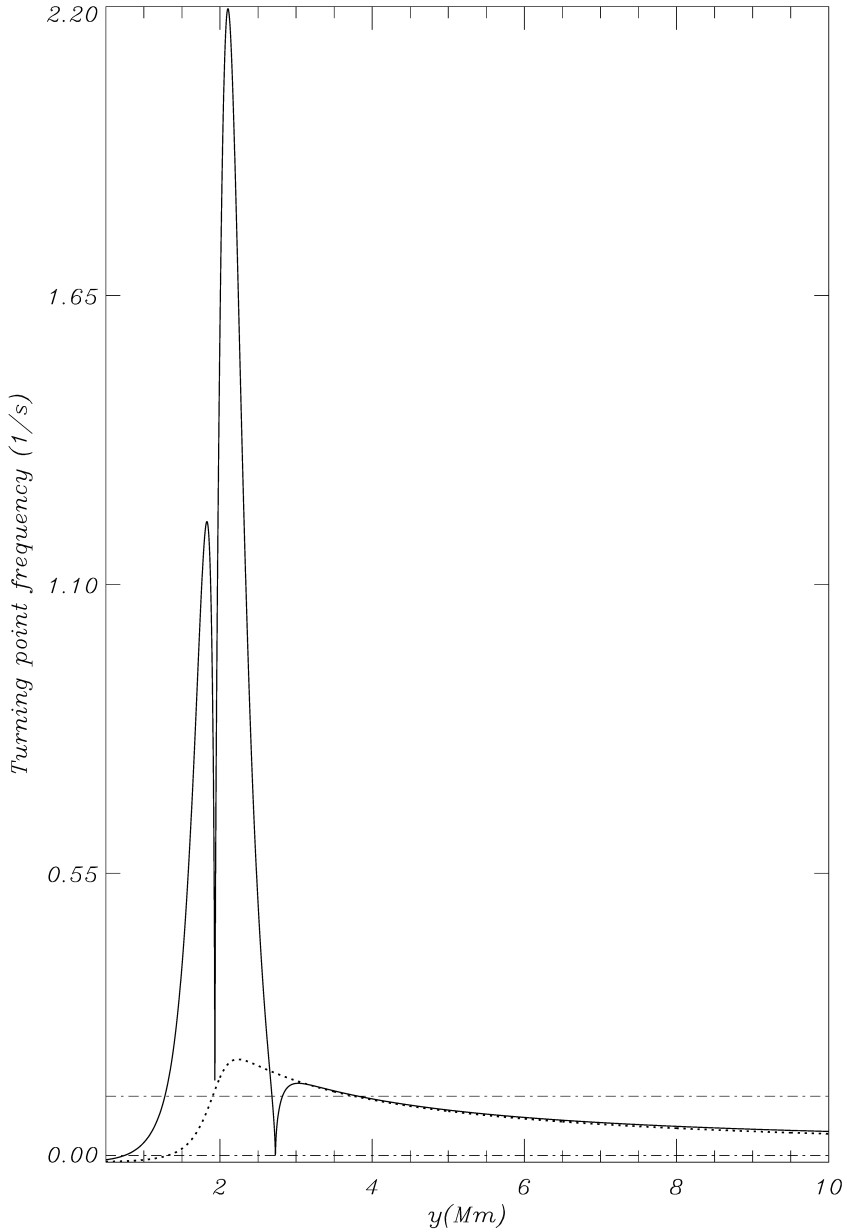

Figure 5.11: Plots of approximate turning point frequencies versus the atmospheric height for velocity and magnetic field perturbations given by dotted and solid lines, respectively.

and the obtained results are shown in Fig. 5.14. Similarly the transition points were taken from the critical frequency plot which is not shown here.

Figure (5.12) represents the wave profile for the transformed velocity perturbation, $v(\mathrm{t}, \tau)$ as given by Eq. (5.17), versus the atmospheric height with the transition and turning points depicted by the dotted and dashed vertical lines, respectively. In Fig. 5.12, it is clearly seen that the transition and turning points coincide with each other for all the considered wave frequencies and that their location gets closer to zero by reducing the size of the oscillatory region, when the frequency (period) decreases (increases). Also note that those points are located after the last maximum of velocity after last zero. For higher (lower) frequencies (periods), we see that the waves oscillate more in the solar atmosphere and if we further decrease the frequency beyond the minimum shown in the figure, there will be no oscillatory region at all within the computational domain we consider in this chapter. Similarly Fig. 5.13 presents the transformed magnetic field perturbation versus the solar atmospheric height with the transition and turning points given by the dotted and dashed vertical lines. Here also the location for both the transition and turning points are the same except the last panel for P = 500 s with the former being higher than the latter. This is due to the t_{ac} term in the turning point frequency expression and it effects only those transition or turning points that are closer to starting point, which is $y = 0.5$ Mm. However the effect is negligible for all other frequencies. If we further compare the locations of those points for both the velocity and magnetic field wave variables, we clearly see that those are not the same and therefore they must be treated separately.

5.6 Relevance to observations

Recently, according to McIntosh et al. (2011), Alfvén waves with periods ranging from 100 s to 500 s are observed and Alfvén waves with period of 45 s are ob-

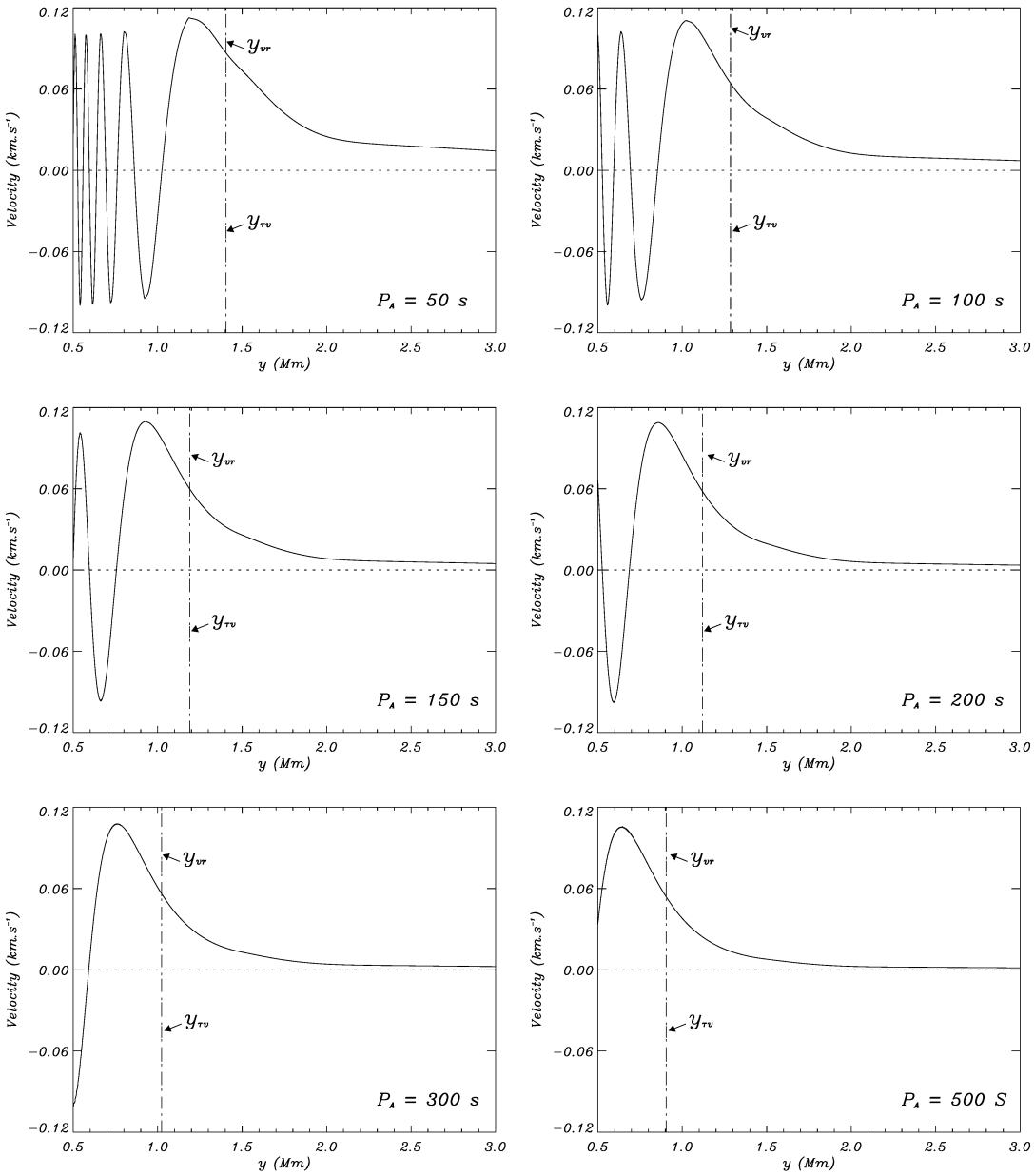

Figure 5.12: Plots of the transformed velocity perturbation: $[v(t,\tau) = (C_{\rm A0}/C_{\rm A})^{1/2} v_z(t,\tau)]$ versus atmospheric height with the location of the transition, $y_{\rm vr}$ and turning points $y_{\tau \rm v}$ depicted by vertical dotted and dashed lines, respectively.

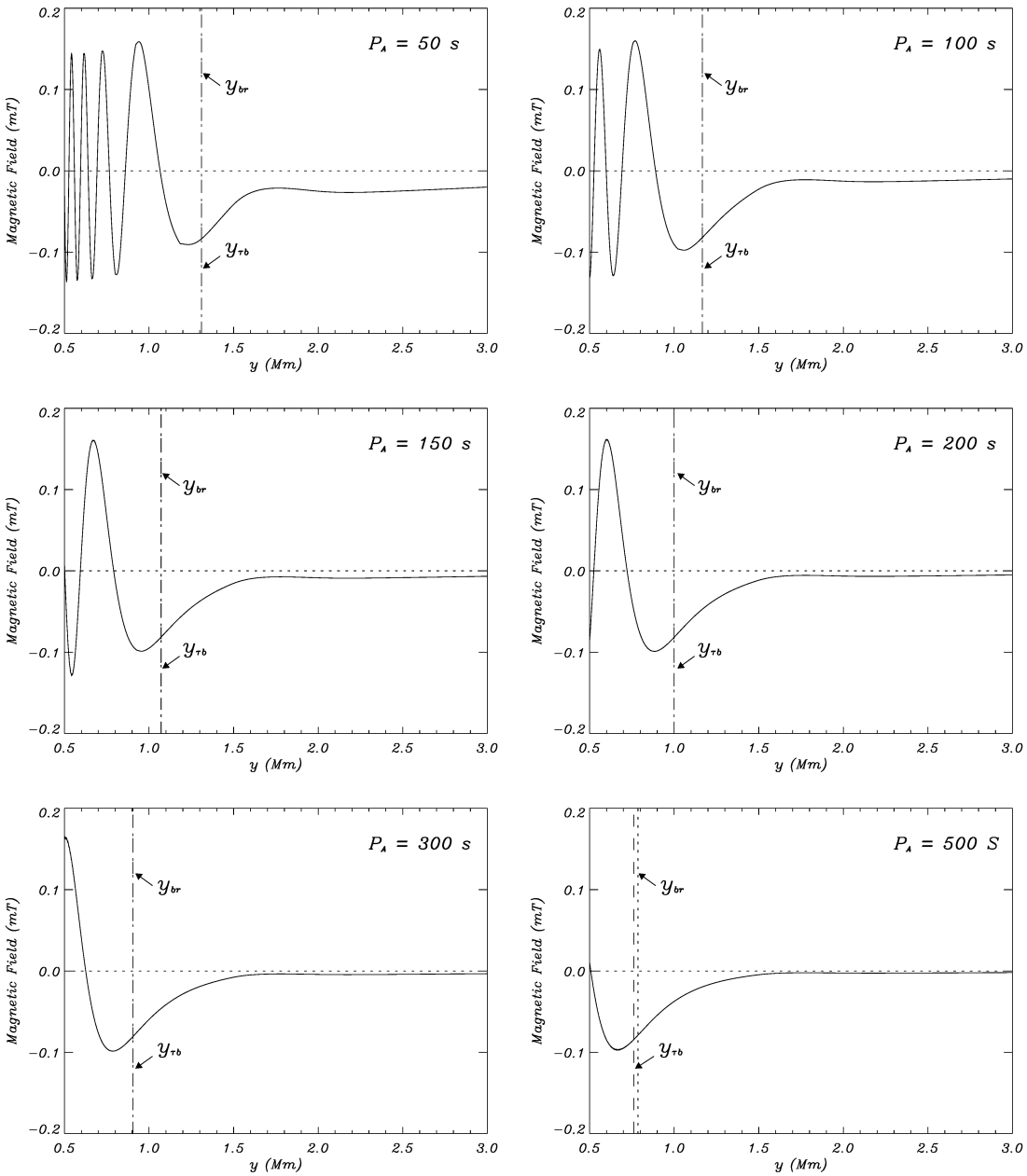

Figure 5.13: Plots of the transformed magnetic field perturbation: $[b(t,\tau) = (C_{\rm A}/C_{\rm A0})^{1/2} b_z(t,\tau)]$ versus atmospheric height with the location of the transition, $y_{\rm br}$ and turning points $y_{\tau \rm b}$ depicted by vertical dotted and dashed lines, respectively.

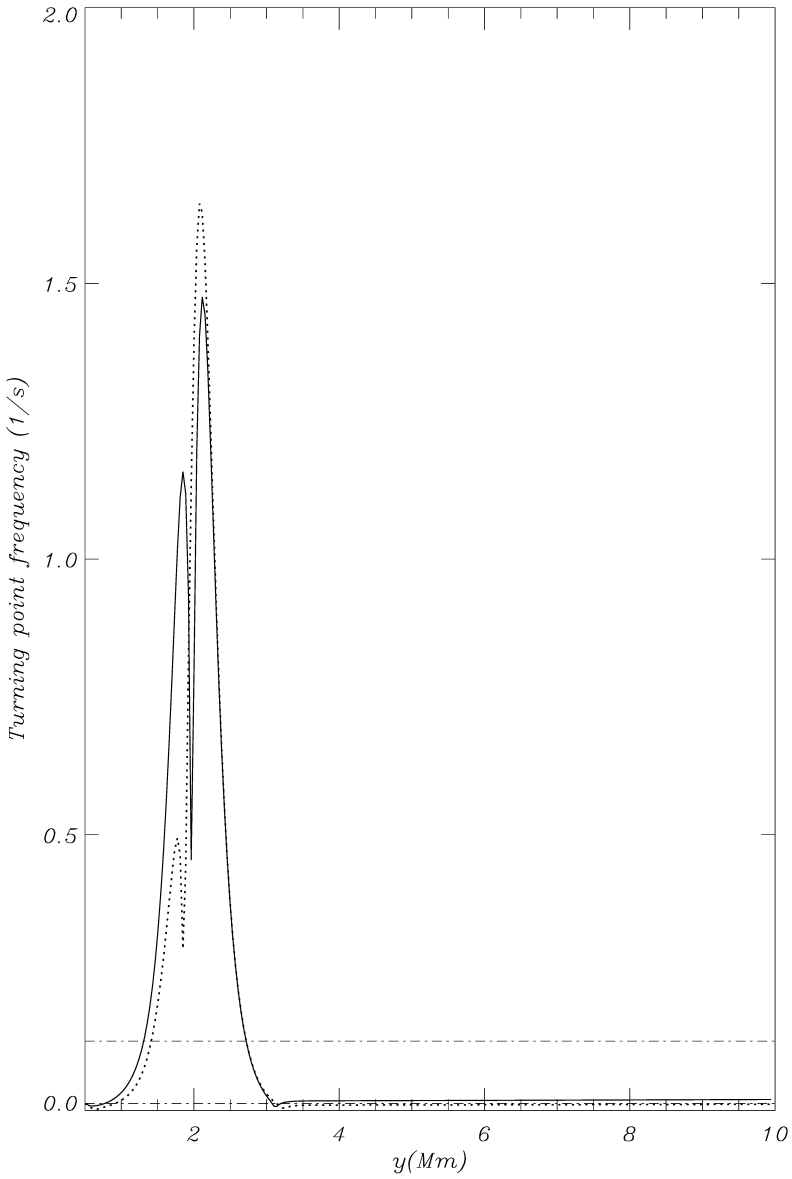

Figure 5.14: Plots of actual turning point frequencies versus the atmospheric height for velocity and magnetic field perturbations given by dotted and solid lines respectively.

served by Okamoto & De Pontieu (2011) are propagating or evanescent. Comparison of our theoretically established cutoff frequencies to the observational data shows that Alfvén waves with periods ranging from 50 s to 500 s are partially propagating within our computational domain, whose physical parameters are described by the non-isothermal solar atmosphere, and partially evanescent in the upper part of the domain; as shown in Figs 5.7 through 5.13, the result is a sensitive function of wave period.

According to our results, Alfvén waves with periods higher than 500 s are evanescent in the entire computational domain while periods below 4 s (see Fig. 5.14) will propagate throughout the whole domain without going through any turning point and will escape to the solar corona before it sees a turning point and starts non-propagating.

We compared only our theoretical predictions obtained here for the MM model of the solar atmosphere, which has the temperature distribution considered originally by Murawski & Musielak (2010). The reason is that the MM model approximates well a more realistic temperature in the solar atmosphere given by the VAL C model (see Vernazza et al. (1981)).

5.7 Summary

We investigated numerically the propagation of linear Alfvén waves in the non-isothermal solar atmospheres using two different models: the power law and MM model. In both models, we discovered that the temperature gradient does affect the locations of the turning and transition points but the effect is rather mild. On the other hand, our results show that the cutoff frequency is effected by the temperature variations in the MM model and reaches its maximum around the height where the temperature gradient is the steepest, which is at ($y = 2$ Mm). After the maximum

it decreases gradually at the higher atmospheric heights, similar to the isothermal model as explained in Chapter 4.

According to the cutoff frequency figure for the MM model, it is clear that waves can travel through multiple turning points rather than one turning point. Our results show only the first turning point, which lies within our computational domain. Also in terms of wave periods, we can not go below 5 s due to some numerical limitations. The waves with periods between 4 s and 500 s are effected by more than one turning point and according to mathematical definition the wave's behavior is oscillatory until the first turning point and it is non-oscillatory between the first and second turning points, and then again it becomes propagating after the second turning point, with the trend to continue. As a result the waves will not be evanescent completely after it reaches the first turning point, but it will be non-propagating for a certain range and show some oscillations again after the second turning point. This may effect the energy carried by Alfvén waves and detailed studies of such a wave tunneling is outside of the scope of this research.

Our main and most important result is that overall the differences between the non-isothermal and isothermal models are only significant, as expected, in the solar transition region (see Perera et al. (2014)). Another interesting result is that there is no one unique cutoff frequency for Alfvén waves but instead we have a number of cutoffs whose specific forms depend on the method used to define them as well as on the choice of the wave variable used to describe the waves. Finally, it is important to point out that our theoretical predictions can be used to determine whether Alfvén waves observed in the solar atmosphere (see Chapter 1) are propagating or not; this information cannot be be easily obtained from the data.

CHAPTER 6

CONDITIONS FOR WAVE PROPAGATION AND OSCILLATION THEOREMS

6.1 Basic definitions

From a mathematical point of view (e.g., Swanson (1968); Teschl (2011)), solutions to wave equations are called *non-oscillatory* in a given interval if every non-trivial solution has at most one zero in this interval. Now, the solutions are called *oscillatory* in a given interval if every non-trivial solution has an infinite number of zeros in this interval. There are also solutions for which a number of zeros in a given interval is more than one but finite. In this chapter, we identify the oscillatory and non-oscillatory solutions with *propagating* and *non-propagating* Alfvén waves' respectively. However, the solutions with a finite number of zeros, we identify with *standing* Alfve'en waves that are confined to a well-defined cavity.

Such standing wave pattern is formed by Alfvén waves in our model of isothermal atmosphere without the displacement current (DC). The reason is that in this model the Alfvén velocity is unlimited and as a result Alfvén waves reach infinity in a finite time. Hence, a well-defined cavity exists and this cavity extends from an atmospheric height at which the waves are generated, say at $y = 0$, to infinity at which $\rho_e(y = \infty) = 0$. On the other hand, in our model with the DC, the maximum velocity of Alfvén waves is the speed of light and therefore the waves cannot reach infinity. Physically it means that there is no cavity for Alfvén waves in our model with the DC.

In a stratified homogeneous medium that is considered in this dissertation, the waves show reflections at each point due to stratification; the process of reflection can

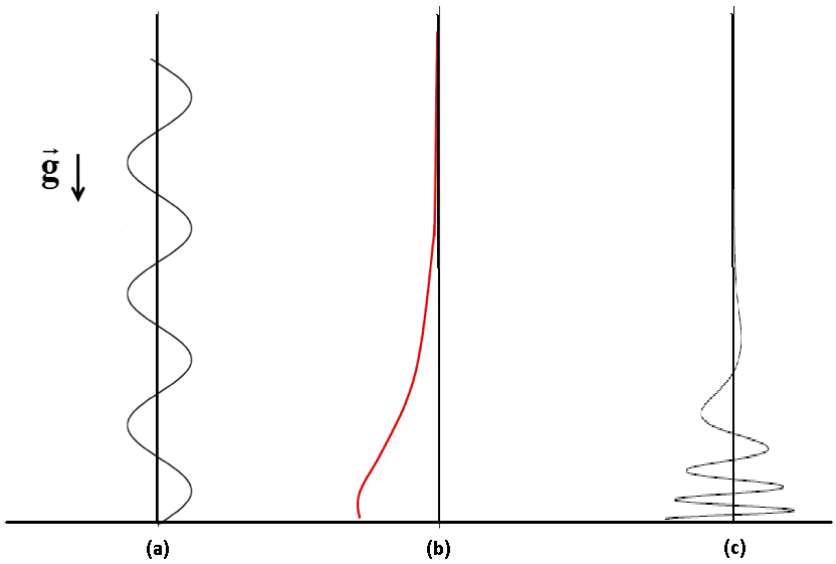

Figure 6.1: Schematic illustration of propagating (a), non-propagating (b) and standing waves (c).

be either destructive or constructive depending on the interfere between the ongoing and reflected waves. However if frequency of the launched wave is greater than a local cutoff frequency (see Chapter 5), then the wave will be propagating. It is also possible that both propagating and non-propagating solutions appear in the same domain; the requirement is that the cutoff frequency is a function of atmospheric height.

Now there are well-known oscillation theorems used by mathematicians to determine whether a given equation has oscillatory or non-oscillatory solutions (e.g., Swanson (1968); Teschl (2011)); such theorems are very powerful as they allowed obtaining the desired results without formally solving the equation. One of the goals of this dissertation is to used the theorems to establish the conditions for propagating and non-propagating waves. Before the specific results obtained by using the oscillation theorems are presented (see Chapter 7), we first give a general overview of these theorems.

6.2 Oscillation theorems

Starting with the original work of Sturm (1836), mathematicians have been interested in developing general methods to determine whether a given differential equation has periodic or non-periodic solutions, without formally solving this equation. Sturm considered the following differential equation

$$\psi'' + f(x)\psi = 0 \ , \tag{6.1}$$

where ψ is a dependent variable, ψ'' is the second derivative of ψ with respect to the independent variable x, and $f(x)$ is a continuous function of x, and showed that solutions to this equation are oscillatory if $f(x) > 0$ for all x in a given interval and non-oscillatory if $f(x) \leq 0$ in this interval. Thus, oscillatory and non-oscillatory solutions are mutually exclusive. Kneser (1893) assumed that $f(x) > 0$, introduced $\gamma = \lim_{x\to\infty} x^2 f(x)$, and used the Euler equation and its solutions (e.g., Murphy (2011)) to demonstrate that solutions to the above equation are oscillatory if $\gamma > 1/4$, and that they are non-oscillatory if $\gamma < 1/4$. He also showed that the case of $\gamma = 1/4$ was inconclusive.

Other established oscillation theorems typically involve the behavior of the integral over $f(x)$. According to a theorem proved by Leighton (1950), solutions to Eq. (6.1) are oscillatory if $f(x) > 0$ and

$$\int^{\infty} f(x)dx = \infty \ . \tag{6.2}$$

Actually, a more general version of this theorem was given early by Wintner (1949) who did not impose any condition on sign of $f(x)$ and demonstrated that the solutions are oscillatory if

$$\lim_{x\to\infty} \frac{1}{x} \int^x \int^s f(\xi) d\xi ds = \infty \ . \tag{6.3}$$

An interesting result is that an oscillation theorem formulated even earlier by Hille (1948) happened to be be general enough to include the Kneser, Leighton and Wintner theorems as special cases. Hille defined

$$g(x) = x \int_x^\infty f(\xi) d\xi \ , \tag{6.4}$$

introduced

$$g_* = \lim_{x\to\infty} \inf \ g(x) \qquad \text{and} \qquad g^* = \lim_{x\to\infty} \sup \ g(x) \ , \tag{6.5}$$

and proved that $g_* > 1/4$ is a sufficient condition for Eq. (6.1) to have oscillatory solutions. However, $g_* \leq 1/4$ and $g^* \leq 1/4$ are necessary conditions and $g^* < 1/4$ is a sufficient condition for Eq. (6.1) to have non-oscillatory solutions.

Further extensions and generalizations of the above oscillation theorems were given by Hartman (1952), Nehari (1954), Coles (1968), Kamenev (1978), Yan (1986), Philos (1989), Yu (1991), Saker et al. (2003), Lee et al. (2005), and more recently by Bohner & Saker (2006), Tyagi (2009), and Teschl (2011); note that this list is not complete and that more references can be found in Swanson (1968) and Teschl (2011).

Having established the nature of solutions to Eq. (6.1) by using one of the above oscillation theorems, the result can be used to determine the nature of solutions to other equations of similar forms. Sturm (1836) was first to formulate the required conditions for this comparison to give mathematically valid answers. To present the

basic idea, we follow Kahn (1990) who assumes that all solutions to Eq. (6.1) are known and that they are oscillatory. Then he considers the following equation

$$z'' + p(x)z = 0 \ , \tag{6.6}$$

and proves that all solutions to this equations are also oscillatory if $p(x) \geq f(x)$. This theorem is known as Sturm's comparison theorem and it was used by Musielak et al. (2006) to study the existence of oscillatory and non-oscillatory solutions to a certain class of wave equations. They compared their wave equations to the Euler equation, whose solutions are well-known (e.g., Murphy (2011)), however, for which the above theorems are not applicable (e.g., Wong (1999); Aghajani & Roomi (2012)). The comparison allowed these authors to establish conditions for wave propagation for different inhomogeneous media.

There are also oscillation theorems that apply to other ordinary differential equations (ODE's), specifically, to second order self-adjoint ODE's given in the following form

$$[a(x)u']' + c(x)u = 0 \ , \tag{6.7}$$

on a bounded open interval $\alpha < x < \beta$, where $a(x)$ and $c(x)$ are real-valued continuous functions and $a(x) > 0$ on the interval $[\alpha, \beta]$. According to Leighton's oscillation theorem (Leighton (1962)), solutions to Eq. (7.27) are oscillatory if

$$\int^{\infty} \frac{dx}{a(x)} = \int^{\infty} c(x)dx = \infty \ . \tag{6.8}$$

The above equation was also studied by Leighton (1949), who showed that if $a(x) > 0$ near $x = +\infty$, and if

$$\int_1^\infty \frac{dx}{a(x)} = \int_1^\infty c(x)dx = \infty \ , \tag{6.9}$$

then every solution of Eq. (6.8) has an infinite number of zeros in the interval $1 < x < \infty$. Similarly, if $a(x) > 0$ near $x = 0+$, and if

$$\int_0^1 \frac{dx}{a(x)} = \int_1^\infty c(x)dx = \infty \ , \tag{6.10}$$

then every solution of Eq. (6.8) has an infinite number of zeros in the interval $0 < x < 1$.

Leighton (1949) also investigated the so-called normal equation

$$[xu']' + c(x)u = 0 \ , \tag{6.11}$$

and demonstrated that if $x > 0$ and $0(x^\kappa)$, with $\kappa > 1$, for x large, a non-null solution of Eq. (6.11) has at most a finite number of zeros on $1 < x < \infty$. Moreover, if $x > 0$ and $0(x^\kappa)$, with $\kappa < 1$, for x near $x = 0+$, then a non-null solution of Eq. (6.11) has at most a finite number of zeros on $0 < x < 1$.

More generalized oscillation theorems that can be applicable to this equation are also available (e.g., Swanson (1968); Teschl (2011), and references therein). Once it is established that the solutions to the above equations are oscillatory, the Sturm comparison theorem can be used to determine the nature of solutions to the following equation

$$[A(x)v']' + C(x)v = 0 \ . \tag{6.12}$$

Leighton (1962) used the variational analysis to introduce $V[u]$, which is a functional given by

$$V[u] = \int_{\alpha}^{\beta} [(a - A)u'^2 + (C - c)u^2]dx \ , \tag{6.13}$$

and proved that if there exists a nontrivial real solution for u in (α, β) such that $u(\alpha) = u(\beta) = 0$ and $V[u] > 0$, then every real solution for v has at least one zero in (α, β).

For even more generalized form of differential equation given by

$$[A(x)v']' + B(x)v' + C(x)v = 0 \ , \tag{6.14}$$

the variational function $V[u]$ has to be written in the following form

$$V[u] = \int_{\alpha}^{\beta} [(a - A)u'^2 + (b' - B' + C - c - G)u^2]dx \ , \tag{6.15}$$

where G is continuous function satisfying $G \geq B^2/A$. Moreover, if there exists a nontrivial real solution for u in (α, β) such that $u(\alpha) = u(\beta) = 0$ and $V[u] > 0$, then every real solution for v has at least one zero in (α, β).

Applications of the Sturm comparison theorem to wave propagation in the solar atmosphere was first considered by Musielak & Moore (1995), who investigated propagation of Alfvén waves in an isothermal solar atmosphere. Schmitz & Fleck (1998) also used it to study propagation of acoustic waves in the solar atmosphere. In more recent work, the theorem was used by Musielak et al. (2006), Routh et al. (2007, 2010), Hammer et al. (2010), Murawski & Musielak (2010), and by Routh et al. (2013). From this point on, we do not restrict ourselves to only one theorem but instead we apply the most appropriate oscillation theorems to the problem of wave propagation the isothermal solar atmosphere without and with the DC.

CHAPTER 7

APPLICATIONS OF OSCILLATION THEOREMS

7.1 Model and Formulation

In our model of isothermal solar atmosphere considered in Chapter 4, we investigated the propagation of linear Alfvén waves. Since the waves are linear, they are purely transverse and they are not coupled to the other (fast and slow) MHD waves. We consider only one-dimensional wave propagation along the $y-$axis. Studies of Alfvén waves in this specific model of the solar atmosphere were performed in many papers (e.g., Ferraro & Plumpton (1958); Thomas (1983); An et al. (1989); Musielak et al. (1992); Musielak & Moore (1995); Cally (2012).

As pointed out by these authors, the most striking feature of this model is the fact that Alfvén waves reach infinity because their characteristic (Alfvén) velocity is unlimited. This lack of physical limit on the Alfvén velocity is caused by the gas density decreasing to zero when $y \to \infty$, and by the background magnetic field whose strength remains the same in the entire model. Since the waves reached infinity at which they are totally reflected (e.g., Cally (2012)), the waves form a standing wave pattern described mathematically by solutions given in terms of Bessel functions of different kinds (Ferraro & Plumpton (1958)).

A way to prevent Alfvén waves in the model of isothermal atmosphere to reach infinity is to formally include in the MHD equations the displacement currents (DC) as originally suggested by Leroy (1983). As a result of this modification, the Alfvén wave velocity is limited by the speed of light, which means that at a certain atmospheric height Alfvén waves propagate with the speed of light. Since the velocity of the wave

propagation is now finite and constant, the waves never reach infinity in a finite time. From a physical point of view, this obviously does not mean that Alfvén waves become electromagnetic waves but rather that our description of these waves sets the well-defined limit on the Alfvén wave velocity, which forces the waves to be propagating waves, instead of standing waves (see above for the model without the DC).

We perform our studies of the propagation of Alfvén waves in both the isothermal solar model without the DC and in the model with the DC. In both cases, we determine conditions for the wave propagation by using analytical and numerical methods. Our results shed a new light on the concept of cutoff frequency and its physical meaning for propagating and standing Alfvén waves.

7.2 Ferraro and Plumpton original work

In their original paper on Alfvén waves in an isothermal solar atmosphere, Ferraro & Plumpton (1958) transformed their wave equations, similar to Eqs (7.27) and (7.28), into the following Bessel equations

$$\eta^2 \frac{d^2\tilde{v}_z}{d\eta^2} + \eta \frac{d\tilde{v}_z}{d\eta} + \alpha^2\eta^2\tilde{v}_z = 0 \ , \tag{7.1}$$

and

$$\eta^2 \frac{d^2\tilde{b}_{1z}}{d\eta^2} + \eta \frac{d\tilde{b}_{1z}}{d\eta} + \left(\alpha^2\eta^2 - 1\right)\tilde{b}_{1z} = 0 \ , \tag{7.2}$$

where the transformation was done using $\eta(y) = \exp(-y/2H)$, with H being the pressure scale. In the isothermal atmosphere $H = c_s^2/\gamma g =$ constant, with c_s being the sound speed and γ the ratio of specific heats, and the pressure and density (H_ρ) scale heights are the same. In addition, $\alpha = 2\omega H/C_{A0}$, where C_{A0} is a height-

independent Alfvén velocity specified at one given atmospheric height, which means that we can write $C_A(y) = C_{A0}/\eta(y)$.

The general solutions to Eqs (7.1) and (7.2) are given in terms of Bessel functions of the first (J) and second (Y) kind, and they can be written as

$$\tilde{v}_z(\eta) = C_1 J_0(\alpha\eta) + C_2 Y_0(\alpha\eta) \ , \tag{7.3}$$

and

$$\tilde{b}_{1z}(\eta) = C_3 J_1(\alpha\eta) + C_4 Y_1(\alpha\eta) \ , \tag{7.4}$$

where C_1, C_2, C_3 and C_4 are integration constants that can be evaluated once boundary conditions are specified.

Since the functions Y_0 and Y_1 become infinite as $\eta \to 0$, the parts of the solutions described by these functions are typically eliminated by taking $C_2 = 0$ and $C_4 = 0$ (e.g., An et al. (1989)). However, recently Cally (2012) pointed out that these assumptions about C_2 and C_4 are equivalent to imposing a perfectly reflecting boundary conditions at infinity, and suggested that a radiation boundary can be imposed at the infinity and the solution then will be in Hankel function rather than Bessel.

Now, in this isothermal model of the solar atmosphere, Alfvén waves do reach infinity because their characteristic speed is unlimited (see Section 7.1), therefore, one boundary condition is $\eta(\infty) = 0$. The other boundary condition must be set up at a height in the atmosphere where the waves are launched; let us specify this height to be $y = 0$, which gives $\eta(0) = 1$. Actually, the boundary conditions form a wave cavity that extends from $\eta = 1$ to $\eta = 0$ and makes the waves trapped in it. As a result, the waves are standing waves in this cavity.

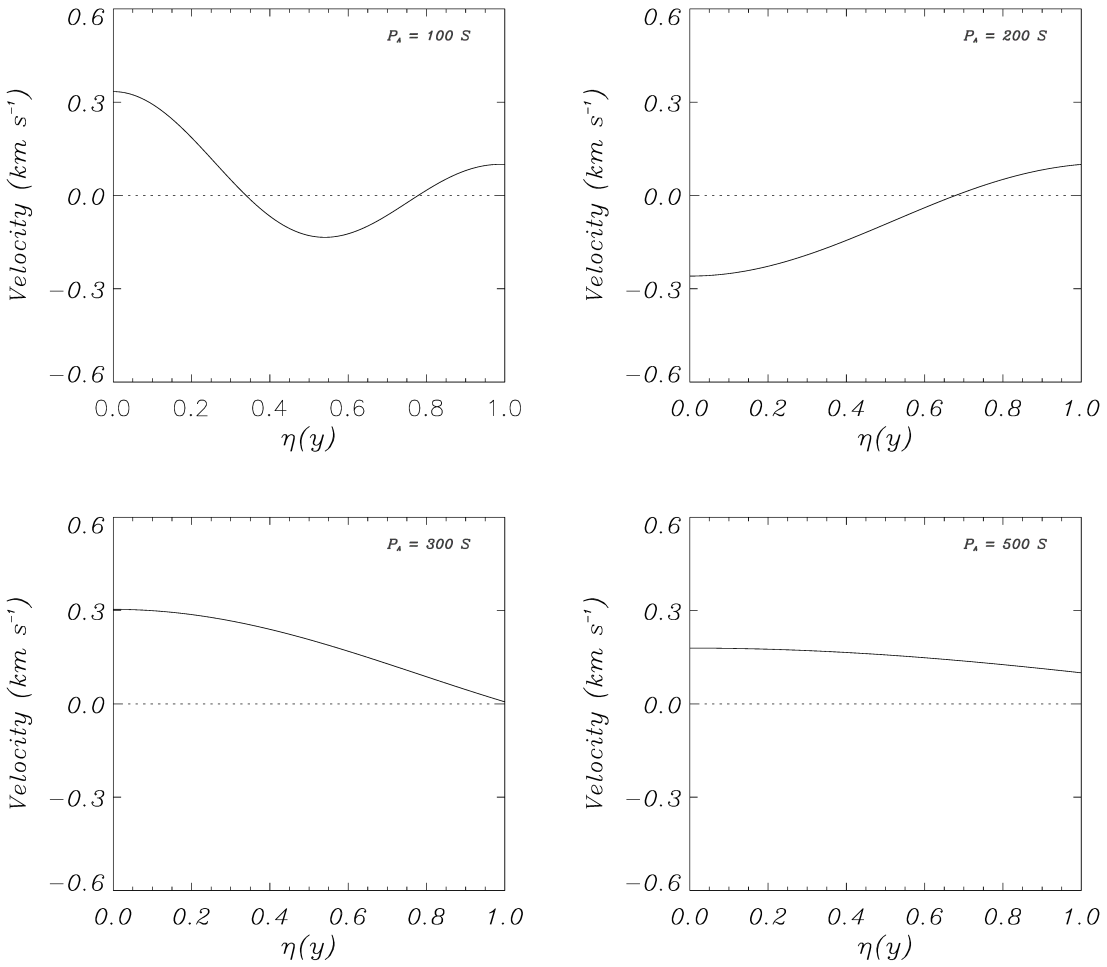

Figure 7.1: Plots of velocity perturbations ($\tilde{v}_z$) versus transformed atmospheric heights (η)

We solve Eqs (7.1) and (7.2) numerically by imposing boundary conditions at $\eta = 1$ ($y = \infty$), $\tilde{v}_z(\eta = 1) = v_0$ and $\tilde{v}'_z(\eta = 0) = 0$, and $\tilde{b}_{1z}(\eta = 1) = b_0$ and $\tilde{b}'_{1z}(\eta = 0) = 0$ with $v_0 = 0.1$ km s^{-}1 and $b_0 = 0.001585333$ T. Figures 7.1 and 7.2 represent the numerically obtained solutions for the velocity and magnetic field perturbations respectively. We perform simulations for six different wave frequencies (see Chapter 4) and introduce the concept of global cutoff frequency.

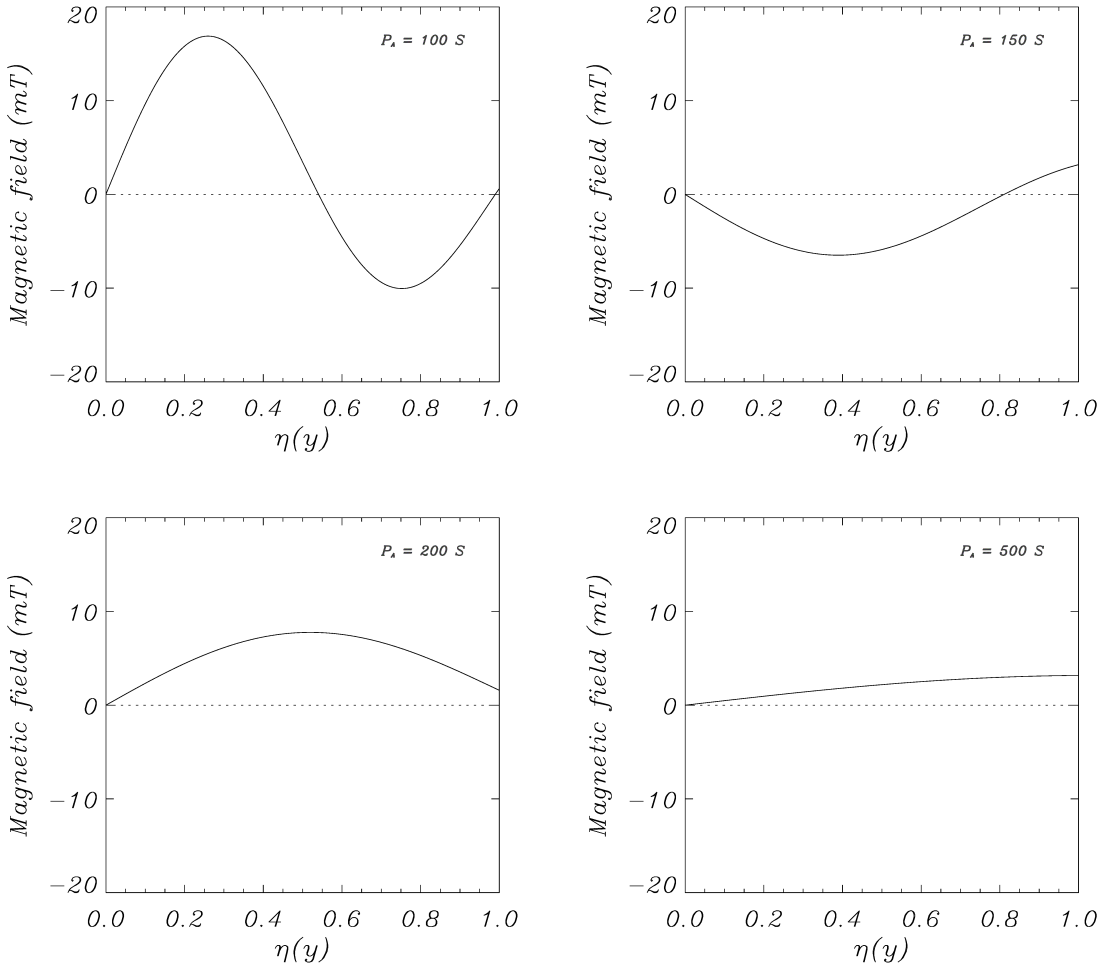

Figure 7.2: Plots of magnetic field perturbations ($\tilde{b}_{1z}$) versus transformed atmospheric heights (η)

7.3 Applications of oscillation theorems to Ferraro and Plumpton equations

We now briefly review oscillation theorem that will be used in this section. Beginning with the original work of Sturm (1836), mathematicians have developed general methods to determine the periodicity of solutions of differential equations without formally solving them. Sturm considered the following general differential equation

$$\frac{d}{dx}\left[a(x)\frac{du}{dx}\right] + b(x)\frac{du}{dx} + c(x)u = 0 \tag{7.5}$$

on a bounded open interval (α, β), where $a(x)$, $b(x)$ and $c(x)$ are real-valued continuous functions and $a(x) > 0$.

Once it is established that the solutions to the above equation are oscillatory in that interval, the Sturm comparison theorem can be used to determine the nature of solutions of the following equation

$$\frac{d}{dx}\left[A(x)\frac{dw}{dx}\right] + B(x)\frac{dw}{dx} + C(x)w = 0, \tag{7.6}$$

knowing that $A(x)$, $B(x)$ and $C(x)$ are real-valued continuous functions and $A(x) > 0$ in the interval (α, β). Note that the Ferraro & Plumpton equations for both the velocity and magnetic field perturbations can be cast in the same form.

Comparison theorems analogous to those in the previous chapter will be used to obtain the extended variational function $V[u]$, which is given by (Swanson (1968))

$$V[u] = \int_{\alpha}^{\beta} \left[(a - A)u'^2 + (b' - B' + C - c - G)u^2\right] dx \ , \tag{7.7}$$

where G is a continuous function satisfying $G \geq B^2/A$. If there exists a non trivial real solution for u in (α, β) such that $u(\alpha) = u(\beta) = 0$ and $V[u] > 0$, then every solution for w has at least one zero in (α, β).

In the following sub-sections, we mainly use this theorem to prove the oscillatory conditions involving the frequency intervals originally considered by Ferraro & Plumpton (1958).

7.3.1 Comparison with differential equations

Method 1 : Bessel differential equation

The general Bessel differential equation can be expressed in the following form

$$u'' + \frac{1}{\eta}u' + \left[\xi^2 - \frac{\nu^2}{\eta^2}\right] u = 0 \ , \tag{7.8}$$

which has solutions as follows :

$$u(\eta) = CJ_\nu(\xi\eta) + DY_\nu(\xi\eta) \ . \tag{7.9}$$

The boundary conditions stated in the theorem given above, which are $u(\eta = 0) = u(\eta = 1) = 0$, force ν to be greater than zero, as if $\nu = 0$, these boundary conditions are no longer valid because $J_0(0) = 1$. Furthermore, using the boundary condition $u(\eta = 0) = 0$, we can eliminate second term in the above equation. After considering all the factors and constraints, we set ν to be '1' and then we can reduce the general solution to the following simplified form:

$$u(\eta) = J_1(\xi\eta) \ . \tag{7.10}$$

Also we can pick any value for ξ in such a way that $J_1(\xi) = 0$; and hence we assign $\xi \equiv \xi_1$ to be the first zero of $J_1(\xi_1\eta)$ at the boundary $\eta = 1$. Mathematically, it is allowed that one can consider the corresponding ξ_n of n^{th} zero at $\eta = 1$, where n can be any positive integer greater than or equal to one. But in this case our main goal is to find the minimum global cutoff frequency, so we consider the value corresponds to the first zero of the Bessel function of first kind (ξ_1) which is approximately 3.8317.

Now we can rewrite Eqs (7.1) and (7.2) in the form that allowed us to directly compare them with the Bessel differential equation:

$$\frac{d^2\tilde{v}_z}{d\eta^2} + \frac{1}{\eta}\frac{d\tilde{v}_z}{d\eta} + \alpha^2\tilde{v}_z = 0 \ , \tag{7.11}$$

and

$$\frac{d^2\tilde{b}_{1z}}{d\eta^2} + \frac{1}{\eta}\frac{d\tilde{b}_{1z}}{d\eta} + \left[\alpha^2 - \frac{1}{\eta^2}\right]\tilde{b}_{1z} = 0 \ . \tag{7.12}$$

We determine the variational function given in Eq. (7.7), for the velocity perturbation, V_v, by comparing Eq. (7.11) with Eq. (7.8)

$$V_v[u] = (\alpha^2 - \xi_1^2)\int_0^1 J_1^2(\xi_1\eta)d\eta \ . \tag{7.13}$$

According to the theorem, solutions will have at least one zero if $V_v[u] > 0$. The integral in Eq. (7.13) is positive and hence $(\alpha^2 - \xi_1^2)$ is the effective term which determines positivity of $V_v[u]$; i.e. for all $(\alpha^2 - \xi_1^2) > 0$, $V_v[u]$ is positive and the solutions will have at least one zero in the interval (0,1). Now we use this inequality to find the minimum frequency such that $\alpha = \xi_1$, and obtain

$$\omega > \left(\frac{C_{A0}}{2H}\right)\xi_1 \ . \tag{7.14}$$

Then we obtain the minimum frequency, ω_0, which is given by

$$\omega_{0v} = \left(\frac{C_{A0}}{2H}\right)\xi_1 \tag{7.15}$$

This minimum frequency, ω_{0v}, can be used to determine the cutoff frequency, a frequency that separates the oscillatory and non-oscillatory regions. Henceforth, we call

this ω_{0v} as the global cutoff frequency for velocity perturbations. We also determine similar global cutoff frequency, ω_{0b}, for the magnetic field perturbation.

It is clearly seen that for all waves with frequencies $\omega > \omega_{0v}$, there is at least one zero in $(0, 1)$. Note that one can also obtain a different ω_{0v} as it depends on ξ, which is a zero of the Bessel function. Since ξ_1 is the minimum, this ω_{0v} will also be the minimum. Hence we can guarantee that if a wave has frequency less than ω_0, then the solution will not oscillate or form a standing wave within $(0, 1)$. This strongly implies that this is truly a cutoff.

Let us now perform the same method to determine the cutoff frequency for Eq.(7.12). After comparing Eq. (7.12) with Eq. (7.8), we obtain the variational function in the following form:

$$V_b[u] = (\alpha^2 - \xi_1^2) \int_0^1 J_1^2(\xi_1 \eta) d\eta - \int_0^1 \frac{J_1^2(\xi_1 \eta)}{\eta^2} d\eta \ . \tag{7.16}$$

Then we evaluate the integrals and follow the method described above to get ω_{0b}

$$\omega_{0b} = \left(\frac{C_{A0}}{2H} \right) Q \ . \tag{7.17}$$

where Q is a value which depends on ξ_1 and $Q > 0$. Approximately Q is equal to 4.920617. Note that for different wave variables, the global cutoff frequencies are also different.

Now we can compare analytically obtained global cutoff frequencies with numerically obtained solutions for different wave frequencies (ω_A) as given in Figs 7.1 and 7.2. Then we evaluate analytically obtained cutoff frequencies for the model we consider and compare the wave behavior when the wave frequency is above and below those frequencies. Fig. 7.1 represents the numerical solutions for the velocity per-

turbations. Comparison of these numerical solutions to those obtained analytically (the global cutoff frequency that is approximately 0.03 s^{-1} or 210 s) shows that the analytical values agree with the numerical solutions; this means that there is no oscillatory behavior for frequencies below the cutoff and that oscillations are only seen above the cutoff frequency. Similarly, for magnetic field perturbations (Fig. 7.2) the analytical value is around 0.04 s^{-1} or 145 s, and the resulting conclusions are the same as for the velocity perturbations.

We want to point out that the turning points introduced in Chapter 4 cannot be clearly seen in the figures because they are very close to zero on the adopted scale. The main purpose of the figures is verify the existence of global cutoff frequencies. We must also emphasize that the presented results were obtained for one specific case, namely, when the Bessel equation was used in the comparison theorem. In principle, a different differential equation can be used and the comparison theorem would give a new global cutoff frequency. The result is shown below.

Method 2:

Consider the differential equation ;

$$y'' - \frac{1}{\eta} y' + (2\pi x)^2 y = 0 \ , \tag{7.18}$$

which has general solutions in the form

$$y(x) = E\cos(\pi x^2) + F\sin(\pi x^2) \ , \tag{7.19}$$

where E & F are arbitrary constants which can be evaluated using the boundary conditions.

However, in order to apply the oscillation theorem, this equation should satisfy certain boundary conditions: $y(0) = y(\pi) = 0$. So we pick the most simplest but still valid, solution

$$y(x) = \sin(\pi x^2) \ . \tag{7.20}$$

Let us now compare Ferraro & Plumpton type equations with Eq. (7.18) and follow the same procedure described in the previous section to find the minimum or global cutoff frequency for each wave variable. After evaluating the variational function $V[y]$ by using Eq. (7.7), we find the global cutoff frequencies for the velocity and magnetic field perturbations:

$$\omega_{0v} = \left(\frac{C_{A0}}{2H}\right) Q_1 \ , \tag{7.21}$$

and

$$\omega_{0b} = \left(\frac{C_{A0}}{2H}\right) Q_2 \ , \tag{7.22}$$

where $Q_1 = 3.9075$ and $Q_2 = 4.25715$.

Method 3:

Let us adopt the same method to determine the global cutoff frequencies for the following differential equation that has sinusoidal solutions

$$w''(x) + \pi^2 w(x) = 0 \ . \tag{7.23}$$

The most simplified version of the general solution to the above differential equation that also satisfies the boundary conditions $w(0) = w(\pi) = 0$ can be given as

$$w(x) = \sin(\pi x) \ . \tag{7.24}$$

We then calculate the global cutoff frequencies at which the solutions show oscillatory behavior by first evaluating $V[w]$ and hence finding the inequalities to get the minimum frequencies for both velocity and magnetic filed perturbations. We can present those as follows

$$\omega_{0v} = \left(\frac{C_{A0}}{2H}\right)\pi \ , \tag{7.25}$$

and

$$\omega_{0b} = \left(\frac{C_{A0}}{2H}\right)Q_3 \ , \tag{7.26}$$

where $Q_3 = 4.25715$.

We will compare obtained global cutoff frequencies at the end of this chapter in the summary section.

7.4 Wave equations in unbounded interval $[0, \infty]$

We recall the Fourier transformed Alfvén wave equations given in Chapter 4 (see Eqs 4.5 and 4.6) and for convenience write them here again

$$\frac{d^2\tilde{v}_z}{dy^2} + \frac{\omega_A^2}{C_A^2(y)}\tilde{v}_z = 0 \ , \tag{7.27}$$

and

$$\frac{d^2\tilde{b}_{1z}}{dy^2} + \frac{\omega_A^2 - \Omega_{cr,b}^2(y)}{C_A^2(y)}\tilde{b}_{1z} = 0 \ . \tag{7.28}$$

These two equations are valid throughout the whole atmosphere starting from $y = 0$ to $y = \infty$.

Oscillation theorems are important because we can directly conclude the oscillatory or non-oscillatory behavior of the solutions without even solving the equations. Even though there are many oscillation theorems (see Chapter 6), only some are applicable depending on the specific physical problem considered. Here, we carefully

picked two oscillation theorems, which are applicable to Eqs (7.27) and (7.28) and used them to determine the periodicity of the equations.

1. Leighton's Oscillation Theorem

   The differential equation under consideration is

$$[a(x)\,u']' + c(x)\,u = 0\ , \tag{7.29}$$

   where $0 < x < \infty$ and $a(x) > 0$. Here $a, a'$and c are continuous functions and $a(x) > 0$ in this interval. The following notations will be used :

$$a_\infty = \lim_{x\to\infty} \int_1^x \frac{dt}{a(t)}\ ,$$

   and

$$c_\infty = \lim_{x\to\infty} \int_1^x c(t)\,dt\ .$$

   Here $C_v = \omega^2/C_A^2(y)$ and $C_b = \left(\omega^2 - \Omega_{crit}^2(y)\right)/C_A^2(y)$.

   When we use this theorem to see whether the solutions of Eq. (7.27) and Eq. (7.28) are oscillatory or non-oscillatory, we have to find a_∞ and c_∞ first. Compare to the Eq. (7.27), $a(y) = 1$ and hence $a_\infty = \infty$ and $C_{v\infty} = (\omega_A^2 H/C_{A0}^2)\exp(-1/H)$ and $C_{b\infty} = -\infty$. Since both $C_{v\infty}\&C_{b\infty} \neq \infty$, according to the Leighton's oscillation theorem we can conclude that the corresponding wave variables are not-oscillatory.

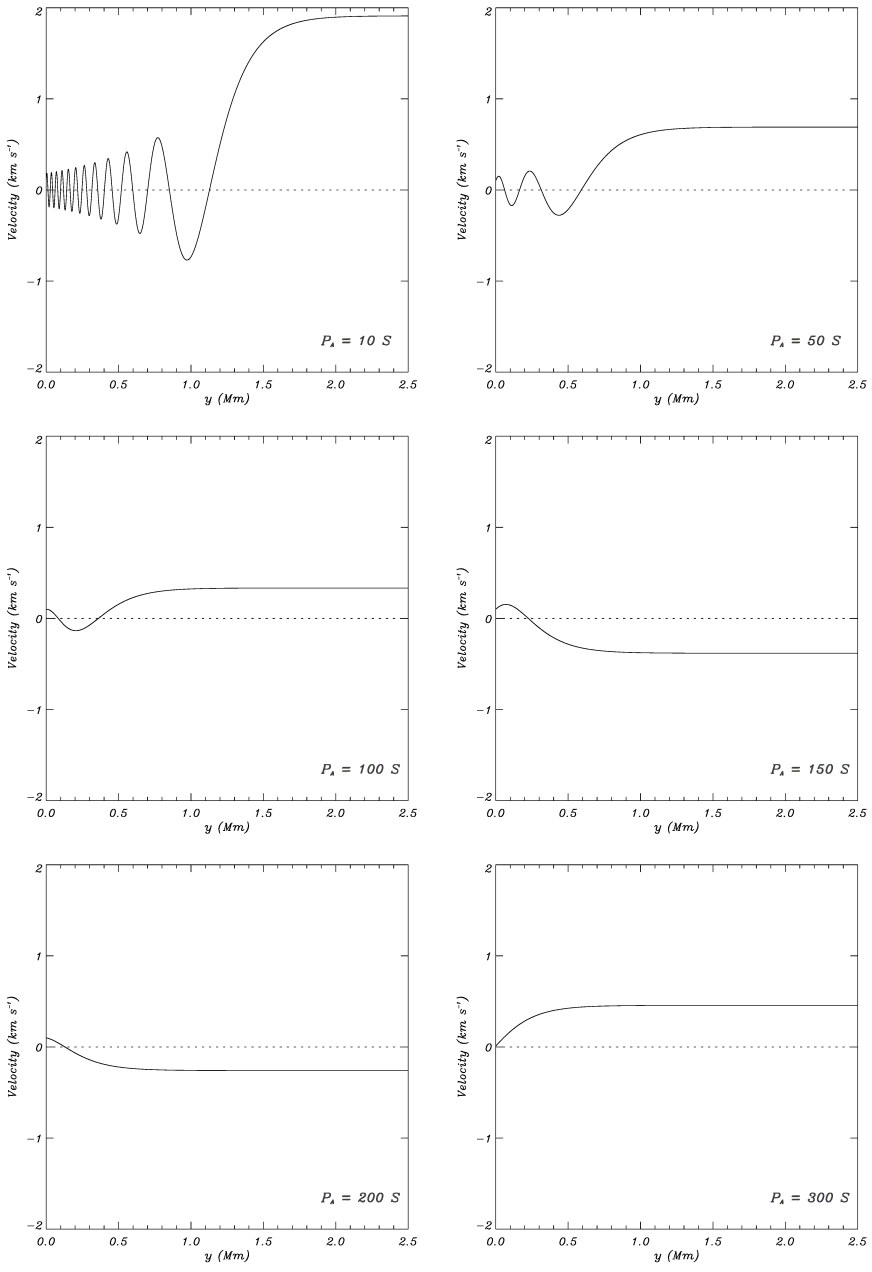

Figure 7.3: Velocity perturbations ($\tilde{v}_z$) vs atmospheric heights ($y(Mm)$)

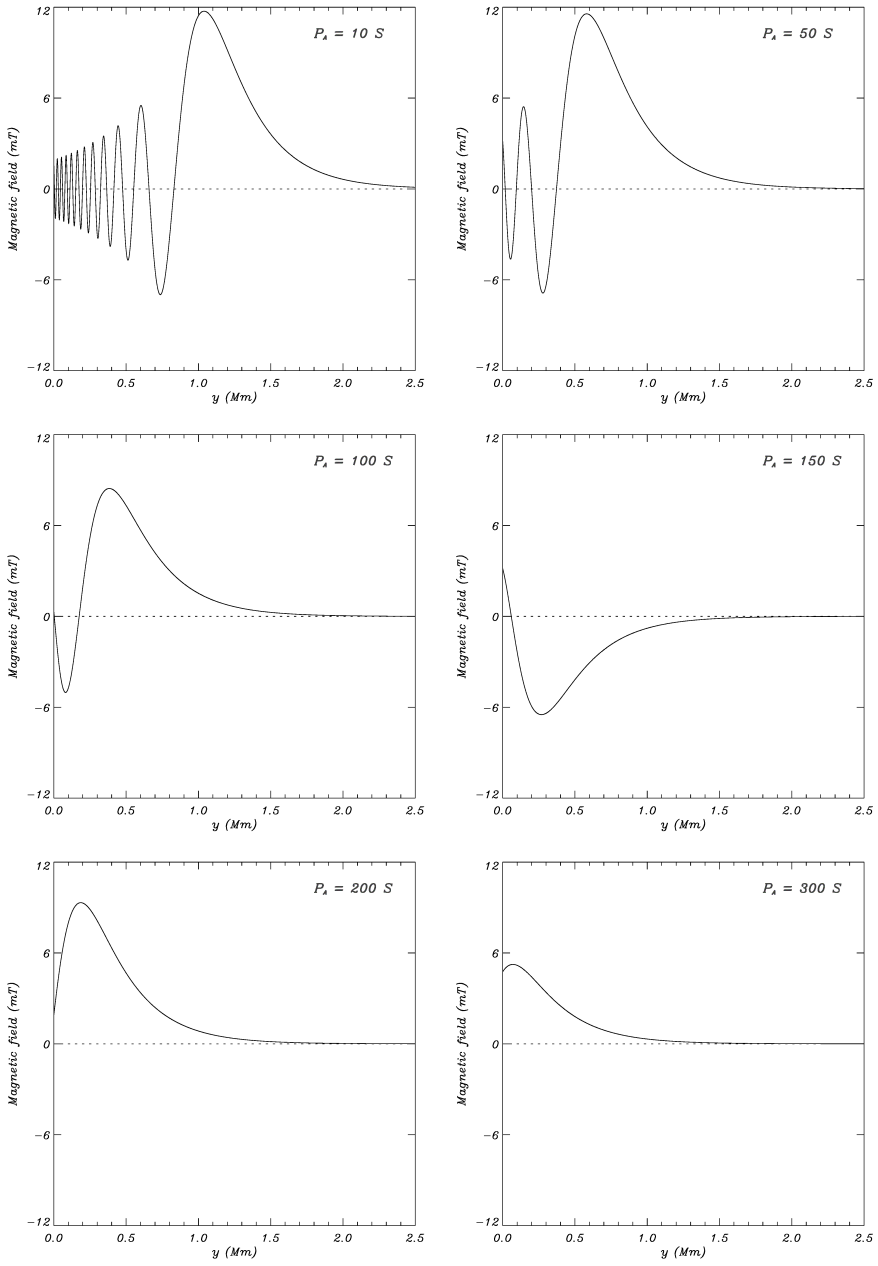

Figure 7.4: Plots of magnetic field perturbations ($\tilde{b}_z$) versus atmospheric heights ($y(Mm)$)

2. Hille's Kneser type oscillation criteria

Now let us consider the differential equation in the following form

$$u'' + c(x)u = 0 \ . \tag{7.30}$$

Let

$$\tilde{\omega}^* = \limsup_{x\to\infty} x^2 c(x) \ ,$$

and

$$\tilde{\omega}_* = \liminf_{x\to\infty} x^2 c(x) \ .$$

According to this theorem, the solutions of the differential equation given above are oscillatory (have infinite number of zeros) if $\tilde{\omega}_* > 1/4$ and non-oscillatory (no zeros at all) if $\tilde{\omega}^* < 1/4$; the solutions can also be either oscillatory or non-oscillatory if $\tilde{\omega}^* = \tilde{\omega}_* = 1/4$. When we compare this differential equation with Eq. (7.27) and Eq. (7.28), we determine $\tilde{\omega}*_v$ and $\tilde{\omega}*_b$, and obtain

$$\tilde{\omega}*_v = \frac{4H^2\omega^2}{C_{A0}^2 \exp 2} \ , \tag{7.31}$$

and

$$\tilde{\omega}*_b = \frac{4H^2\omega^2}{C_{A0}^2 \exp 2} - 1 \ . \tag{7.32}$$

and also $\tilde{\omega}_{*v} = 0$ and $\tilde{\omega}_{*b} = -\infty$ for the velocity and magnetic field, respectively. The theorem states that if $\tilde{\omega}* < 1/4$ the solutions are non-oscillatory. Hence we obtain the maximum frequency at which the corresponding solutions have no zeros at all. Also we obtain another result using the other condition in the theorem. If $\tilde{\omega}_* > 1/4$, the solutions are oscillatory. Since our results for both wave variables are less than $1/4$, we conclude that the solutions are not

oscillatory (no infinite number of zeros). This clearly shows that there are three types of solutions: oscillatory, non-oscillatory or it can be neither oscillatory nor non-oscillatory. We define the third type as a standing solution.

However, now we go back to the first condition and evaluate the minimum frequency of waves, which could have solutions with finite number of zeros given by

$$\omega_{0v} = \left(\frac{C_{A0}}{2H}\right) \frac{\exp 1}{2} \ , \tag{7.33}$$

$$\omega_{0b} = \left(\frac{C_{A0}}{2H}\right) \frac{\sqrt{5}\exp 1}{2} \ . \tag{7.34}$$

This means that all solutions with frequency greater than that of given above have finite number of zeros and below that frequency have at most one zero in the domain $(0, \infty)$.

Note that all the above conclusions are highly mathematical. In order to be oscillatory, it has to have infinite number of zeros within the considered range. The numerical results given in Figs. 7.3 and 7.4 clarify above conclusions.

The Figures 7.3 and 7.4 illustrate the solutions to Eqs (7.27) and (7.27) for the velocity and magnetic field, respectively. These figures clearly show that there are no infinite number of zeros in all panels for given frequencies. It also convinces that, even for higher (lower) frequencies (periods) than that of given in the figures, the solutions eventually become evanescent after showing number of oscillations. The range of oscillations depends upon the frequency of the wave. So, the wave shows infinite number of zeros i.e. becomes oscillatory according to mathematical definition, only when the frequency of the wave becomes infinity. This can also be proved by using the oscillation theorem as explained above: when $\omega_A \to \infty$ both $C_{v\infty}$ and $C_{b\infty}$

terms become infinity as well. Then according to the theorem, this implies that the solutions to Eqs (7.27) and (7.28) are oscillatory throughout the whole region and no local cutoff frequency is present for that particular case when $\omega_A = \infty$. This special case exists only in the mathematics and in the physical picture we cannot launch waves with frequency being infinity and this fact also proves that cutoff frequency effects all the waves with any frequency, at least for the model we consider in this chapter.

7.4.1 Wave equations in actual wave travel time

We already discussed in Chapter 4 how Alfvén wave equations can be transformed using actual wave travel time. We recall these Fourier transformed Alfvén wave equations and write them again here as

$$\frac{d^2\tilde{v}}{d\tau^2} + \left[\omega^2 - \Omega^2_{cr,v}(\tau)\right]\tilde{v} = 0 \,, \tag{7.35}$$

$$\frac{d^2\tilde{b}}{d\tau^2} + \left[\omega^2 - \Omega^2_{cr,b}(\tau)\right]\tilde{b} = 0 \,, \tag{7.36}$$

where

$$\Omega^2_{cr,v}(\tau) = \frac{1}{2}\left[\frac{3}{2}\left(\frac{C'_A(\tau)}{C_A(\tau)}\right)^2 - \frac{C''_A(\tau)}{C_A(\tau)}\right] \,, \tag{7.37}$$

and

$$\Omega^2_{cr,b}(\tau) = \frac{1}{2}\left[\frac{C''_A(\tau)}{C_A(\tau)} - \frac{1}{2}\left(\frac{C'_A(\tau)}{C_A(\tau)}\right)^2\right] \,. \tag{7.38}$$

Now we can evaluate τ for the isothermal solar atmosphere and obtain

$$\begin{aligned}\tau(y) &= \int_0^y \frac{d\tilde{y}}{C_A\tilde{y}} \,, \\ &= \frac{2H}{C_{A0}}\left(1-\exp\left(-\frac{y}{2H}\right)\right) \,,\end{aligned}$$

and hence we can calculate $C_A(\tau)$,$C'_A(\tau)$ and $C''_A(\tau)$ as follows

$$\begin{aligned}C_A(\tau) &= \frac{C_{A0}}{\left(1-\frac{C_{A0}}{2H}\tau\right)} \,, \\ C'_A(\tau) &= \frac{C_A^2}{2H} \,, \\ C''_A(\tau) &= \frac{C_A^3}{2H^2} \,.\end{aligned}$$

Using these we can obtain the most simplified critical frequencies $\Omega^2_{cr,v}(\tau) = -\left(C_A/4H\right)^2$ and $\Omega^2_{cr,b}(\tau) = 3\left(C_A/4H\right)^2$ for the velocity and magnetic field, respectively.

7.4.2 General Solutions and application of oscillation theorems

Now we can re-write Eq.(7.35) and Eq.(7.36) as

$$\left(1-\frac{C_{A0}}{2H}\tau\right)^2\tilde{v}'' + \left[\omega^2\left(1-\frac{C_{A0}}{2H}\tau\right)^2 + \frac{C_{A0}^2}{16H^2}\right]\tilde{v} = 0 \,, \tag{7.39}$$

$$\left(1-\frac{C_{A0}}{2H}\tau\right)^2\tilde{b}'' + \left[\omega^2\left(1-\frac{C_{A0}}{2H}\tau\right)^2 - \frac{3C_{A0}^2}{16H^2}\right]\tilde{b} = 0 \,. \tag{7.40}$$

Using the transformation

$$\tilde{\tau} = 1-\frac{C_{A0}}{2H}\tau \tag{7.41}$$

we can transform the differential equations for $\tilde{v}$ and $\tilde{b}$ as

$$\hat{v}(\tau)'' + \left[\left(\frac{2H\omega}{C_{A0}}\right)^2 + \frac{1}{4\tilde{\tau}^2}\right]\hat{v}(\tau) = 0\ , \tag{7.42}$$

$$\hat{b}(\tau)'' + \left[\left(\frac{2H\omega}{C_{A0}}\right)^2 - \frac{3}{4\tilde{\tau}^2}\right]\hat{b}(\tau) = 0\ . \tag{7.43}$$

Then we solve these two second order differential equations analytically and get

$$\hat{v}(\tilde{\tau}) = \sqrt{\tilde{\tau}}\left[C_4 J_0(\lambda\tilde{\tau}) + C_5 Y_0(\lambda\tilde{\tau})\right]\ , \tag{7.44}$$

$$\hat{b}(\tilde{\tau}) = \sqrt{\tilde{\tau}}\left[C_6 J_1(\lambda\tilde{\tau}) + C_7 Y_1(\lambda\tilde{\tau})\right] \tag{7.45}$$

where $\lambda = \frac{2H\omega}{C_{A0}}$ and C_4, C_5, C_6 & C_7 are arbitrary constants and can be evaluated when boundary conditions are introduced. $\tilde{\tau}$ goes from 1 to 0 when τ goes from 0 to τ_{max}, which is a finite positive value. So we must treat these two equations as bounded and then we have to choose the most applicable oscillation theorem to find global cutoff frequencies, which are similar to the case discussed in sec. 7.3. Since in both cases; Fearraro & Plumpton case and Eqs (7.42) and (7.43), the location of the boundaries are the same (0,1) and we can take the same differential equations to compare with, but not the equations including the first derivative as the Eqs (7.42) and (7.43) do not have the first derivative terms. So it is more appropriate to compare these with Eq. (7.23), which has solutions satisfying the boundary conditions $w(0) = w(1) = 0$.

After setting up the stage, we now apply Leighton's theorem as explained in sec. 7.3 and obtain the variational functions $V_v[w]$ and $V_b[w]$ for both the wave variables. Then we use the same procedure to find the minimum frequencies, which could make

above variational functions positive, as required by the theorem. Then we get the global cutoff frequencies for the velocity and magnetic field perturbations given by

$$\omega_{0v} = \frac{C_{A0}}{2H} Q_4 \ , \tag{7.46}$$

and

$$\omega_{0b} = \frac{C_{A0}}{2H} Q_5 \ , \tag{7.47}$$

where $Q_4 \approx 2.764413$ and $Q_5 \approx 4.068475$ and all the solutions with frequency greater than those global cutoff frequencies will have at least one zero within the interval (0,1).

Figures 7.5 and 7.6 present numerical solutions to differential equations given by Eqs (7.42) and (7.43) for four different frequencies below and above the analytically calculated global cutoff frequencies as shown by Eqs (7.46) and (7.47). The figures clearly illustrate that above the analytical cutoff frequency, the solutions do not have any zeros. The boundary conditions used to obtain these numerical results are also the same as in the sec. 7.2. Furthermore, we compare all these cutoff frequencies in summary section below.

7.5 Summary

It is clear that the cutoff frequencies discussed in Chapter 4 is different than the cutoff derived in this Chapter. The former was obtained by introducing the turning point frequencies, however, the latter was derived by using some oscillation theorems. To see how these cutoff frequencies work, we should first consider the global cutoff frequency; if $\omega_A > \omega_0$, the wave can be launched and once the wave is launched then

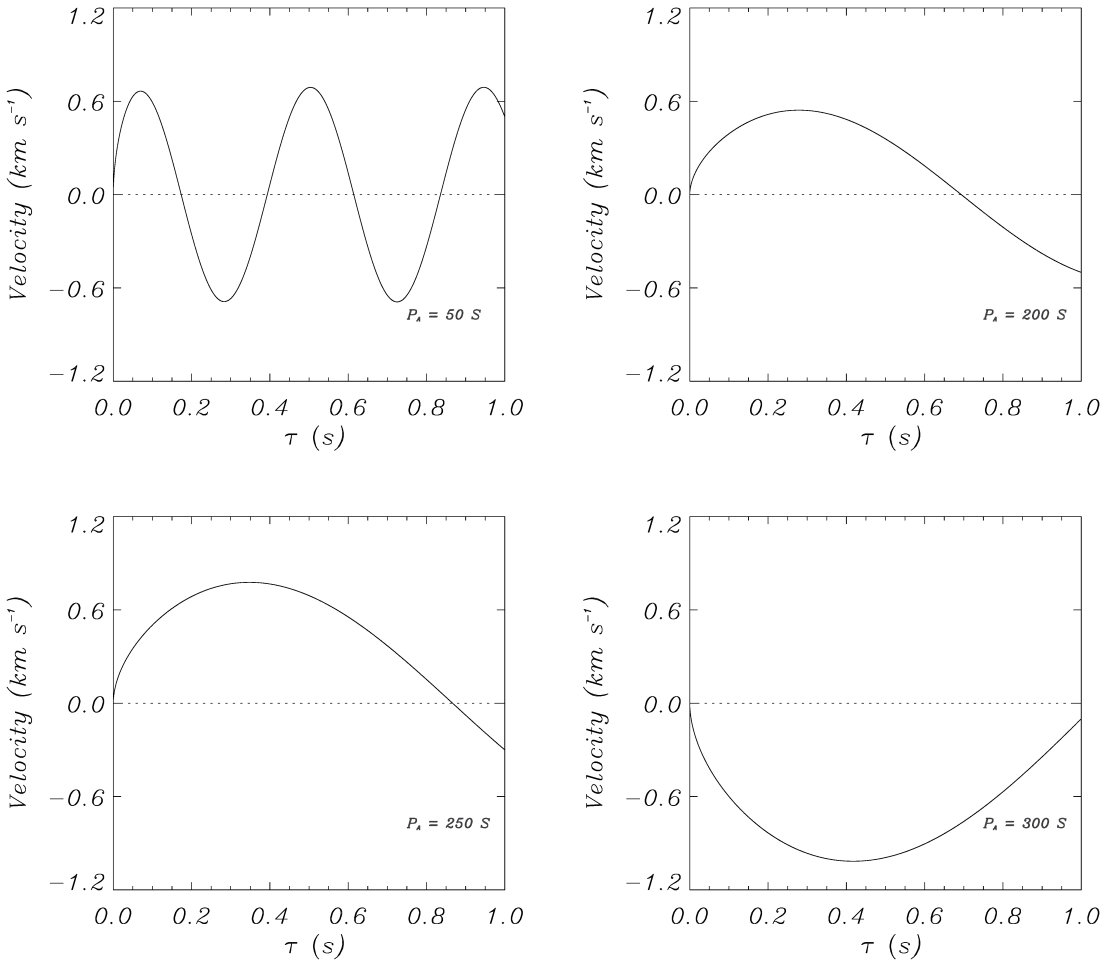

Figure 7.5: Plots of velocity perturbations ($\tilde{v}_z$) versus transformed actual wave travel time $\tilde{\tau}$ (s)

we calculate the other (local) cutoff frequency to see how far this wave will propagate in the solar atmosphere.

We first determined the so-called global cutoff frequencies for the Ferraro-Plumpton type equations comparing with three different differential equations. Then, we evaluated the cutoff frequencies for the velocity and magnetic field perturbations using the concepts of the approximate and actual wave travel times. The obtained results are summarized in Table 7.1.

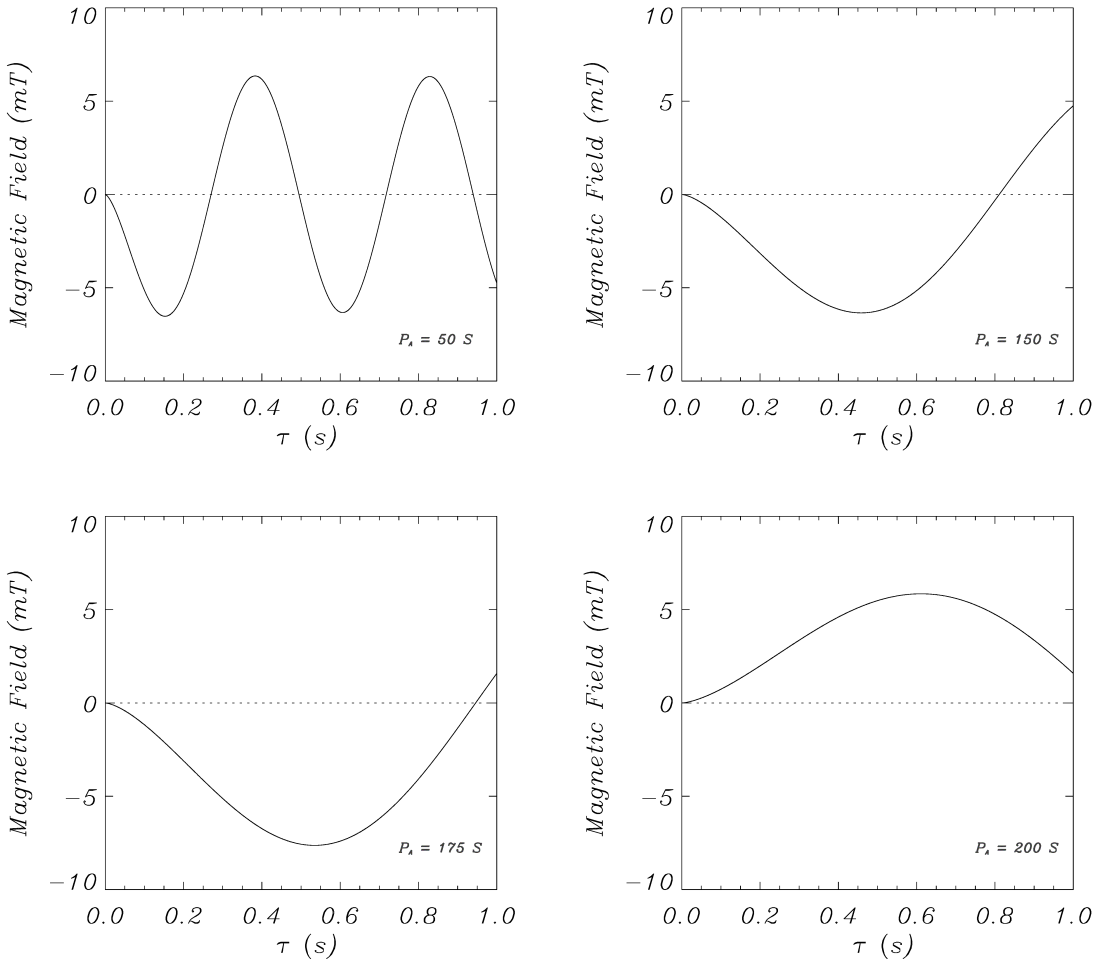

Figure 7.6: Plots of magnetic field perturbations ($\tilde{b}_z$) versus transformed actual wave travel time $\tilde{\tau}$ (s)

It is interesting that these global cutoff frequencies for both velocity and magnetic field perturbations are not the same but all three methods give comparable values for each variable. For velocity, method 1 & 2 gives closer values and the value obtained from method 3 is relatively off while for magnetic field, method 2 & 3 give similar values and method 1 gives a little bit higher value compare to the other two. Method 4 shows the cutoff frequencies in the y - space and method 5 shows the cutoff frequencies for the τ - space.

Table 7.1. Comparison of global cutoff frequencies

Method	ω_{0v} (s^{-1}) [P_{0v} (s)]	ω_{0b} (s^{-1}) [P_{0b} (s)]
1	0.034 [185]	0.044 [143]
2	0.035 [180]	0.038 [165]
3	0.028 [224]	0.038 [165]
4	0.025 [256]	0.036 [174]
5	0.012 [522]	0.027 [233]

Comparing all the values obtained for the cutoff frequencies, we conclude that there is a range of the global cutoff frequencies for each wave variable instead of a single value.

CHAPTER 8

ALFVÉN WAVES WITH DISPLACEMENT CURRENTS

8.1 Background and governing equations

Up to this point, we have talked about the situation when the displacement current (DC) was not included in the MHD equations (see Eqs 2.13 through 2.16). Now, we take the DC into account, derive the wave equations and apply the oscillation theorems. This would help us to understand the concept of cutoff frequencies for Alfvén waves with the DC. We follow Leroy (1983) and write the Ampere's law for perfectly conducting fluid in the following form:

$$\nabla \times \mathbf{B} = \frac{4\pi}{c}\mathbf{j} - \frac{1}{c^2}\frac{\partial}{\partial t}\left(\mathbf{V} \times \mathbf{B}\right) \ , \tag{8.1}$$

which can be re-arranged as

$$\mathbf{j} = \frac{c}{4\pi}\left[\nabla \times \mathbf{B} + \frac{1}{c^2}\frac{\partial}{\partial t}\left(\mathbf{V} \times \mathbf{B}\right)\right] \ , \tag{8.2}$$

and inserted into the conservation of momentum equation given by

$$\rho\left[\frac{\partial \mathbf{V}}{\partial t} + \left(\mathbf{V} \cdot \nabla\right)\right] = -\nabla p + \rho\mathbf{g} + \frac{1}{c}\left(\mathbf{j} \times \mathbf{B}\right) \ . \tag{8.3}$$

8.2 Wave equations in y space

The wave equations for the velocity and magnetic perturbations become

$$\frac{\partial^2 u}{\partial t^2} = V_{AC}^2 \frac{\partial^2 u}{\partial y^2} \ , \tag{8.4}$$

and

$$\frac{\partial^2 b}{\partial t^2} = \frac{\partial}{\partial y}\left(V_{AC}^2 \frac{\partial b}{\partial z} \right) \ , \tag{8.5}$$

where now $V_{AC}^2 = C_A^2 / \left(1 + C_A^2/c^2\right)$.

In this model the gas density drops to zero as y goes to infinity and, as a result, the Alfvén velocity C_A goes to infinity, however, $V_{AC}^2 \to c$ when C_A becomes very large, which implies that the wave is propagating with the speed of light c; this does not mean that Alfvén waves turn into pure electromagnetic waves. Note also that in the limit of $C_A << c$, $V_{AC} \approx C_A$, and the wave equations are reduced to Eqs (4.1) and (4.2), respectively, which is the case without the DC.

Now we can eliminate the first derivative from Eq. (8.5) by using the transformation $b(y,t) = b_1(y,t) exp\left[-\int^y 1/2H d\tilde{y}\right]$ and then making the Fourier transform in time by taking $u(y,t) = \tilde{u}(y) \exp -i\omega t$ and $b_1(y,t) = \tilde{b}(y) \exp -i\omega t$. We obtain the following wave equations:

$$\frac{d^2\tilde{u}}{dy^2} + \frac{\omega^2}{V_{AC}^2}\tilde{u} = 0 \ , \tag{8.6}$$

$$\frac{d^2\tilde{b}}{dy^2} + \left(\frac{\omega^2 - \Omega_{crit}^2}{V_{AC}^2} \right) \tilde{b} = 0 \ , \tag{8.7}$$

where $\Omega_{crit}^2 = V_{AC}^2 / 4H^2$.

8.2.1 Oscillation Theorems

Let us re-write Eqs (8.6) and (8.7) by taking $C_{\tilde{u}}(y) = \omega^2/V_{AC}^2$ and $C_{\tilde{b}}(y) = (\omega^2 - \Omega_{crit}^2)/V_{AC}^2$. The results are:

$$\frac{d^2\tilde{u}}{dy^2} + C_{\tilde{u}}(y) = 0 \ , \tag{8.8}$$

$$\frac{d^2\tilde{b}}{dy^2} + C_{\tilde{b}}(y) = 0 \ . \tag{8.9}$$

In order to apply oscillation theorems we should first check whether the functions $C_{\tilde{u}}(y)$ and $C_{\tilde{b}}(y)$ are positive or not. Note that $C_{\tilde{u}}(y)$ is always positive, regardless the value of ω, but $C_{\tilde{b}}(y)$ can be either negative or positive depending on the value of ω. If $\omega \geq c/2H$ then $C_{\tilde{b}}(y) > 0$ and if $\omega < c/2H$, then $C_{\tilde{b}}(y) < 0$. Again if $C_{\tilde{b}}(y) < 0$, then the solutions of Eq. (8.7) is always non-oscillatory (Kneser's non oscillation theorem). From this point on, we assume $C_{\tilde{b}}(z)$ is positive.

We take $g_u(y) = y\int_y^\infty C_{\tilde{u}}(t)dt$ and $g_b(y) = y\int_z^\infty C_{\tilde{b}}(t)dt$ and find that both $g_u(y)$ and $g_b(y)$ are infinite and so are g_{u*} , g_{b*} ,g_u^* and g_b^*. According to the theorem, if $g_* > 1/4$ the differential equation has oscillatory solutions. Therefore both Eqs (8.6) and (8.7) have oscillatory solutions.

Nehari's Theorem (Nehari (1954)):

Consider the oscillatory Euler equation $u'' + \gamma(x+1)^{-1}u = 0$ when $\gamma > 1/4$. Let $\gamma = \mu = 1$. Here the theorem explains in terms of $h(x), h_*$ and h^*, where $h(x)$ is defined by

$$h(x) = \int_x^\infty \tilde{c}(t)dt / \int_x^\infty \tilde{C}(t)dt \ , \tag{8.10}$$

and the numbers h_* and h^* are defined by

$$h_* = \liminf_{x\to\infty} h(x) \ , \tag{8.11}$$

$$h^* = \limsup_{x\to\infty} h(x) \ . \tag{8.12}$$

When we apply our functions we get $h_u(z), h_b(z) = \infty$ and then $h_{u*}, h_{b*}, h_u^*, h_u^* = \infty$. According to the theorem, if $h_* > \mu$ then the solutions are oscillatory. Therefore, both Eqs (8.6) and (8.7) have oscillatory solutions.

Leighton's Oscillation Theorem (Leighton (1962)):

As described in Chapter 6, for this case we have $a(x) = 1$ and hence $a_\infty = \infty$ and $C_{\tilde{u}}$ and $C_{\tilde{b}}$ are continuous functions in this interval. Now, we can calculate C_∞'s and $C_{\tilde{b}\infty}, C_{\tilde{b},\infty} = \infty$. Then according to the theorem, those two equations have oscillatory solutions. Note that $\tilde{c}(x)$ is not required to be positive for these theorems, which means that the solutions to these equations are always oscillatory regardless of the value of ω.

8.2.2 General Solutions

To get the general solutions let us re-write Eqs (8.6) and (8.7) by using the transformation $\eta = \exp(-y/H)$, and obtain

$$\eta^2 \frac{d^2\tilde{u}}{d\eta^2} + \eta \frac{d\tilde{u}}{d\eta} + \left(\frac{4H^2\omega^2}{c^2} + \frac{4H^2\omega^2}{C_{A0}^2}\eta \right) \tilde{u} = 0 \ , \tag{8.13}$$

$$\eta^2 \frac{d^2\tilde{b}}{d\eta^2} + \eta \frac{d\tilde{b}}{d\eta} + \left[\left(\frac{4H^2\omega^2}{c^2} - 1 \right) + \frac{4H^2\omega^2}{C_{A0}^2}\eta \right] \tilde{b} = 0 \ . \tag{8.14}$$

which has the solutions in the form of Bessel functions and they can be written as

$$\tilde{u}(\eta) = C_1 J_{i\mu}\left(\frac{4H\omega}{C_{A0}}\eta^{1/2}\right) + C_2 J_{-i\mu}\left(\frac{4H\omega}{C_{A0}}\eta^{1/2}\right) \ , \tag{8.15}$$

$$\tilde{b}(\eta) = C_3 J_{i\nu}\left(\frac{4H\omega}{C_{A0}}\eta^{1/2}\right) + C_4 J_{-i\nu}\left(\frac{4H\omega}{C_{A0}}\eta^{1/2}\right) \ , \tag{8.16}$$

where $\mu = 4H\omega/c$ and $\nu = 2\sqrt{4H^2\omega^2\ c^2 - 1}$. C_1, C_2, C_3 and C_4 are integration constants.

We may calculate integration constants by using the boundary conditions imposed in Leroy's paper. Since the waves are propagating with the speed of light, they cannot reach infinity in a finite time, thus there is no reflection at infinity imposed by the boundary conditions (see Cally (2012)); hence, $C_2, C_4 = 0$. Also using the other boundary condition given in the paper and modifying according to our situation we finally obtain

$$\tilde{u}(y) = u_0 \frac{J_{i\mu}\left(\frac{4H\omega}{C_{A0}} exp(-y/2H)\right)}{J_{i\mu}\left(4H\omega/C_{A0}\right)} \ , \tag{8.17}$$

$$\tilde{b}(y) = b_0 \frac{J_{i\nu}\left(\frac{4H\omega}{C_{A0}} exp(-y/2H)\right)}{J_{i\nu}\left(4H\omega/C_{A0}\right)} \ , \tag{8.18}$$

where u_0 and b_0 are the amplitudes of the velocity and magnetic field perturbations respectively, at $y = 0$.

8.3 Summary

We modified the original ideal MHD equations by taking into account the displacement current (DC). The wave equations describing Alfvén waves with the DC were derived and several oscillations theorems were applied to determine whether the solutions were oscillatory or non-oscillatory. As expected, only oscillatory solutions

were found. This result is consistent with the physics of the problem as in the model with the DC Alfvén waves are always propagating waves and their speed of propagation is finite and reaches the speed of light in the solar atmospheric models considered in this PhD dissertation.

CHAPTER 9

CONCLUSIONS AND FUTURE WORK

9.1 Conclusions

A study of propagation of linear Alfvén waves in the solar atmosphere with uniform vertical magnetic field has been performed analytically and numerically. Both isothermal and non-isothermal models were considered. The analytical results showed that Alfvén waves have the cutoff frequencies and the numerical results confirmed that they depend on the wave variable chosen to describe the waves. The study has been done by refining both analytical and numerical methods, including a temperature distribution characteristic for the solar chromosphere, transition region and corona, and considering the sinusoidally generated waves. The main analytical result is that the cutoff frequencies obtained with the approximate and actual wave travel time are local quantities and their variations with height are used to identify regions in the solar atmosphere where waves change their behavior from oscillatory to non-oscillatory. To verify this prediction of the analytical theory, the resulting wave equations have been solved numerically and compared to the results of numerical simulations with those obtained analytically. The numerical results were obtained for the finite time wave propagation while the analytical results were obtained for the infinite time Fourier transformed wave equations; it was demonstrated that the height at which the turning point is located depends on the frequency of the excited wave. A good agreement between the analytical predictions of the atmospheric height at which the wave become evanescent and the numerical results have been found.

One of the main results of this PhD dissertation is that there is no one unique cutoff frequency for Alfvén waves, but instead there is a number of cutoffs whose specific forms depend on the methods used to define them as well as on the choice of the wave variable used to describe the waves. We used the cutoffs to establish a range of frequencies corresponding to the propagating Alfvén waves and compared it to some recent solar observations of these waves. The results presented in this PhD dissertation give strong evidence for the existence of cutoff frequencies for Alfvén waves propagating in both isothermal and more realistic non-isothermal solar atmospheres.

Another important result of this PhD dissertation is the global cutoff frequency obtained using different applicable oscillation theorems. This study was done for Alfvén waves propagating in the isothermal atmosphere for the velocity and magnetic field perturbations. It showed the existence of the global cutoff frequency and demonstrated that this cutoff frequency is different than the other (local) cutoff frequencies. Different methods along with applicable oscillation theorems have been used to obtain global cutoff frequencies and the obtained results showed that a range of frequencies can be uniquely defined using these cutoffs.

Finally, the original ideal MHD equations were modified by taking into account the displacement current (DC). The wave equations describing Alfvén waves with the DC were derived and several oscillations theorems were applied to determine whether the solutions were oscillatory or non-oscillatory. As expected, only oscillatory solutions were found. This result is consistent with the physics of the problem because in the model with the DC, Alfvén waves they are always propagating waves and their speed of propagation are finite; they do reach the speed of light in the considered solar models.

9.2 Future Work

The method developed in this PhD dissertation will be used to obtain the cutoff frequencies for the semi-empirical model developed by Avrett & Loeser (2008), and the theoretical predictions based on this model will be compared with the recent solar observations of Alfvén waves.

The sinusoidally generated waves will be replaced with more realistic randomly generated trains of pulses with known range of frequencies instead of one monochromatic wave frequency.

All studies performed in this PhD dissertation are one-dimensional (1D) and linear, which is well-justified by the physical properties of the considered Alfvén waves. However, there are well known Alfvén-like (torsional and transverse) waves in solar magnetic flux tubes and studies of such waves require 2D and 3D treatments. Moreover, nonlinear phenomena are commonly present and their effects on the wave propagation should be explored numerically. Therefore, one of the important future steps in investigating the propagation of Alfvén waves in the solar atmosphere is to take into account both 2D and 3D magnetic structures, and to include nonlinear effects.

APPENDIX A

NUMERICAL CODE : CLAWPACK VERSION 4.0

```
      program driver_com
c
c  Generic driver routine for claw1ez
c
c  Author: Randall J. LeVeque
c  Version of March, 1999 --  CLAWPACK Version 4.0
c
c
      implicit double precision (a-h,o-z)

c     # set parameters for maximum array sizes used in declarations
c     # these must be increased for larger problems.
c
c
      parameter (maxmx = 40000)
      parameter (mwork = 640064)

      parameter (mbc = 2)
      parameter (meqn = 2)
      parameter (mwaves = 2)
      parameter (maux = 2)
c
      dimension q(1-mbc:maxmx+mbc, meqn)

      dimension  aux(1-mbc:maxmx+mbc, maux)

      dimension work(mwork)
      dimension mthlim(mwaves)

      open(11,file='ts.dat',status='unknown',form='formatted')

      call claw1ez(maxmx,meqn,mwaves,mbc,maux,mwork,mthlim,
     &           q,work,aux)

      close(11)

      stop
      end
c
c
c =========================================================
       subroutine qinit(maxmx,meqn,mbc,mx,xlower,dx,q,maux,aux)
c =========================================================
c
c     # Set initial conditions for q.
c     # Pulse in pressure, zero velocity
c
c
      implicit double precision (a-h,o-z)
      dimension q(1-mbc:maxmx+mbc, meqn)
      dimension aux(1-mbc:maxmx+mbc, *)
      common /cqinit/ beta,ic,i_d
      common /driver/ omega_d, period_d
c
c
      pi  = 4.*datan(1.d0)
      x_d = 5.0d-1 ! detection point
```

```
      i_d = (x_d-(xlower+0.5*dx))/dx
      print*,'  x_d = ', xlower + (i_d-0.5d0)*dx

!      period_d = 2.0                !  waveperiod       of the driver
      period_d = 50.0               !  waveperiod       of the driver
!      period_d = 0.5                !  waveperiod       of the driver
      omega_d  = 2.*pi / period_d   !  cyclic frequency of the driver

c      x0  = 0.00  !  initial position of the pulse
      x0  = 0.05 * (xlower + (mx-0.5d0)*dx)  !  initial position of the pulse
      wpx = 0.3   !  width of the initial pulse, in x, in units of 10^6 m


      do 150 i=1,mx
         xcell = xlower + (i-0.5d0)*dx

c         go to (10,20,30) ic


c   10    continue
c         # half ellipse:
c         if (xcell.gt.-4d0 .and. xcell.lt.-2d0) then
c             q(i,1) = dsqrt(1.d0 - (xcell+3.d0)**2)
c            else
c             q(i,1) = 0.d0
c            endif
c         q(i,2) = q(i,1)
c         go to 150
c
c   20    continue
c         # single discontinuity:
c         if (xcell .lt. -2.d0) then
c             q(i,1) = 1.d0
c            else
c             q(i,1) = 0.d0
c            endif
c         q(i,2) = q(i,1)
c         go to 150

c   30    continue
c         # Gaussian and square pulse:
c         q(i,1) = dexp(-beta*(xcell+2.0d0)**2)
c         if (dabs(q(i,1)) .lt. 1d-30) q(i,1) = 0.d0
c         if (xcell.gt.-4.d0 .and. xcell.lt.-3.d0) then
c            q(i,1) = q(i,1) + 0.5d0
c            endif
c         q(i,2) = q(i,1)
c         go to 150

c         q(i,2) = dexp(-(xcell/wpx)**2)             !  V_theta
c         q(i,2) = -dsin(0.5*pi/xlower*(xcell-xlower))     !  V_theta

c         q(i,2) = dsin(omega_d*xcell)
         q(i,1) = 0.d0                                    !  B_theta
c         q(i,2) = 0.d0                                     !  V_theta
c         if(xcell.lt.1.5)
c         q(i,2) = dexp(-(((xcell-x0)/wpx)**2))             !  V_theta
```

```
c        q(i,1) = -dexp(-(((xcell-x0)/wpx)**2))             !  B_theta
        q(i,2) = 0.d0                                     !  V_theta
c

  150    continue
c
      return
      end
c
c
c     =============================================
      subroutine setaux(maxmx,mbc,mx,xlower,dx,maux,aux)
c     =============================================
c
c     # set auxiliary arrays
c     # variable coefficient acoustics
c     #  aux(i,1) = impedance Z in i'th cell
c     #  aux(i,2) = sound speed c in i'th cell
c
c     # Piecewise constant medium with single interface at x=0
c     # Density and sound speed to left and right are set in setprob.f
c
c
      implicit double precision (a-h,o-z)
      real*8 mean_mass, int_1, int_2, masde_ref_lvl, p_cor
      real*8 H, H_Mm, rho0_Mm, mu0, mu0_Mm, c_s0, time_inf
      dimension aux(1-mbc:maxmx+mbc, 2)
      common /comaux/ rhol,cl,rhor,cr

      open(unit=31,file='fort.aux',status='unknown',form='formatted')
c
c****************************** for normalization
******************************
c****************************** to chromospheric values
******************************

c       r0          = 5.e+5       ! a unit of length, in m
c       V0          = 1.e+4       ! velocity unit = Alfven speed, in m/s
c       t0          = r0 / V0      ! time unit
c       rho0  = 2.e-4             ! mass density unit, in kg/m^3
c      p0    = rho0*V0*V0         ! pressure unit, in Pa
c      B0    = sqrt(rho0)*V0      ! B unit, in T
c       Temp0 = 6.e+3              ! temperature unit, in K

c      grav_phys   = 274.0        ! gravity acceleration, in m/s^2
c       grav = t0*grav_phys/V0     ! normalized gravity
      p_cor = 0.01               ! normalized gas pressure in the solar
corona
c*********************************************************************************
******

c      sim_gamma = 5./3.
       Boltzman  = 1.3807e-23               ! Boltzman constant, in J/K
       mean_mass = 1.27*1.6726e-27          ! mean mass
       grav_phys   = 274.0                  ! gravity acceleration, in m/s^2
c       Temp0 = 5.e+3
c       rho0  = 1.e-4
```

```
       mu0   = 1.25664e-6        ! T.m/A
       mu0_Mm = 1.25664e-12      ! T.Mm/A

       y0_Mm          = 1.d0        ! reference level in Mm
       r0          = 5.e+3       ! a unit of length, in m
       V0          = 1.e+4       ! velocity unit = Alfven speed, in m/s
       t0          = r0 / V0      ! time unit
       rho0  = 2.e-4             ! mass density unit, in kg/m^3
       rho0_Mm = rho0 * 1.e18    ! mass density in kg/Mm^3

c      p0    = rho0*V0*V0         ! pressure unit, in Pa
c      B0    = sqrt(rho0)*V0      ! B unit, in T
       Temp0 = 5.e+3              ! temperature unit, in K

c      grav_phys   = 274.0        ! gravity acceleration, in m/s^2
c       grav = t0*grav_phys/V0

       H0  = Boltzman * Temp0 / (mean_mass * grav_phys)  ! Scale height at
reference level, in m
       H0_Mm = H0 * 1.e-6                                ! Scale height at
reference level , in Mm

      coef_p   = mean_mass*grav_phys*r0 / (Boltzman*Temp0)  ! coefficient for
the pressure profile (Mm^-1)
      coef_rho = 1.e+12 * coef_p / grav_phys                ! coefficient for
the rho profile (Mm)

       B_cor = 0.0015
       c_s0 = B_cor / dsqrt( rho0_Mm * mu0_Mm)
       time_inf = 2*H0_Mm/c_s0

c      print*,'  coef_rho  = ', coef_rho
       print*,'  H0  = ', H0_Mm
       print*,'  rho0  = ', rho0_Mm
       print*,'  c_s0  = ', c_s0
       print*,'  time to reach infinity  = ', time_inf


      y_ref_lvl = 1.0e+1             ! reference level for coronal plasma
c      v_Acor =   1.0e+6              ! Alfven speed in the solar corona, in
m/s
c      c_scor = 100.0e+3              ! sound  speed in the solar corona, in
m/s
cc     c_sph  =  c_scor/10.           ! sound  speed in the solar
photosphere, in m/s
c      beta = 2.*c_scor*c_scor / v_Acor / v_Acor / sim_gamma
c      B_cor = dsqrt(2.*p_cor/beta)   ! B at y=y_ref_lvl



cc      B_cor  =   B_cor  * 10. /8.
c      print*,'  beta = ', beta
c      print*,'  p_cor = ', p_cor
c      print*,'  B_cor = ', B_cor

cc     tem_rat = (c_sph/c_scor)**2   ! temperature ratio: T_ph / T_corona
      tem_rat = 1./200.            ! temperature ratio: T_ph / T_corona
```

```
c      c_sph  = sqrt(tem_rat)*c_scor ! sound  speed in the solar photosphere,
in m/s
cc      print*,'  c_sph  = ', c_sph
      y_w     = 2.0e-1              ! width of the transition region  !!!
decreasing this may end up with numerical problems
c!      y_w     = 1.0e-1              ! width of the transition region  !!!
decreasing this may end up with numerical problems
      y_t     = 2.00                ! location of the transition region
      y_s     = y_ref_lvl           ! reference level
      y_sn    = (y_s - y_t) / y_w   ! normalized reference level
      int_2   = y_w/(2.*tem_rat) * ( 2.*y_sn + (tem_rat-1.)*
     &           dlog(tem_rat+dexp(2.*y_sn)) )   !  integral at y_sn

c      print*,'   int_2 = ', int_2


c mass density and gas pressure at reference level
c      yi = (y_ref_lvl - y_t) / y_w
c      int_1 = y_w/(2.*tem_rat) * ( 2.*yi + (tem_rat-1.)
c     &       *dlog(tem_rat+dexp(2.*yi)) )
c      press_ref_lvl =  p_cor * dexp( -coef_p*(int_1-int_2) )
c      help = dexp(2.*yi)
c      masde_ref_lvl = press_ref_lvl*coef_rho*(help+1.)/(help+tem_rat)

c       print*,'  p_cor  = ', p_cor

       do i=1-mbc,mx+mbc
c
          xcell = xlower + (i-0.5d0)*dx
c          yy = (xcell - y_t) / y_w

          yy  = xcell
          yi = (yy - y_t) / y_w
          int_1 = y_w/(2.*tem_rat) * ( 2.*yi + (tem_rat-1.)*
     &           dlog(tem_rat+dexp(2.*yi)) )

          pres =  p_cor * dexp( -coef_p*(int_1-int_2) )
          help = exp(2.*yi)
          rho = pres*coef_rho*(help+1.)/(help+tem_rat)
          c_s = B_cor / dsqrt(rho*mu0_Mm)
c          rho = pres*coef_rho / dsqrt(1.+dabs(xcell))
c          c_s = (B_cor * exp (dabs(xcell)/(2*H))) /dsqrt(rho0*mu0)

c        Rho from Matlab!
c           rho = ((0.0002905527926*dexp(-0.04213967987*xcell)*
c     &          (1598123445.0*dtanh(5.0*xcell - 10.0) +
c     &          1614184988.0)**(0.8385795855))/((0.003234837103*
c     &          dtanh(5.0*xcell - 10.0) + 0.003267348031)*
c     &          (dtanh(5.0*xcell - 10.0) + 1.0)**(0.8385795855)))

c           c_s = B_cor / dsqrt( rho*mu0_Mm )

c       rho = 1.0 / (1.+dabs(xcell))**1.95
c          rho = rho0
c          c_s = B_cor / dsqrt(rho)
```

```
c          print*,'  c_s  = ', c_s
c          print*,'  rho  = ', rho
c  ---------------------------------------
c  specific conditions for p to propagate
cc          c_s = (xcell/((xlower + (mx-0.5d0)*dx)*0.1)) **( 2./3.)
cc          rho = (xcell/((xlower + (mx-0.5d0)*dx)*0.1)) **(-4./3.)
c          c_s = (5.*xcell) **( 2./3.)
c          rho = (5.*xcell) **(-4./3.)
c  ---------------------------------------

c  ---------------------------------------
c  specific conditions for V to propagate
c          c_s = (xcell/(xlower + (mx-0.5d0)*dx)) **( 2.)
c          rho = (xcell/(xlower + (mx-0.5d0)*dx)) **(-4.)
c  ---------------------------------------

          aux(i,1) = rho*c_s
          aux(i,2) = c_s
c
          enddo

        write(31,*) mx
        do i=1,mx
          xcell = xlower + (i-0.5d0)*dx

c          print*,'xcell,aux(i,1)/aux(i,2),aux(i,2)=',xcell,
c     &           aux(i,1)/aux(i,2), aux(i,2)
          write(31,701) xcell, aux(i,1)/aux(i,2), aux(i,2)
  701     format(3f16.6)
          enddo

       close(unit=31)
c
       return
       end
c
c
c     =====================================================================
      subroutine bc1(maxmx,meqn,mbc,mx,xlower,dx,q,maux,aux,t,dt,mthbc)
c     =====================================================================
c
c     # Standard boundary condition choices for claw2
c
c     # At each boundary  k = 1 (left),  2 (right):
c     #   mthbc(k) =  0  for user-supplied BC's (must be inserted!)
c     #            =  1  for zero-order extrapolation
c     #            =  2  for periodic boundary coniditions
c     #            =  3  for solid walls, assuming this can be implemented
c     #                  by reflecting the data about the boundary and then
c     #                  negating the 2'nd component of q.
c     ------------------------------------------------
c
c     # Extend the data from the computational region
c     #      i = 1, 2, ..., mx2
c     # to the virtual cells outside the region, with
c     #      i = 1-ibc  and   i = mx+ibc   for ibc=1,...,mbc
c
```

```
      implicit double precision (a-h,o-z)
      dimension q(1-mbc:maxmx+mbc, meqn)
      dimension aux(1-mbc:maxmx+mbc, *)
      dimension mthbc(2)

      integer*4  iflag/0/
      real*8  v(100),x(100)

      common /driver/ omega_d, period_d

c      print*,'  omega_d = ', omega_d
c      print*,'        t = ', t

c
c
c-----------------------------------------------------
c     # left boundary:
c-----------------------------------------------------
      go to (100,110,120,130,140) mthbc(1)+1
c
  100 continue
c     # user-specified boundary conditions go here in place of error output
c      write(6,*) '*** ERROR *** mthbc(1)=0 and no BCs specified in bc1'
c      stop
      do 105 m=1,meqn
         do 105 ibc=1,mbc
               q(1-ibc,m) = q(ibc,m)
  105       continue
c     # the normal velocity is represented by a periodic driver
c      if(t.gt.3.*period_d) go to 199

c     # random train of pulses

c        do 106 ibc=1,mbc
c          do i = 1, 100
c           x(i) = (i-1)*5.d-2
c           v(i) = drand( iflag )

c           if ( v(i) .lt. 7.5d-1 ) then
c             v(i) = 0.d0
c           else
c             v(i) = dsin((1/v(i))*x(i))
c             if ( v(i) .lt. 0.d0 ) then
c               v(i) = 0.d0
c             endif
c           endif
c           q(1-ibc,2)=v(i)
c           t=x(i)
c        enddo


c  106   continue

c      # Sinusoidal driver
          do 106 ibc=1,mbc
              q(1-ibc,2) =1.e-4 * dsin(omega_d * t)
```

```
c     # the half rectifying driver
c         do 106 ibc=1,mbc
c            if ( dsin(omega_d * t) .lt. 0.d0) then
c                q(1-ibc,2) = 0.d0
c             else
c                q(1-ibc,2) = dsqrt( dsin(omega_d * t) )
c             endif

c         do 106 ibc=1,mbc
c             q(1-ibc,2) = 0.d0

  106      continue


      go to 199
c
  110 continue
c     # zero-order extrapolation:
      do 115 m=1,meqn
         do 115 ibc=1,mbc
               q(1-ibc,m) = q(1,m)
  115       continue
      go to 199

  120 continue
c     # periodic:
      do 125 m=1,meqn
         do 125 ibc=1,mbc
               q(1-ibc,m) = q(mx+1-ibc,m)
  125       continue
      go to 199

  130 continue
c     # solid wall (assumes 2'nd component is velocity or momentum in x):
      do 135 m=1,meqn
         do 135 ibc=1,mbc
               q(1-ibc,m) = q(ibc,m)
  135       continue
c     # negate the normal velocity:
      do 136 ibc=1,mbc
            q(1-ibc,2) = -q(ibc,2)
  136    continue
      go to 199

  140 continue

c     # line-tying (assumes 2'nd component is velocity or momentum in x):
      do 145 m=1,meqn
         do 145 ibc=1,mbc
               q(1-ibc,m) = q(ibc,m)
  145       continue
c     # zero the normal velocity:
      do 146 ibc=1,mbc
            q(1-ibc,2) = 0.d0
  146    continue
      go to 199
```

```
  199 continue

c
c-----------------------------------------------------
c     # right boundary:
c-----------------------------------------------------
      go to (200,210,220,230,240) mthbc(2)+1
c
  200 continue
c     # user-specified boundary conditions go here in place of error output
      write(6,*) '*** ERROR *** mthbc(2)=0 and no BCs specified in bc2'
      stop
      go to 299

  210 continue
c     # zero-order extrapolation:
      do 215 m=1,meqn
         do 215 ibc=1,mbc
               q(mx+ibc,m) = q(mx,m)
  215       continue
      go to 299

  220 continue
c     # periodic:
      do 225 m=1,meqn
         do 225 ibc=1,mbc
               q(mx+ibc,m) = q(ibc,m)
  225       continue
      go to 299

  230 continue
c     # solid wall (assumes 2'nd component is velocity or momentum in x):
      do 235 m=1,meqn
         do 235 ibc=1,mbc
               q(mx+ibc,m) = q(mx+1-ibc,m)
  235       continue
      do 236 ibc=1,mbc
            q(mx+ibc,2) = -q(mx+1-ibc,2)
  236    continue
      go to 299

  240 continue
c     # line-tying (assumes 2'nd component is velocity or momentum in x):
      do 245 m=1,meqn
         do 245 ibc=1,mbc
               q(mx+ibc,m) = q(mx+1-ibc,m)
  245       continue
      do 246 ibc=1,mbc
            q(mx+ibc,2) = 0.d0
  246    continue
      go to 299

  299 continue
c
      return
      end
c
```

```
c
c
c     =====================================================
      subroutine rp1(maxm,meqn,mwaves,mbc,mx,ql,qr,auxl,auxr,
     &                   wave,s,amdq,apdq)
c     =====================================================
c
c     # Riemann solver for the acoustics equations in 1d, with
c     #  variable coefficients (heterogeneous media)
c
c     # auxl(i,1) should contain the impedance Z in cell i
c     # auxl(i,2) should contain the sound speed c in cell i
c
c     # On input, ql contains the state vector at the left edge of each cell
c     #           qr contains the state vector at the right edge of each cell
c
c     # On output, wave contains the waves,
c     #            s the speeds,
c     #
c     #            amdq = A^- Delta q,
c     #            apdq = A^+ Delta q,
c     #                   the decomposition of the flux difference
c     #                       f(qr(i-1)) - f(ql(i))
c     #                   into leftgoing and rightgoing parts respectively.
c     #
c
c     # Note that the i'th Riemann problem has left state qr(i-1,:)
c     #                                    and right state ql(i,:)
c     # From the basic clawpack routines, this routine is called with ql = qr
c
c
      implicit double precision (a-h,o-z)
c
      dimension auxl(1-mbc:maxm+mbc, 2)
      dimension auxr(1-mbc:maxm+mbc, 2)
      dimension wave(1-mbc:maxm+mbc, meqn, mwaves)
      dimension    s(1-mbc:maxm+mbc, mwaves)
      dimension   ql(1-mbc:maxm+mbc, meqn)
      dimension   qr(1-mbc:maxm+mbc, meqn)
      dimension apdq(1-mbc:maxm+mbc, meqn)
      dimension amdq(1-mbc:maxm+mbc, meqn)
      common /comlim/ mylim,mrplim(2)
c
c     local arrays
c     ------------
      dimension delta(2)
c
c
c     # split the jump in q at each interface into waves
c
c     # find a1 and a2, the coefficients of the 2 eigenvectors:
      do 20 i = 2-mbc, mx+mbc
         delta(1) = ql(i,1) - qr(i-1,1)
         delta(2) = ql(i,2) - qr(i-1,2)

c        # impedances:
         zi = auxl(i,1)
```

```
         zim = auxl(i-1,1)

         a1 = (-delta(1) + zi*delta(2)) / (zim + zi)
         a2 =  (delta(1) + zim*delta(2)) / (zim + zi)
c
c        # Compute the waves.
c
         wave(i,1,1) = -a1*zim
         wave(i,2,1) = a1
         s(i,1) = -auxl(i-1,2)
c
         wave(i,1,2) = a2*zi
         wave(i,2,2) = a2
         s(i,2) = auxl(i,2)
c
   20    continue
c
c
c     # compute the leftgoing and rightgoing fluctuations:
c     # Note s(i,1) < 0   and   s(i,2) > 0.
c
      do 220 m=1,meqn
         do 220 i = 2-mbc, mx+mbc
            amdq(i,m) = s(i,1)*wave(i,m,1)
            apdq(i,m) = s(i,2)*wave(i,m,2)
  220       continue
c
      return
      end
c
c -----------------------------------------------------
c
      subroutine setprob
      implicit double precision (a-h,o-z)
      common /cqinit/ beta,ic,i_d
      common /comaux/ rhol,cl,rhor,cr
      common /comlim/ mylim,mrplim(2)
c
c     # Set the material parameters for the acoustic equations
c
      open(unit=7,file='setprob.data',status='old',form='formatted')

c     # choice of initial data:
      read(7,*) ic
c     # beta for initial conditions:
      read(7,*) beta
c
c     # Piecewise constant medium with single interface at x=0
c     # Density and sound speed to left and right:
      read(7,*) rhol
      read(7,*) cl
      read(7,*) rhor
      read(7,*) cr
c
c     # if mylim>0 then limiter is applied in rp1 rather than using
c     # default clawpack limiter.
c     # mrplim(p) tells which limiter to use for the p'th wave.
```

```
c     # if mylim>0 then you should set mthlim(p)=0 in claw1ez.data!
c
      read(7,*) mylim
      read(7,*) mrplim(1), mrplim(2)

      return
      end
c
c
c     ============================================================
      subroutine claw1ez(maxmx,meqn,mwaves,mbc,maux,mwork,mthlim,
     &                   q,work,aux)
c     ============================================================
c
c     An easy-to-use clawpack driver routine for simple applications
c     Documentation is available at
c                 http://www.amath.washington.edu/~claw/doc.html
c
c     Author: Randall J. LeVeque
c     Version of August, 2002 --  CLAWPACK Version 4.1
c
      implicit double precision (a-h,o-z)
      external bc1,rp1,src1,b4step1

      dimension    q(1-mbc:maxmx+mbc, meqn)
      dimension  aux(1-mbc:maxmx+mbc, maux)
      dimension work(mwork)
      dimension mthlim(mwaves)
c
      dimension method(7),dtv(5),cflv(4),nv(2),mthbc(2)
      dimension tout(100)
      logical outt0

      common /cqinit/ beta,ic,i_d
c
      open(55,file='claw1ez.data',status='old',form='formatted')
      open(10,file='fort.info',status='unknown',form='formatted')
c
c
c     # Read the input in standard form from claw1ez.data:
c     # For a description of input parameters see the documentation at
c                 http://www.amath.washington.edu/~claw

c     Number of grid cells:
      read(55,*) mx

c     i/o variables
      read(55,*) nout
      read(55,*) outstyle
      if (outstyle.eq.1) then
          read(55,*) tfinal
          nstepout = 1
        elseif (outstyle.eq.2) then
          read(55,*) (tout(i), i=1,nout)
          nstepout = 1
        elseif (outstyle.eq.3) then
          read(55,*) nstepout, nstop
```

```
        nout = nstop
        endif

c     timestepping variables
      read(55,*) dtv(1)
      read(55,*) dtv(2)
      read(55,*) cflv(1)
      read(55,*) cflv(2)
      read(55,*) nv(1)
c

c     # input parameters for clawpack routines
      read(55,*) method(1)
      read(55,*) method(2)
      read(55,*) method(3)
      read(55,*) method(4)
      read(55,*) method(5)
      read(55,*) method(6)
      read(55,*) method(7)

      read(55,*) meqn1
      read(55,*) mwaves1
      read(55,*) (mthlim(mw), mw=1,mwaves1)

c     # physical domain:
      read(55,*) t0
      read(55,*) xlower
      read(55,*) xupper
c
c     # boundary conditions:
      read(55,*) mbc1
      read(55,*) mthbc(1)
      read(55,*) mthbc(2)

      if (method(7) .ne. maux) then
         write(6,*) '*** ERROR ***  maux set wrong in input or driver'
         stop
         endif

      if (meqn1 .ne. meqn) then
         write(6,*) '*** ERROR ***  meqn set wrong in input or driver'
         stop
         endif
      if (mwaves1 .ne. mwaves) then
         write(6,*) '*** ERROR ***  mwaves set wrong in input or driver'
         stop
         endif
      if (mbc1 .ne. mbc) then
         write(6,*) '*** ERROR ***  mbc set wrong in input or driver'
         stop
         endif
c
      if ((mthbc(1).eq.2 .and. mthbc(2).ne.2) .or.
     &    (mthbc(2).eq.2 .and. mthbc(1).ne.2)) then
         write(6,*) '*** ERROR ***  periodic boundary conditions'
         write(6,*) ' require mthbc(1) and mthbc(2) BOTH be set to 2'
         stop
```

```
         endif

c
c     # check that enough storage has been allocated:
c

      mwork1 = (maxmx + 2*mbc) * (2 + 4*meqn + mwaves + meqn*mwaves)
c
      if (mx.gt.maxmx .or. mwork.lt.mwork1) then
c        # insufficient storage
         maxmx1 = max0(mx,maxmx)

         mwork1 = (maxmx1 + 2*mbc) * (2 + 4*meqn + mwaves + meqn*mwaves)

         write(6,*) ' '
         write(6,*) '*** ERROR *** Insufficient storage allocated'
         write(6,*) 'Recompile after increasing values in driver.f:'
         write(6,611) maxmx1
         write(6,613) mwork1
 611     format(/,'parameter (maxmx = ',i5,')')
 613     format('parameter (mwork = ',i7,')',/)
         stop
         endif

c
c
      write(6,*) 'running...'
      write(6,*) ' '
c
c     # grid spacing
      dx = (xupper - xlower) / float(mx)
c

c     # time increments between outputing solution:
      if (outstyle .eq. 1) then
         dtout = (tfinal - t0)/float(nout)
         endif
c
c
c     # call user's routine setprob to set any specific parameters
c     # or other initialization required.
c
      call setprob
c
c     # set aux array:
c
      if (maux .gt. 0)  then
         call setaux(maxmx,mbc,mx,xlower,dx,maux,aux)
         endif
c
c     # set initial conditions:
c
      call qinit(maxmx,meqn,mbc,mx,xlower,dx,q,maux,aux)
c
      outt0 = .true.
      if (outt0) then
c        # output initial data
```

```
         call out1(maxmx,meqn,mbc,mx,xlower,dx,q,t0,0,aux,maux)
         write(6,601) 0, t0
         endif

c      write(11,700) t0, q(mx/2,1), q(mx/2,2)    !# time-signature
       write(11,700) t0, q(i_d,1), q(i_d,2)    !# time-signature
c      write(11,700) t0, q(251,1), q(251,2)    !# time-signature

       print*,'  detection point at x = ', xlower + (i_d-0.5d0)*dx

c
c     ----------
c     Main loop:
c     ----------
c
      tend = t0
      do 100 n=1,nout
         tstart = tend
         if (outstyle .eq. 1)  tend = tstart + dtout
         if (outstyle .eq. 2)  tend = tout(n)
         if (outstyle .eq. 3)  tend = tstart - 1.d0  !# single-step mode
c
         call claw1(maxmx,meqn,mwaves,mbc,mx,
     &           q,aux,xlower,dx,tstart,tend,dtv,cflv,nv,method,mthlim,
     &           mthbc,work,mwork,info,bc1,rp1,src1,b4step1)

c
c        # check to see if an error occured:
         if (info .ne. 0) then
            write(6,*) '*** ERROR in claw1 ***  info =',info
            if (info.eq.1) then
               write(6,*) '***   either mx > maxmx or mbc < 2'
               endif
            if (info.eq.2) then
               write(6,*) '***   dt does not divide (tend - tstart)'
               write(6,*) '***   and dt is fixed since method(1)=0'
               endif
            if (info.eq.3) then
               write(6,*) '***   method(1)=1 and cflv(2) > cflv(1)'
               endif
            if (info.eq.4) then
               write(6,*) '***   mwork is too small'
               endif
            if (info.eq.11) then
               write(6,*) '***   Too many times steps, n > nv(1)'
               endif
            if (info.eq.12) then
               write(6,*)
     &          '***   The Courant number is greater than cflv(1)'
               write(6,*) '***   and dt is fixed since method(1)=0'
               endif

            go to 999
            endif
c
         dtv(1) = dtv(5)  !# use final dt as starting value on next call
c
```

```
c        # output solution at this time
c        ----------------------------
c
c        # if outstyle=1 or 2, then nstepout=1 and we output every time
c        # we reach this point, since claw1 was called for the entire time
c        # increment between outputs.
c
c        # if outstyle=3 then we only output if we have taken nstepout
c        # time steps since the last output.

c        # iframe is the frame number used to form file names in out1
         iframe = n/nstepout
       if (iframe*nstepout .eq. n) then
            call out1(maxmx,meqn,mbc,mx,xlower,dx,q,tend,iframe,
     &                aux,maux)
            write(6,601) iframe,tend
            write(10,1010) tend,info,dtv(3),dtv(4),dtv(5),
     &           cflv(3),cflv(4),nv(2)
         endif
c
c        # formats for writing out information about this call to claw:
c
  601    format('CLAW1EZ: Frame ',i4,
     &           ' matlab plot files done at time t =',
     &           d12.4,/)
  700    format(2x,f10.4,2(2x,f16.8))
c
 1010    format('tend =',d15.4,/,
     &       'info =',i5,/,'smallest dt =',d15.4,/,'largest dt =',
     &       d15.4,/,'last dt =',d15.4,/,'largest cfl =',
     &         d15.4,/,'last cfl =',d15.4,/,'steps taken =',i4,/)
c
  100    continue
c
  999 continue
c
      return
      end
c
c
c     ============================================
      subroutine b4step1(maxmx,mbc,mx,meqn,q,
     &            xlower,dx,t,dt,maux,aux)
c     ============================================
c
c     # called from claw1 before each call to step1.
c     # use to set time-dependent aux arrays or perform other tasks
c     # which must be done every time step.
c
c     # dummy routine
c
c
      implicit double precision (a-h,o-z)
      dimension q(1-mbc:maxmx+mbc, meqn)
      dimension aux(1-mbc:maxmx+mbc, *)
c
      return
```

```
      end
c
c
c =========================================================
      subroutine out1(maxmx,meqn,mbc,mx,xlower,dx,q,t,iframe,aux,maux)
c =========================================================
c
c     # Output the results for a general system of conservation laws
c     # in 1 dimension
c
c     # Write the results to the file fort.q<iframe>
c     # Use format required by matlab script  plotclaw1.m
c     # The same format is used by the amrclaw package.
c     # Here it's adapted to output just the single grid.
c
c     # set outaux = .true. to also output the aux arrays to fort.a<iframe>
c
c
      implicit double precision (a-h,o-z)
      dimension q(1-mbc:maxmx+mbc, meqn)
      dimension aux(1-mbc:maxmx+mbc, maux)
      character*10 fname1, fname2, fname3
      logical outaux

      outaux = .false.
c
c     # Write the results to the file fort.q<iframe>
c     # Use format required by matlab script  plotclaw1.m
c     # The same format is used by the amrclaw package.
c     # Here it's adapted to output just the single grid.
c
c     # first create the file name and open file
c
         fname1 = 'fort.qxxxx'
         fname2 = 'fort.txxxx'
         fname3 = 'fort.axxxx'
         nstp = iframe
         do 55 ipos = 10, 7, -1
            idigit = mod(nstp,10)
            fname1(ipos:ipos) = char(ichar('0') + idigit)
            fname2(ipos:ipos) = char(ichar('0') + idigit)
            fname3(ipos:ipos) = char(ichar('0') + idigit)
            nstp = nstp / 10
 55      continue

         open(unit=50,file=fname1,status='unknown',form='formatted')
         open(unit=60,file=fname2,status='unknown',form='formatted')

c
c     # the following parameters are used in amrclaw where there are
c     # multiple grids.  Here they are all set to 1:
      ngrids = 1
      mptr = 1
      level = 1

      write(50,1001) mptr,level,mx
 1001 format(i5,'                grid_number',/,
```

```
     &       i5,'                AMR_level',/,
     &       i5,'                mx')

      write(50,1002) xlower,dx
 1002 format(e18.8,'    xlow', /,
     &       e18.8,'    dx', /)
c
        do 10 i=1,mx
          do m=1,meqn
c            # exponents with more than 2 digits cause problems reading
c            # into matlab... reset tiny values to zero:
             if (dabs(q(i,m)) .lt. 1d-99) q(i,m) = 0.d0
             enddo
c
          write(50,1005) (q(i,m), m=1,meqn)
 1005     format(4e16.8)
c
 10       continue
       write(50,*) ' '
 20    continue
      write(50,*) ' '


      if (outaux) then
c        # also output the aux arrays:
         open(unit=70,file=fname3,status='unknown',form='formatted')
         write(70,1001) mptr,level,mx
         write(70,1002) xlower,dx
         do 110 i=1,mx
            do m=1,maux
c              # exponents with more than 2 digits cause problems reading
c              # into matlab... reset tiny values to zero:
               if (dabs(aux(i,m)) .lt. 1d-99) aux(i,m) = 0.d0
            enddo
c
            write(70,1005) (aux(i,m), m=1,maux)
c
  110       continue
         write(70,*) ' '
         close(unit=70)
         endif

      write(60,1000) t,meqn,ngrids,maux

 1000 format(e26.16,'    time', /,
     &       i5,'                meqn'/,
     &       i5,'                ngrids'/,
     &       i5,'                maux'/,/)
c

      close(unit=50)
      close(unit=60)

      return
      end
c
c     =============================================================
```

```
      subroutine claw1(maxmx,meqn,mwaves,mbc,mx,
     &           q,aux,xlower,dx,tstart,tend,dtv,cflv,nv,method,mthlim,
     &           mthbc,work,mwork,info,bc1,rp1,src1,b4step1)
c     ============================================================
c
c  Solves a hyperbolic system of conservation laws in one space dimension
c  of the general form
c
c     capa * q_t + A q_x = psi
c
c  The "capacity function" capa(x) and source term psi are optional
c  (see below).
c
c  For a more complete description see the documentation at
c      http://www.amath.washington.edu/~claw
c
c  Sample driver programs and user-supplied subroutines are available.
c  See the the directories claw/clawpack/1d/example* for some examples, and
c  codes in claw/applications for more extensive examples.
c
c  ----------------------------------------------------------
c
c  The user must supply the following subroutines:
c
c    bc1, rp1        subroutines specifying the boundary conditions and
c                    Riemann solver.
c                    These are described in greater detail below.
c
c    b4step1            The routine b4step1 is called each time step and
c                       can be supplied by the user in order to perform
c                       other operations that are necessary every time
c                       step.  For example, if the variables stored in
c                       the aux arrays are time-dependent then these
c                       values can be set.
c
c  In addition, if the equation contains source terms psi, then the user
c  must provide:
c
c    src1               subroutine that solves capa * q_t = psi
c                       over a single time step.
c
c  These routines must be declared EXTERNAL in the main program.
c  For description of the calling sequences, see below.
c
c  Dummy routines b4step1.f and src1.f are available in
c       claw/clawpack/1d/lib
c
c
c
c  Description of parameters...
c  ----------------------------
c
c
c    maxmx is the maximum number of interior grid points in x,
c          and is used in declarations of the array q.
c
c    meqn is the number of equations in the system of
```

```
c         conservation laws.
c
c    mwaves is the number of waves that result from the
c           solution of each Riemann problem.  Often mwaves = meqn but
c           for some problems these may be different.
c
c    mbc is the number of "ghost cells" that must be added on to each
c       side of the domain to handle boundary conditions.  The cells
c       actually in the physical domain are labelled from 1 to mx in x.
c       The arrays are dimensioned actually indexed from 1-mbc to mx+mbc.
c       For the methods currently implemented, mbc = 2 should be used.
c       If the user implements another method that has a larger stencil and
c       hence requires more ghost cells, a larger value of mbc could be used.
c       q is extended from the physical domain to the ghost cells by the
c       user-supplied routine bc1.
c
c    mx is the number of grid cells in the x-direction, in the
c       physical domain.  In addition there are mbc grid cells
c       along each edge of the grid that are used for boundary
c       conditions.
c       Must have mx .le. maxmx
c
c    q(1-mbc:maxmx+mbc, meqn)
c        On input:  initial data at time tstart.
c        On output: final solution at time tend.
c        q(i,m) = value of mth component in the i'th cell.
c        Values within the physical domain are in q(i,m)
c                for i = 1,2,...,mx
c        mbc extra cells on each end are needed for boundary conditions
c        as specified in the routine bc1.
c
c    aux(1-mbc:maxmx+mbc, maux)
c        Array of auxiliary variables that are used in specifying the
problem.
c        If method(7) = 0 then there are no auxiliary variables and aux
c                         can be a dummy variable.
c        If method(7) = maux > 0 then there are maux auxiliary variables
c                         and aux must be dimensioned as above.
c
c        Capacity functions are one particular form of auxiliary variable.
c        These arise in some applications, e.g. variable coefficients in
c        advection or acoustics problems.
c        See Clawpack Note # 5 for examples.
c
c        If method(6) = 0 then there is no capacity function.
c        If method(6) = mcapa > 0  then there is a capacity function and
c            capa(i), the "capacity" of the i'th cell, is assumed to be
c            stored in aux(i,mcapa).
c            In this case we require method(7).ge.mcapa.
c
c    dx = grid spacing in x.
c         (for a computation in ax <= x <= bx,  set dx = (bx-ax)/mx.)
c
c    tstart = initial time.
c
c    tend = Desired final time (on input).
c              If tend<tstart, then claw1 returns after a single successful
```

```
c                time step has been taken (single-step mode).
c              Otherwise, as many steps are taken as needed to reach tend,
c                up to a maximum of nv(1).
c         = Actual time reached (on output).
c
c    dtv(1:5) = array of values related to the time step:
c               (Note: method(1)=1 indicates variable size time steps)
c         dtv(1) = value of dt to be used in all steps if method(1) = 0
c                = value of dt to use in first step if method(1) = 1
c         dtv(2) = unused if method(1) = 0.
c                = maximum dt allowed if method(1) = 1.
c         dtv(3) = smallest dt used (on output)
c         dtv(4) = largest dt used (on output)
c         dtv(5) = dt used in last step (on output)
c
c    cflv(1:4) = array of values related to Courant number:
c         cflv(1) = maximum Courant number to be allowed.  With variable
c                   time steps the step is repeated if the Courant
c                   number is larger than this value.  With fixed time
c                   steps the routine aborts.  Usually cflv(1)=1.0
c                   should work.
c         cflv(2) = unused if method(1) = 0.
c                 = desired Courant number if method(1) = 1.
c                   Should be somewhat less than cflv(1), e.g. 0.9
c         cflv(3) = largest Courant number observed (on output).
c         cflv(4) = Courant number in last step (on output).
c
c    nv(1:2) = array of values related to the number of time steps:
c         nv(1) = unused if method(1) = 0
c               = maximum number of time steps allowed if method(1) = 1
c         nv(2) = number of time steps taken (on output).
c
c    method(1:7) = array of values specifying the numerical method to use
c         method(1) = 0 if fixed size time steps are to be taken.
c                       In this case, dt = dtv(1) in all steps.
c                   = 1 if variable time steps are to be used.
c                       In this case, dt = dtv(1) in the first step and
c                       thereafter the value cflv(2) is used to choose the
c                       next time step based on the maximum wave speed seen
c                       in the previous step.  Note that since this value
c                       comes from the previous step, the Courant number will
c                       not in general be exactly equal to the desired value
c                       If the actual Courant number in the next step is
c                       greater than 1, then this step is redone with a
c                       smaller dt.
c
c         method(2) = 1 if Godunov's method is to be used, with no 2nd order
c                       corrections.
c                   = 2 if second order correction terms are to be added,
with
c                       a flux limiter as specified by mthlim.
c
c         method(3)  is not used in one-dimension.
c
c         method(4) = 0 to suppress printing
c                   = 1 to print dt and Courant number every time step
c
```

```
c         method(5) = 0 if there is no source term psi.  In this case
c                     the subroutine src1 is never called so a dummy
c                     parameter can be given.
c                   = 1 if there is a source term.  In this case
c                     the subroutine src1 must be provided and a
c                     fractional step method is used.
c                     In each time step the following sequence is followed:
c                          call bc to extend data to ghost cells
c                          call step1 to advance hyperbolic eqn by dt
c                          call src1 to advance source terms by dt
c                   = 2 if there is a source term and Strang splitting is to
c                     be used instead of the Godunov splitting above.
c                     In each time step the following sequence is followed:
c                          call bc to extend data to ghost cells
c                          call src1 to advance source terms by dt/2
c                          call step1 to advance hyperbolic equation by dt
c                          call src1 to advance source terms by dt/2
c                     For most problems 1 is recommended rather than 2
c                     since it is less expensive and works essentially as
c                     well on most problems.

c
c         method(6) = 0 if there is no capacity function capa.
c                   = mcapa > 0 if there is a capacity function.  In this
case
c                     aux(i,mcapa) is the capacity of the i'th cell and you
c                     must also specify method(7) .ge. mcapa and set aux.
c
c         method(7) = 0 if there is no aux array used.
c                   = maux > 0  if there are maux auxiliary variables.
c
c
c         The recommended choice of methods for most problems is
c            method(1) = 1,  method(2) = 2.
c
c    mthlim(1:mwaves) = array of values specifying the flux limiter to be
used
c                       in each wave family mw.  Often the same value will be
used
c                       for each value of mw, but in some cases it may be
c                       desirable to use different limiters.  For example,
c                       for the Euler equations the superbee limiter might be
c                       used for the contact discontinuity (mw=2) while another
c                       limiter is used for the nonlinear waves.  Several
limiters
c                       are built in and others can be added by modifying the
c                       subroutine philim.
c
c        mthlim(mw) = 0 for no limiter
c                   = 1 for minmod
c                   = 2 for superbee
c                   = 3 for van Leer
c                   = 4 for monotonized centered
c
c
c    work(mwork) = double precision work array of length at least mwork
c
```

```
c    mwork = length of work array.  Must be at least
c                (maxmx + 2*mbc) * (2 + 4*meqn + mwaves + meqn*mwaves)
c            If mwork is too small then the program returns with info = 4
c            and prints the necessary value of mwork to unit 6.
c
c
c    info = output value yielding error information:
c         = 0 if normal return.
c         = 1 if mx.gt.maxmx   or  mbc.lt.2
c         = 2 if method(1)=0 and dt doesn't divide (tend - tstart).
c         = 3 if method(1)=1 and cflv(2) > cflv(1).
c         = 4 if mwork is too small.
c         = 11 if the code attempted to take too many time steps, n > nv(1).
c              This could only happen if method(1) = 1 (variable time steps).
c         = 12 if the method(1)=0 and the Courant number is greater than 1
c              in some time step.
c
c           Note: if info.ne.0, then tend is reset to the value of t actually
c           reached and q contains the value of the solution at this time.
c
c    User-supplied subroutines
c    -------------------------
c
c    bc1 = subroutine that specifies the boundary conditions.
c         This subroutine should extend the values of q from cells
c         1:mx to the mbc ghost cells along each edge of the domain.
c
c          The form of this subroutine is
c  ------------------------------------------------
c     subroutine bc1(maxmx,meqn,mbc,mx,xlower,dx,q,maux,aux,t,mthbc)
c     implicit double precision (a-h,o-z)
c     dimension   q(1-mbc:maxmx+mbc, meqn)
c     dimension aux(1-mbc:maxmx+mbc, *)
c     dimension mthbc(2)
c  ------------------------------------------------
c
c    The routine claw/clawpack/1d/lib/bc1.f can be used to specify
c    various standard boundary conditions.
c
c
c    rp1 = user-supplied subroutine that implements the Riemann solver
c
c          The form of this subroutine is
c  ------------------------------------------------
c     subroutine
rp1(maxmx,meqn,mwaves,mbc,mx,ql,qr,auxl,auxr,wave,s,amdq,apdq)
c     implicit double precision (a-h,o-z)
c     dimension   ql(1-mbc:maxmx+mbc, meqn)
c     dimension   qr(1-mbc:maxmx+mbc, meqn)
c     dimension auxl(1-mbc:maxmx+mbc, *)
c     dimension auxr(1-mbc:maxmx+mbc, *)
c     dimension wave(1-mbc:maxmx+mbc, meqn, mwaves)
c     dimension    s(1-mbc:maxmx+mbc, mwaves)
c     dimension amdq(1-mbc:maxmx+mbc, meqn)
c     dimension apdq(1-mbc:maxmx+mbc, meqn)
c  ------------------------------------------------
c
```

```
c         On input, ql contains the state vector at the left edge of each
cell
c                   qr contains the state vector at the right edge of each
cell
c                 auxl contains auxiliary values at the left edge of each
cell
c                 auxr contains auxiliary values at the right edge of each
cell
c
c         Note that the i'th Riemann problem has left state qr(i-1,:)
c                                             and right state ql(i,:)
c         In the standard clawpack routines, this Riemann solver is
c         called with ql=qr=q along this slice.  More flexibility is allowed
c         in case the user wishes to implement another solution method
c         that requires left and rate states at each interface.

c         If method(7)=maux > 0 then the auxiliary variables along this slice
c         are passed in using auxl and auxr.  Again, in the standard routines
c         auxl=auxr=aux in the call to rp1.
c
c          On output,
c              wave(i,m,mw) is the m'th component of the jump across
c                           wave number mw in the ith Riemann problem.
c              s(i,mw) is the wave speed of wave number mw in the
c                           ith Riemann problem.
c              amdq(i,m) = m'th component of A^- Delta q,
c              apdq(i,m) = m'th component of A^+ Delta q,
c                     the decomposition of the flux difference
c                         f(qr(i-1)) - f(ql(i))
c                     into leftgoing and rightgoing parts respectively.
c
c           It is assumed that each wave consists of a jump discontinuity
c           propagating at a single speed, as results, for example, from a
c           Roe approximate Riemann solver.  An entropy fix can be included
c           into the specification of amdq and apdq.
c
c    src1 = subroutine for the source terms that solves the equation
c                capa * q_t = psi
c           over time dt.
c
c           If method(5)=0 then the equation does not contain a source
c           term and this routine is never called.  A dummy argument can
c           be used with many compilers, or provide a dummy subroutine that
c           does nothing (such a subroutine can be found in
c           claw/clawpack/1d/lib/src1.f)
c
c          The form of this subroutine is
c  ------------------------------------------------
c     subroutine src1(maxmx,meqn,mbc,mx,xlower,dx,q,maux,aux,t,dt)
c     implicit double precision (a-h,o-z)
c     dimension   q(1-mbc:maxmx+mbc, meqn)
c     dimension aux(1-mbc:maxmx+mbc, *)
c  ------------------------------------------------
c      If method(7)=0  or the auxiliary variables are not needed in this
solver,
c      then the latter dimension statement can be omitted, but aux should
c      still appear in the argument list.
```

```
c
c      On input, q(i,m) contains the data for solving the
c               source term equation.
c      On output, q(i,m) should have been replaced by the solution to
c                 the source term equation after a step of length dt.
c
c
c      b4step1 = subroutine that is called from claw1 before each call to
c                step1.  Use to set time-dependent aux arrays or perform
c                other tasks which must be done every time step.
c
c          The form of this subroutine is
c
c  -------------------------------------------------
c      subroutine b4step1(maxmx,mbc,mx,meqn,q,xlower,dx,time,dt,maux,aux)
c      implicit double precision (a-h,o-z)
c      dimension   q(1-mbc:maxmx+mbc, meqn)
c      dimension aux(1-mbc:maxmx+mbc, *)
c  -------------------------------------------------
c
c
c
c
c =====================================================================
c
c  Copyright 1994 -- 2002 R. J. LeVeque
c
c  This software is made available for research and instructional use only.
c  You may copy and use this software without charge for these non-commercial
c  purposes, provided that the copyright notice and associated text is
c  reproduced on all copies.  For all other uses (including distribution of
c  modified versions), please contact the author at the address given below.
c
c  *** This software is made available "as is" without any assurance that it
c  *** will work for your purposes.  The software may in fact have defects,
so
c  *** use the software at your own risk.
c
c  --------------------------------------
c    CLAWPACK Version 4.1,  August, 2002
c    Webpage: http://www.amath.washington.edu/~claw
c  --------------------------------------
c    Author:  Randall J. LeVeque
c             Applied Mathematics
c             Box 352420
c             University of Washington,
c             Seattle, WA 98195-2420
c             rjl@amath.washington.edu
c =====================================================================
c
c
c
c
c    ================================================================
c    Beginning of claw1 code
c    ================================================================
c
```

```
      implicit double precision (a-h,o-z)
      external bc1,rp1,src1,b4step1
      dimension q(1-mbc:maxmx+mbc, meqn)
      dimension aux(1-mbc:maxmx+mbc, *)
      dimension work(mwork)
      dimension mthlim(mwaves),method(7),dtv(5),cflv(4),nv(2)
      dimension mthbc(2)
      common /comxt/ dtcom,dxcom,tcom
      common /cqinit/ beta,ic,i_d
c
c
      info = 0
      t = tstart
      maxn = nv(1)
      dt = dtv(1)   !# initial dt
      cflmax = 0.d0
      dtmin = dt
      dtmax = dt
      nv(2) = 0
      maux = method(7)
c
c     # check for errors in data:
c
      if (mx .gt. maxmx) then
         info = 1
         go to 900
         endif
c
      if (method(1) .eq. 0) then
c        # fixed size time steps.  Compute the number of steps:
         if (tend .lt. tstart) then
c             # single step mode
            maxn = 1
          else
            maxn = (tend - tstart + 1d-10) / dt
            if (dabs(maxn*dt - (tend-tstart)) .gt.
     &                           1d-5*(tend-tstart)) then
c               # dt doesn't divide time interval integer number of times
                info = 2
                go to 900
                endif
         endif
         endif
c
      if (method(1).eq.1 .and. cflv(2).gt.cflv(1)) then
         info = 3
         go to 900
         endif
c
c     # partition work array into pieces for passing into step1:
      i0f = 1
      i0wave = i0f + (maxmx + 2*mbc) * meqn
      i0s = i0wave + (maxmx + 2*mbc) * meqn * mwaves
      i0dtdx = i0s + (maxmx + 2*mbc) * mwaves
      i0qwork = i0dtdx + (maxmx + 2*mbc)
      i0amdq = i0qwork + (maxmx + 2*mbc) * meqn
      i0apdq = i0amdq + (maxmx + 2*mbc) * meqn
```

```
      i0dtdx = i0apdq + (maxmx + 2*mbc) * meqn
      i0end = i0dtdx + (maxmx + 2*mbc) - 1
c
      if (mwork .lt. i0end) then
         write(6,*) 'mwork must be increased to ',i0end
         info = 4
         go to 900
         endif
c
c     -----------
c     # main loop
c     -----------
c
      if (maxn.eq.0) go to 900
      do 100 n=1,maxn
         told = t   !# time at beginning of time step.

c        # adjust dt to hit tend exactly if we're near end of computation
c        #  (unless tend < tstart, which is a flag to take only a single
step)
         if (told+dt.gt.tend .and. tstart.lt.tend) dt = tend - told

         if (method(1).eq.1) then
c           # save old q in case we need to retake step with smaller dt:
            call copyq1(maxmx,meqn,mbc,mx,q,work(i0qwork))
            endif
c
   40    continue
         dt2 = dt / 2.d0
         thalf = t + dt2  !# midpoint in time for Strang splitting
         t = told + dt    !# time at end of step

         write(11,700) t, q(i_d,1), q(i_d,2)      !# time-signature
c         write(11,700) t, q(mx/2,1), q(mx/2,2)      !# time-signature
c         write(11,700) t, q(251,1), q(251,2)      !# time-signature
  700    format(2x,f10.4,2(2x,f16.8))

c        # store dt and t in the common block comxt in case they are needed
c        # in the Riemann solvers (for variable coefficients)
         tcom = told
         dtcom = dt
         dxcom = dx
c
c        ------------------------------------------------------------------
c        # main steps in algorithm:
c        ------------------------------------------------------------------
c
c        # extend data from grid to bordering boundary cells:
         call bc1(maxmx,meqn,mbc,mx,xlower,dx,q,maux,aux,told,dt,mthbc)
c
c
c        # call user-supplied routine which might set aux arrays
c        # for this time step, for example.

         call b4step1(maxmx,mbc,mx,meqn,q,
     &                xlower,dx,told,dt,maux,aux)
```

```
c
c
         if (method(5).eq.2) then
c            # with Strang splitting for source term:
             call src1(maxmx,meqn,mbc,mx,xlower,dx,q,maux,aux,told,dt2)
             endif
c
c        # take a step on the homogeneous conservation law:
         call step1(maxmx,meqn,mwaves,mbc,mx,q,aux,dx,dt,
     &             method,mthlim,cfl,work(i0f),work(i0wave),
     &             work(i0s),work(i0amdq),work(i0apdq),work(i0dtdx),
     &             rp1)
c
         if (method(5).eq.2) then
c            # source terms over a second half time step for Strang
splitting:
c            # Note it is not so clear what time t should be used here if
c            # the source terms are time-dependent!
             call src1(maxmx,meqn,mbc,mx,xlower,dx,q,maux,aux,thalf,dt2)
             endif

         if (method(5).eq.1) then
c            # source terms over a full time step:
             call src1(maxmx,meqn,mbc,mx,xlower,dx,q,maux,aux,t,dt)
             endif
c


c
c        ------------------------------------------------------------
c
         if (method(4) .eq. 1) write(6,601) n,cfl,dt,t
  601    format('CLAW1... Step',i4,
     &                  '   Courant number =',f6.3,'  dt =',d12.4,
     &                  '  t =',d12.4)
c
         if (method(1) .eq. 1) then
c           # choose new time step if variable time step
            if (cfl .gt. 0.d0) then
                dt = dmin1(dtv(2), dt * cflv(2)/cfl)
                dtmin = dmin1(dt,dtmin)
                dtmax = dmax1(dt,dtmax)
              else
                dt = dtv(2)
              endif
            endif
c
c        # check to see if the Courant number was too large:
c
         if (cfl .le. cflv(1)) then
c               # accept this step
                cflmax = dmax1(cfl,cflmax)
              else
c               # reject this step
                t = told
                call copyq1(maxmx,meqn,mbc,mx,work(i0qwork),q)
c
                if (method(4) .eq. 1) then
```

```
                write(6,602)
  602           format('CLAW1 rejecting step... ',
     &                     'Courant number too large')
                endif
              if (method(1).eq.1) then
c                 # if variable dt, go back and take a smaller step
                  go to 40
                else
c                 # if fixed dt, give up and return
                  cflmax = dmax1(cfl,cflmax)
                  go to 900
                endif
              endif
c
c       # see if we are done:
        nv(2) = nv(2) + 1
        if (t .ge. tend) go to 900
c
  100   continue
c
  900  continue
c
c     # return information
c
      if (method(1).eq.1 .and. t.lt.tend .and. nv(2) .eq. maxn) then
c        # too many timesteps
         info = 11
         endif
c
      if (method(1).eq.0 .and. cflmax .gt. cflv(1)) then
c        # Courant number too large with fixed dt
         info = 12
         endif
      tend = t
      cflv(3) = cflmax
      cflv(4) = cfl
      dtv(3) = dtmin
      dtv(4) = dtmax
      dtv(5) = dt
      return
      end
c
c
c =====================================================================
      subroutine step1(maxmx,meqn,mwaves,mbc,mx,q,aux,dx,dt,
     &              method,mthlim,cfl,f,wave,s,amdq,apdq,dtdx,rp1)
c =====================================================================
c
c     # Take one time step, updating q.
c
c     method(1) = 1   ==>  Godunov method
c     method(1) = 2   ==>  Slope limiter method
c     mthlim(p)  controls what limiter is used in the pth family
c
c
c     amdq, apdq, wave, s, and f are used locally:
c
```

```
c     amdq(1-mbc:maxmx+mbc, meqn) = left-going flux-differences
c     apdq(1-mbc:maxmx+mbc, meqn) = right-going flux-differences
c        e.g. amdq(i,m) = m'th component of A^- \Delta q from i'th Riemann
c                         problem (between cells i-1 and i).
c
c     wave(1-mbc:maxmx+mbc, meqn, mwaves) = waves from solution of
c                                           Riemann problems,
c           wave(i,m,mw) = mth component of jump in q across
c                          wave in family mw in Riemann problem between
c                          states i-1 and i.
c
c     s(1-mbc:maxmx+mbc, mwaves) = wave speeds,
c           s(i,mw) = speed of wave in family mw in Riemann problem between
c                     states i-1 and i.
c
c     f(1-mbc:maxmx+mbc, meqn) = correction fluxes for second order method
c           f(i,m) = mth component of flux at left edge of ith cell
c     ----------------------------------------------------------------
c
      implicit double precision (a-h,o-z)
      dimension    q(1-mbc:maxmx+mbc, meqn)
      dimension  aux(1-mbc:maxmx+mbc, *)
      dimension    f(1-mbc:maxmx+mbc, meqn)
      dimension    s(1-mbc:maxmx+mbc, mwaves)
      dimension wave(1-mbc:maxmx+mbc, meqn, mwaves)
      dimension amdq(1-mbc:maxmx+mbc, meqn)
      dimension apdq(1-mbc:maxmx+mbc, meqn)
      dimension dtdx(1-mbc:maxmx+mbc)
      dimension method(7),mthlim(mwaves)
      logical limit
c
c     # check if any limiters are used:
      limit = .false.
      do 5 mw=1,mwaves
         if (mthlim(mw) .gt. 0) limit = .true.
    5    continue
c
      mcapa = method(6)
      do 10 i=1-mbc,mx+mbc
         if (mcapa.gt.0) then
             if (aux(i,mcapa) .le. 0.d0) then
                write(6,*) 'Error -- capa must be positive'
                stop
                endif
             dtdx(i) = dt / (dx*aux(i,mcapa))
           else
             dtdx(i) = dt/dx
           endif
   10    continue
c
c
c
c     # solve Riemann problem at each interface
c     -----------------------------------------
c
      call rp1(maxmx,meqn,mwaves,mbc,mx,q,q,aux,aux,wave,s,amdq,apdq)
c
```

```
c     # Modify q for Godunov update:
c     # Note this may not correspond to a conservative flux-differencing
c     # for equations not in conservation form.  It is conservative if
c     # amdq + apdq = f(q(i)) - f(q(i-1)).
c
      do 40 i=1,mx+1
         do 40 m=1,meqn
            q(i,m) = q(i,m) - dtdx(i)*apdq(i,m)
            q(i-1,m) = q(i-1,m) - dtdx(i-1)*amdq(i,m)
   40       continue

c
c     # compute maximum wave speed:
      cfl = 0.d0
      do 50 mw=1,mwaves
         do 45 i=1,mx+1
c          # if s>0 use dtdx(i) to compute CFL,
c          # if s<0 use dtdx(i-1) to compute CFL:
           cfl = dmax1(cfl, dtdx(i)*s(i,mw), -dtdx(i-1)*s(i,mw))
   45      continue
   50    continue
c
      if (method(2) .eq. 1) go to 900
c
c     # compute correction fluxes for second order q_{xx} terms:
c     -----------------------------------------------------------
c
      do 100 m = 1, meqn
            do 100 i = 1-mbc, mx+mbc
               f(i,m) = 0.d0
  100          continue
c
c      # apply limiter to waves:
      if (limit) call limiter(maxmx,meqn,mwaves,mbc,mx,wave,s,mthlim)
c
      do 120 i=1,mx+1
         do 120 m=1,meqn
            do 110 mw=1,mwaves
               dtdxave = 0.5d0 * (dtdx(i-1) + dtdx(i))
               f(i,m) = f(i,m) + 0.5d0 * dabs(s(i,mw))
     &             * (1.d0 - dabs(s(i,mw))*dtdxave) * wave(i,m,mw)
  110          continue
  120       continue
c
c
  140 continue
c
c     # update q by differencing correction fluxes
c     ============================================
c
c     # (Note:  Godunov update has already been performed above)
c
      do 150 m=1,meqn
         do 150 i=1,mx
            q(i,m) = q(i,m) - dtdx(i) * (f(i+1,m) - f(i,m))
  150       continue
c
```

```
  900 continue
      return
      end
c
c
c =========================================================
      subroutine copyq1(maxmx,meqn,mbc,mx,q1,q2)
c =========================================================
c
c     # copy the contents of q1 into q2
c
      implicit double precision (a-h,o-z)
      dimension q1(1-mbc:maxmx+mbc, meqn)
      dimension q2(1-mbc:maxmx+mbc, meqn)
c
      do 10 i = 1-mbc, mx+mbc
          do 10 m=1,meqn
             q2(i,m) = q1(i,m)
   10        continue
      return
      end
c
c
c     =====================================================
      subroutine limiter(maxm,meqn,mwaves,mbc,mx,wave,s,mthlim)
c     =====================================================
c
c     # Apply a limiter to the waves.
c     # The limiter is computed by comparing the 2-norm of each wave with
c     # the projection of the wave from the interface to the left or
c     # right onto the current wave.  For a linear system this would
c     # correspond to comparing the norms of the two waves.  For a
c     # nonlinear problem the eigenvectors are not colinear and so the
c     # projection is needed to provide more limiting in the case where the
c     # neighboring wave has large norm but points in a different direction
c     # in phase space.
c
c     # The specific limiter used in each family is determined by the
c     # value of the corresponding element of the array mthlim, as used in
c     # the function philim.
c     # Note that a different limiter may be used in each wave family.
c
c     # dotl and dotr denote the inner product of wave with the wave to
c     # the left or right.  The norm of the projections onto the wave are
then
c     # given by dotl/wnorm2 and dotr/wnorm2, where wnorm2 is the 2-norm
c     # of wave.
c
      implicit real*8(a-h,o-z)
      dimension mthlim(mwaves)
      dimension wave(1-mbc:maxm+mbc, meqn, mwaves)
      dimension    s(1-mbc:maxm+mbc, mwaves)
c
c
      do 50 mw=1,mwaves
         if (mthlim(mw) .eq. 0) go to 50
         dotr = 0.d0
```

```
          do 40 i = 0, mx+1
             wnorm2 = 0.d0
             dotl = dotr
             dotr = 0.d0
             do 20 m=1,meqn
                wnorm2 = wnorm2 + wave(i,m,mw)**2
                dotr = dotr + wave(i,m,mw)*wave(i+1,m,mw)
   20        continue
             if (i.eq.0) go to 40
             if (wnorm2.eq.0.d0) go to 40
c
             if (s(i,mw) .gt. 0.d0) then
                 wlimitr = philim(wnorm2, dotl, mthlim(mw))
               else
                 wlimitr = philim(wnorm2, dotr, mthlim(mw))
               endif
c
             do 30 m=1,meqn
                wave(i,m,mw) = wlimitr * wave(i,m,mw)
   30        continue
   40       continue
   50    continue
c
      return
      end
c
c
c     =====================================================
      double precision function philim(a,b,meth)
c     =====================================================
      implicit real*8(a-h,o-z)
c
c     # Compute a limiter based on wave strengths a and b.
c     # meth determines what limiter is used.
c     # a is assumed to be nonzero.
c
c     # NOTE: This routine is obsolete.  Instead of using limiter.f,
c     # which calls philim.f for every wave, it is more efficient to
c     # use inlinelimiter.f, which eliminates all these function calls
c     # to philim.  If you wish to change the limiter function and are
c     # using inlinelimiter.f, the formulas must be changed in that routine.
c
      r = b/a
      go to (10,20,30,40,50) meth

c
   10 continue
c     --------
c     # minmod
c     --------
      philim = dmax1(0.d0, dmin1(1.d0, r))
      return
c
   20 continue
c     ----------
c     # superbee
c     ----------
```

```
      philim = dmax1(0.d0, dmin1(1.d0, 2.d0*r), dmin1(2.d0, r))
      return
c
   30 continue
c     ----------
c     # van Leer
c     ----------
      philim = (r + dabs(r)) / (1.d0 + dabs(r))
      return
c
   40 continue
c     ------------------------------
c     # monotinized centered
c     ------------------------------
      c = (1.d0 + r)/2.d0
      philim = dmax1(0.d0, dmin1(c, 2.d0, 2.d0*r))
      return
c
   50 continue
c     ------------------------------
c     # Beam-Warming
c     ------------------------------
      philim = r

      return
      end

c
c
c =========================================================
      subroutine src1(maxmx,meqn,mbc,mx,xlower,dx,q,maux,aux,t,dt)
c =========================================================
      implicit double precision (a-h,o-z)
      dimension q(1-mbc:maxmx+mbc, meqn)
c
c     do nothing... no source term
c
      return
      end
```

BIBLIOGRAPHY

Aghajani, A., & Roomi, V. 2012, Turkish Journal of Mathematics, 36, 273

Alfvén, H. 1942, *Nature* , 150, 405

An, C.-H., Musielak, Z. E., Moore, R. L., & Suess, S. T. 1989, *ApJ* , 345, 597

Anderson, L. S., & Athay, R. G. 1989, *ApJ* , 336, 1089

Avrett, E. H., & Loeser, R. 2008, *ApJS* , 175, 229

Bohner, M., & Saker, S. H. 2006, Research India Publications, 1, 163

Cally, P. S. 2003, Sol. Phys., 217, 95

Cally, P. S. 2012, Sol. Phys., 280, 33

Cameron, R., & Galloway, D. 2005, *MNRAS* , 358, 1025

Cargill, P. 2013, *Nature* , 493, 485

Cargill, P., & de Moortel, I. 2011, *Nature* , 475, 463

Chmielewski, P., Srivastava, A. K., Murawski, K., & Musielak, Z. E. 2013, *MNRAS* , 428, 40

Cirtain, J. W., Golub, L., Lundquist, L., et al. 2007, Science, 318, 1580

Coles, W. J. 1968, Proc. Amer. Math. Soc., 19, 755

Davidson, P. A. 2001, An Introduction to Magnetohydrodynamics (Cambridge University Press)

De Pontieu, B., McIntosh, S. W., Carlsson, M., et al. 2007, Science, 318, 1574

Dwivedi, B. N., & Srivastava, A. K. 2010, Current Science, 98, 295

Erdélyi, R., & Fedun, V. 2007, Science, 318, 1572

Ferraro, C. A., & Plumpton, C. 1958, *ApJ* , 127, 459

Foukal, P. V. 2004, Solar Astrophysics, 2nd, Revised Edition (Wiley-VCH)

Fujimura, D., & Tsuneta, S. 2009, *ApJ* , 702, 1443

Goedbloed, J. P. H., & Poedts, S. 2004, Principles of Magnetohydrodynamics (Cambridge University Press)

Hammer, R., Musielak, Z. E., & Routh, S. 2010, Astronomische Nachrichten, 331, 593

Hartman, P. 1952, Amer. J. Math., 74, 389

Hille, E. 1948, Trans. Am. Math. Soc., 64, 234

Hollweg, J. V. 1978, Sol. Phys, 56, 305

Hollweg, J. V. 1981, Sol. Phys, 70, 25

Hollweg, J. V. 1985, in Advances in Space Plasma Physics, ed. W. Grossmann, E. M. Campbell, & B. Buti, 77

Hollweg, J. V. 1990, Washington DC American Geophysical Union Geophysical Monograph Series, 58, 23

Hollweg, J. V. 1992, *ApJ* , 389, 731

Hollweg, J. V., & Isenberg, P. A. 2007, Journal of Geophysical Research (Space Physics), 112, 8102

Jess, D. B., Mathioudakis, M., Erdélyi, R., et al. 2009, Science, 323, 1582

Kamenev, I. V. 1978, Math, Notes, 23, 136

Kneser, A. 1893, Math. Ann, 42, 409

Kudoh, T., & Shibata, K. 1999, *ApJ* , 514, 493

Kulsrud, R. M. 1955, *ApJ* , 121, 461

Lamb, H. 1932, Hydrodynamics (Dover Publications, NY)

Lee, C. F., Yeh, C. C., & Gau, C. Y. 2005, Czechoslovak Math. J., 55, 845

Leighton, W. 1949, Proc. Nat. Acad. Sci., 35, 190

—. 1950, Duke J. Math., 17, 57

—. 1962, Proc. Amer. Math. Soc., 13, 603

Leroy, B. 1983, *A&A* , 125, 371

Leveque, R. J. 2002, International Journal for Numerical Methods in Fluids, 40, 93

Linsky, J. L. 1991, in Mechanisms of Chromospheric and Coronal Heating, ed. P. Ulmschneider, E. R. Priest, & R. Rosner, 166

Lopin, I., & Nagorny, I. 2013, *ApJ* , 774, 121

Matsumoto, T., & Shibata, K. 2010, *ApJ* , 710, 1857

McIntosh, S. W., de Pontieu, B., Carlsson, M., et al. 2011, *Nature* , 475, 477

McKenzie, J. F., & Hu, Q. 2010, Annales Geophysicae, 28, 737

Milne-Thomson, L., & Rott, N. 1968, Journal of Applied Mechanics, 35, 846

Murawski, K., & Musielak, Z. E. 2010, *A&A* , 518, A37

Murawski, K., Srivastava, A. K., & Musielak, Z. E. 2014, *ApJ* , 788, 8

Murphy, G. M. 2011, Ordinary differential equations and their solutions (Courier Dover Publications)

Musielak, Z. E., Fontenla, J. M., & Moore, R. L. 1992, Physics of Fluids B, 4, 13

Musielak, Z. E., & Moore, R. L. 1995, *ApJ* , 452, 434

Musielak, Z. E., Musielak, D. E., & Mobashi, H. 2006, Phys. Rev., 73, 036612

Musielak, Z. E., Rosner, R., & Ulmschneider, P. 2000, *ApJ* , 541, 410

Musielak, Z. E., Rosner, R., & Ulmschneider, P. 2002, *ApJ* , 573, 418

Musielak, Z. E., Routh, S., & Hammer, R. 2007, *ApJ* , 659, 650

Nehari, Z. 1954, Amer. J. Math., 76, 689

Ofman, L. 2002, *ApJL* , 568, L135

Okamoto, T. J., & De Pontieu, B. 2011, *ApJL* , 736, L24

Osterbrock, D. E. 1961, *ApJ* , 134, 347

Parker, E. N. 1979, Cosmical magnetic fields: Their origin and their activity (Oxford University Press)

Perera, H. K., Musielak, Z. E., & Murawski, K. 2014, A&A submitted

Perera, H. K., Musielak, Z. E., & Murawski, K. 2014, MNRAS submitted

Petukhov, M. Y., & Petukhov, Y. V. 2002, Astronomy Letters, 28, 335

Philos, C. G. 1989, Arch. Math., 53, 482

Priest, E. R. 1982, Solar magneto-hydrodynamics (D. Reidel Pub. Co.), 74P

Priest, E. R., Heyvaerts, J. F., & Title, A. M. 2002, *ApJ* , 576, 533

Priest, E. R., Longcope, D. W., & Titov, V. S. 2003, *ApJ* , 598, 667

Rae, I. C., & Roberts, B. 1982, *ApJ* , 256, 761

Rahimi Tabar, M. R., & Rouhani, S. 1996, Annals of Physics, 246, 446

Roberts, B. 1983, Sol. Phys, 87, 77

Roberts, B. 2000, Sol. Phys, 193, 139

Roberts, B., & Ulmschneider, P. 1997, in Lecture Notes in Physics, Berlin Springer Verlag, Vol. 489, European Meeting on Solar Physics, ed. G. M. Simnett, C. E. Alissandrakis, & L. Vlahos, 75

Routh, S., Musielak, Z. E., & Hammer, R. 2007, Sol. Phys, 246, 133

Routh, S., Musielak, Z. E., & Hammer, R. 2010, *ApJ* , 709, 1297

Routh, S., Musielak, Z. E., & Hammer, R. 2013, *ApJ* , 763, 44

Saar, S. H. 1996, in IAU Symposium, Vol. 176, Stellar Surface Structure, ed. K. G. Strassmeier & J. L. Linsky, 237

Saar, S. H. 1998, in Astronomical Society of the Pacific Conference Series, Vol. 154, Cool Stars, Stellar Systems, and the Sun, ed. R. A. Donahue & J. A. Bookbinder, 211

Saker, S. H., Pang, P. Y. H., & Agarwal, R. P. 2003, Dynamic Sys. Appl., 12, 307

Schmitz, F., & Fleck, B. 1998, *A&A* , 337, 487

Schrijver, C. J., & Title, A. M. 2003, *ApJL* , 597, L165

Solanki, S. K. 1993, Space Sci. Rev., 63, 1

Stix, M. 2004, The sun : an introduction (Springer)

Sturm, C. 1836, J. Math. Pures Appl., 1, 106

Suzuki, T. K., & Inutsuka, S.-i. 2005, *ApJL* , 632, L49

Swanson, C. A. 1968, Comparison and oscillation theory of linear differential equations (Academic Press)

Teschl, G. 2011, Ordinary Differential Equations and Dynamical Systems (Amer. Math. Soc.)

Thomas, J. H. 1983, Annual Review of Fluid Mechanics, 15, 321

Tyagi, J. 2009, Electronic Journal of Differential Equations, 19, 1

Ulmschneider, P., & Musielak, Z. 2003, in Astronomical Society of the Pacific Conference Series, Vol. 286, Current Theoretical Models and Future High Resolution Solar Observations: Preparing for ATST, ed. A. A. Pevtsov & H. Uitenbroek, 363

Velli, M. 1993, *A&A* , 270, 304

Verdini, A., & Velli, M. 2007, *ApJ* , 662, 669

Verdini, A., Velli, M., & Buchlin, E. 2009, *ApJL* , 700, L39

Vernazza, J. E., Avrett, E. H., & Loeser, R. 1981, *ApJS* , 45, 635

Webb, G. M., McKenzie, J. F., Hu, Q., Dasgupta, B., & Zank, G. P. 2012, AGU Fall Meeting Abstracts, B2222

Wintner, A. 1949, Quat. Appl. Math., 7, 115

Wong, J. S. W. 1999, J. Math. Anal. Appl., 231, 235

Yan, J. 1986, Proc. Amer. Math. Soc., 98, 276

Yu, Y. H. 1991, Math. Nachr., 153, 485

Zhugzhda, I. D., & Locans, V. 1982, Sol. Phys., 76, 77

BIOGRAPHICAL STATEMENT

B.L.Harsha Perera is originally from Sri Lanka. Since her junior high school days she set her mind upon studying Physics and decided to pursue Astrophysics as a career in college. After completing Bachelors in Physics from University of Colombo in Sri Lanka, Harsha became first a teaching assistant then an assistant lecturer at the same institution. However she set her sight on serious research in theoretical Astrophysics and decided to go to US for further education. In 2008 Harsha came to University of Texas at Arlington, USA, to pursue her goal. She was awarded Bonnie Cecil Thompson Award and Scharff Award by the Department of Physics for 2010 and 2013. She defended her doctoral dissertation on November 19, 2014. Her current research interest is theoretical study of Alfvén waves in solar atmosphere. Beyond graduate school she wishes to engage in the cutting edge research in Solar Physics and Astrophysics.